LENS-FREE IMAGING OF DEP MANIPULATED CANCER CELLS

A THESIS SUBMITTED TO
THE GRADUATE SCHOOL OF NATURAL AND APPLIED SCIENCES
OF
MIDDLE EAST TECHNICAL UNIVERSITY

BY

MAHMUT KAMİL ASLAN

IN PARTIAL FULFILLMENT OF THE REQUIREMENTS
FOR
THE DEGREE OF MASTER OF SCIENCE
IN
ELECTRICAL AND ELECTRONICS ENGINEERING

SEPTEMBER 2017

Approval of the thesis:

LENS-FREE IMAGING OF
DEP MANIPULATED CANCER CELLS

Submitted by **MAHMUT KAMİL ASLAN** in partial fulfillment of the requirements for the degree of **Master of Science in Electrical and Electronics Engineering Department, Middle East Technical University** by,

Prof. Dr. Gülbin Dural Ünver
Dean, Graduate School of **Natural and Applied Sciences** _____

Prof. Dr. Tolga Çiloğlu
Head of Department, **Electrical and Electronics Engineering** _____

Prof. Dr. Haluk Külah
Supervisor, **Electrical and Electronics Eng. Dept., METU** _____

Examining Committee Members:

Prof. Dr. Tayfun Akın
Electrical and Electronics Engineering Dept., METU _____

Prof. Dr. Haluk Külah
Electrical and Electronics Engineering Dept., METU _____

Prof. Dr. Gözde Bozdağı Akar
Electrical and Electronics Engineering Dept., METU _____

Assist. Prof. Dr. Serdar Kocaman
Electrical and Electronics Engineering Dept., METU _____

Assist. Prof. Dr. Ender Yıldırım
Mechanical Engineering Dept., Çankaya University _____

Date:

I hereby declare that all information in this document has been obtained and presented in accordance with academic rules and ethical conduct. I also declare that, as required by these rules and conduct, I have fully cited and referenced all material and results that are not original to this work.

Name, Lastname:

Signature:

ABSTRACT

LENS-FREE IMAGING OF DEP MANIPULATED CANCER CELLS

Aslan, Mahmut Kamil
M. Sc., Department of Electrical and Electronics Engineering
Supervisor: Prof. Dr. Haluk Külah

September 2017, 94 pages

Dielectrophoresis (DEP) method is based on manipulating dielectric particles under nonuniform electric field according to their unique electrical properties. With the developments in both MEMS and microfluidics technology, DEP becomes promising technique in cell manipulation. Main advantages of the DEP can be listed as: label free operation, simple implementation and cost effectiveness. However, most of the systems implementing DEP method to manipulate cells, includes microscope, computer and signal generator which are not easily available and limiting portability. Lens-free CMOS imaging is an alternative technique in cell quantification by offering cost effectiveness, easy-to-use operation and portability. In this thesis, a lab-on-a-chip (LOC) system integrating the DEP technique with lens-free CMOS imaging to quantify manipulated cancer cells is developed.

In the design phase of the system, different DEP device designs having various electrode width and interelectrode gaps are proposed. DEP devices are energized with a portable signal generator circuitry. Additionally, CMOS image sensor is operated with a smartphone for processing CMOS image data for cell quantification in stand-alone manner. Finally, mechanical integration of the LOC system is completed with 3D printed holders.

Experimental results shows both functionality of the DEP device designs under different flow rates (0-3 μL/min) and counting accuracy of the CMOS imager integrated with the DEP devices. The counting accuracy of the system is above 90%.

As a future development, the system performance can be increased utilizing different image reconstruction techniques for achieving better resolution. Moreover, DEP designs can be revised to selectively capture rare cells from heterogeneous cell solutions.

Keywords: Dielectrophoresis (DEP), lens-free imaging, lab-on-a-chip, cancer cell, smart phones.

ÖZ

DEP YÖNTEMİ İLE MANİPÜLE EDİLEN KANSER HÜCRELERİNİN LENSSİZ GÖRÜNTÜLENMESİ

Aslan, Mahmut Kamil
Yüksek Lisans, Elektrik ve Elektronik Mühendisliği Bölümü
Tez Yöneticisi: Prof. Dr. Haluk Külah

Eylül 2017, 94 sayfa

Dielektroforez (DEP) yöntemi, dielektrik parçacıkların ayırt edici elektriksel özelliklerine göre değişken elektrik alan altında manipüle edilmesine dayanır. MEMS ve mikroakışkanlar teknolojisindeki gelişmelerle birlikte DEP, hücre manipülasyonunda etkili bir teknik haline gelmektedir. DEP'in başlıca avantajları şu şekildedir: etiket kullanılmasını gerektirmeyen yapısı, basit uygulanması ve düşük maliyet. Bununla birlikte, DEP yöntemini uygulayan sistemlerin çoğunda, hücrelerin tespitinde kolayca bulunmayan ve taşınabilirliği sınırlayan, mikroskop, bilgisayar ve sinyal üreteci gibi cihazlar kullanılmaktadır. Lenssiz CMOS görüntüleme, düşük maliyet, kolay kullanım ve taşınabilirlik gibi avantajlar sunarak hücre incelemesinde alternatif bir teknik haline gelmiştir. Bu tezde, manipüle edilmiş kanser hücrelerini incelemek için DEP tekniğini lenssiz CMOS görüntüleme ile birleştiren bir çip-üstü-laboratuvar sistemi geliştirilmiştir.

Sistemin tasarım aşamasında, çeşitli elektrot genişliği ve aralıklarına sahip farklı DEP cihazı tasarımları yapılmıştır. DEP cihazlarını taşınabilir bir sinyal jeneratör ile çalışmaktadır. Buna ek olarak, CMOS görüntü sensörü, hücre incelenmesi için görüntü verilerini işlemek üzere bir akıllı telefon ile çalıştırılmaktadır. Son olarak, çip-üstü-laboratuvar sisteminin mekanik entegrasyonu üç boyutlu yazıcı ile üretilen tutucular ile tamamlanmaktadır.

Deneysel sonuçlar DEP cihaz tasarımlarının farklı akış hızlarında (0-3 μL / dakika) işlevselliğini ve DEP cihazlarıyla entegre CMOS görüntüleyicinin sayım doğruluğunu göstermiştir. Sistemin sayım doğruluğu %90'nın üzerindedir.

İyileştirme olarak, daha iyi çözünürlük elde etmek için görüntüler farklı yapılandırma teknikleri kullanılarak işlenerek sistem performansı artırılabilir. Ayrıca, DEP tasarımları, heterojen hücre solüsyonlarından nadir bulunan hücreleri seçici olarak yakalamak üzere revize edilebilir.

Anahtar Kelimeler: Dielektroforez (DEP), lenssiz görüntüleme, çip-üstü-laboratuvar, kanser hücresi ve akıllı telefonlar.

To My Family

ACKNOWLEDGEMENTS

I would like to thank Prof. Dr. Tayfun Akın and Prof. Dr. Haluk Külah. I would also like to express my deep thanks to my thesis advisor, Prof. Dr. Haluk Külah for believing and supporting me during my graduate studies. I am also thankful to Prof. Dr. Ufuk Gündüz to collaborate us with providing biological laboratory and cancer cell lines.

I would like to thank Aziz Koyuncuoğlu and Taylan Töral for developing my fabrication procedure and helping me for fabrication of my devices. Many thanks to Kaan Sel, Metin Dündar Özkan, Bedirhan İlik, Salar Chamanian, Hasan Uluşan, Furkan Gökçe, Eren Aydın and Mustafa Kangül to simplify my life and for being good friends.

I would also like to thank all METU-MEMS Center staff for their kind helps in cleanroom. Many thanks particularly to Orhan Akar for sharing his deep knowledge on microfabrication and for his helps in the cleanroom.

I am especially thankful to all my lab friends in the BioMEMS and PowerMEMS groups for being good friends and a peaceful work environment.

I would like to express my deepest thankfulness to family, for their endless, priceless and ineffable patience and support. Moreover, I am thankful to them to give me the freedom for achieving all my dreams.

TABLE OF CONTENTS

LIST OF TABLES

LIST OF FIGURES

CHAPTER 1

INTRODUCTION

According to WHO, cancer is one of the leading causes of mortality in worldwide [1]. In every year, approximately 14 million new cancer cases occur and over next two decades, these new cases are expected to rise about %70. In cancer diagnosis and treatment, one of important steps is early cancer detection. For example, survival rate in breast cancer is 90% when it is detected in stage 1 whereas mortality rate is more than 50% in stage 4. In cancer diagnosis, the most common method is surgical biopsy [2]. Blood examination is an alternative method in cancer diagnosis due to the advantages of less invasive and easier to implement. Additionally, rare cancer cells (e.g. circulating tumor cells) which are correlated with cancer metastasis can be detected from patients' blood. Therefore, analysis of blood is crucial in early cancer detection. Blood analysis (counting blood and cancer cells) is conventionally performed with bulky and expensive tools such as flow cytometry or microscopy. However, only 35% of low-income countries have publicly available pathology services offer these diagnosis tools. Thus, a cost effective, publicly available cell counting and diagnosis tool is needed in cancer detection.

Lab-on-a chip (LOC) systems become popular in recent years by offering several advantages including portability, simplicity, cost effectiveness and high throughput [3]. More specifically, microfluidics which is commonly integrated with LOC systems can be characterized as the study of manipulation of fluids at

micro-scale systems. Especially, advancements in Micro Electromechanical Systems (MEMS) fabrication technologies results in designing sophisticated microfluidic devices. These devices are employed in broad range of application areas including molecular analysis, molecular or cell biology and microelectronics [4]. In the field of cell biology; microfluidics based cell manipulation is an emerging technology by offering a number of capabilities such as making both easy to use and low cost systems, the ability to use small amount of samples or reagents, carrying out high resolution and sensitive analysis, and decreasing analysis time by offering high throughput systems.

With the recent advancements in microfluidics, considerable effort is made in developing cancer cell detection and quantification devices. These devices are promising for cancer diagnosis especially in resource limited regions due to their advantages such as simple implementation, easy to use and cost effectiveness. Cell manipulation techniques can be grouped into five main groups: magnetic, mechanical, acoustic, optical and electrical.

1.1 Cell Manipulation Techniques

1.1.1 Magnetic Manipulation

Magnetic manipulation techniques are based either both generating magnetic field on to particles or keeping particles in a magnetic field. Then, manipulation is achieved according to magnetic susceptibilities of the particles i.e. diamagnetic, paramagnetic or nonmagnetic. In this method, particles under test are generally tagged with magnetic nanoparticles since most of the biological particles have low magnetic permeability. Therefore, target particles are selectively manipulated with magnetostatic forces. Also, particles can be manipulated with this method using their intrinsic magnetic properties without tagging. Different techniques used in magnetic manipulation are illustrated in Figure 1.1.

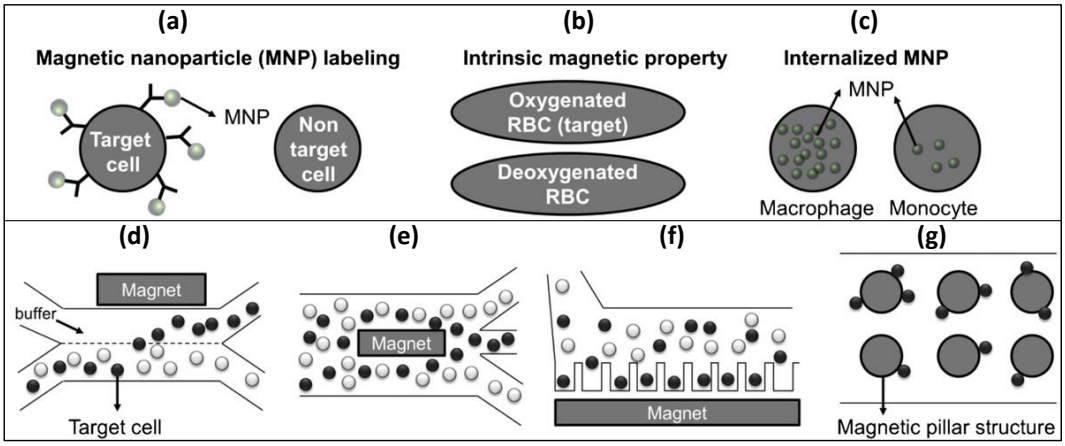

Figure 1.1 (a)-(c) Different magnetic labeling and (d)-(g) manipulation techniques with different microchannel designs [5].

In [6], microfluidic based magnetophoresis device is proposed in order to sort two different types of cells (Figure 1.2). Target cells are magnetically labeled with different magnetic tags. Using ferromagnetic strips (MFS1 and MFS2), high density magnetic fields are generated. Then, cells are separated by directed towards to different outlets. In another application of magnetic manipulation, circulating tumor cells (CTCs) are isolated from whole blood [7]. The system consists of a microfluidic channel which has single inlet and outlet. Using permanent magnet and dead-end side chambers underneath the microfluidic channel, magnetically tagged cells are isolated under continuous flow.

Employing magnetic force, it is also possible to manipulate the cells without tagging due to their intrinsic magnetic properties. Erythrocytes are separated from leukocytes under magnetic field utilizing their distinct magnetic properties [8]. Moreover, when a high density magnetic field is applied, migration velocity of the erythrocytes is correlated to the hemoglobin concentration [9]. Therefore, it is also possible to separate erythrocytes that have different hemoglobin structures by using magnetic manipulation.

Magnetic manipulation technique has advantages such as biocompatibility and it does not cause any damage to the cells. However, most of the cells have weak magnetic properties so that magnetic tagging is needed before applying magnetic field. Magnetic tagging causes loss of label free operation and moreover, tagging is a sensitive process and should be utilized by a trained person.

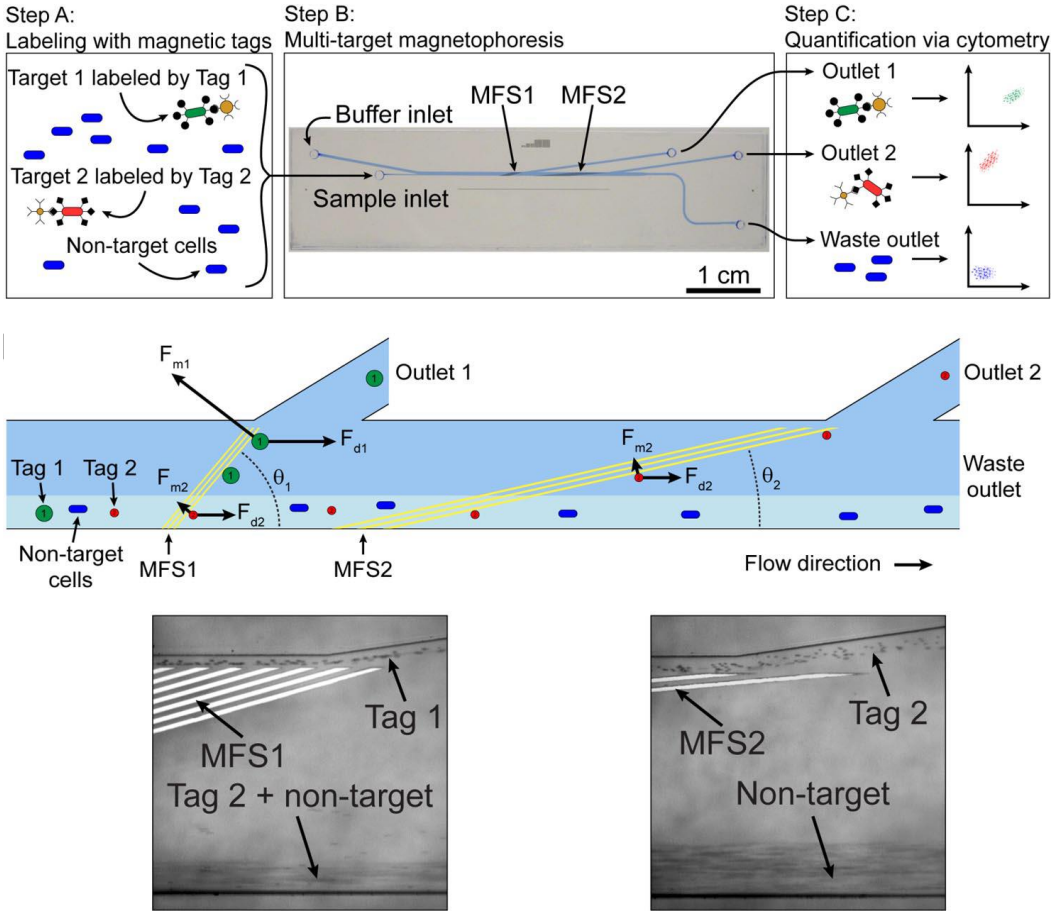

Figure 1.2 Illustration of magnetophoresis based cell sorting device [6].

1.1.2 Mechanical Manipulation

Using cells' distinct mechanical properties such as deformability, stiffness and elasticity or based on their size and shape, cells can be manipulated inside microfluidic channels. For that purpose, there are different types of microfabricated structures such as microfilters [10], [11], microwells [12], [13] or

microgrippers [14] employed in mechanical manipulation techniques. Combining symmetric and asymmetric channel geometries, microfluidics based mechanical manipulation of particles is achieved [15]. In this study, polystyrene beads with different sizes and red blood cells (RBCs) are focused and sorted with inertial forces. In [16], cancers cells are separated from whole blood by using microvortices. The separation is achieved based on the differences between orbits of particles having different sizes inside the microvortices. Therefore, the device mimics the functionality of a centrifuge device by using dynamic properties of the fluids (Figure 1.3).

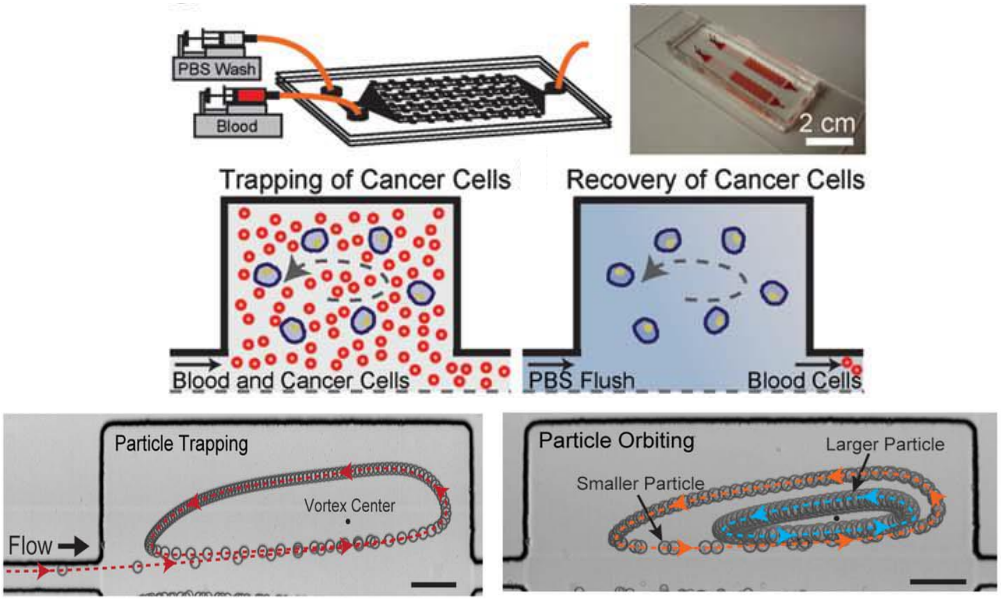

Figure 1.3 Mechanical manipulation based cancer cell separation device [16].

Mechanical techniques provide label free, harmless and simple manipulation of the particles. However, mechanical manipulation is strongly dependent to precise flow controls and also it is not effective in separating the particles have similar sizes, shapes or densities limiting the sensitivity and selectivity.

1.1.3 Optical Manipulation

Optical manipulation technique based on manipulating particles using focused laser beam. In this technique, optical scattering and gradient forces are utilized in order to trap or push the particles. Optical manipulation can be employed in various applications as shown in Figure 1.4.

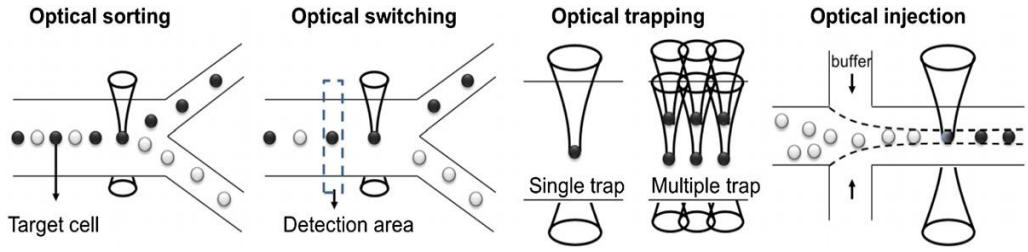

Figure 1.4 Different applications of optical manipulation in cell biology [5].

MacDonald et al [17] introduces an optical manipulation method used in sorting of microscopic particles. The method illustrated in Figure 1.5, is based on optical fractionation, can both be used in size and refractive index based sorting. The efficiency of the proposed method can be achieved to 100%. In another study, size based separation of polystyrene beads is presented [18].

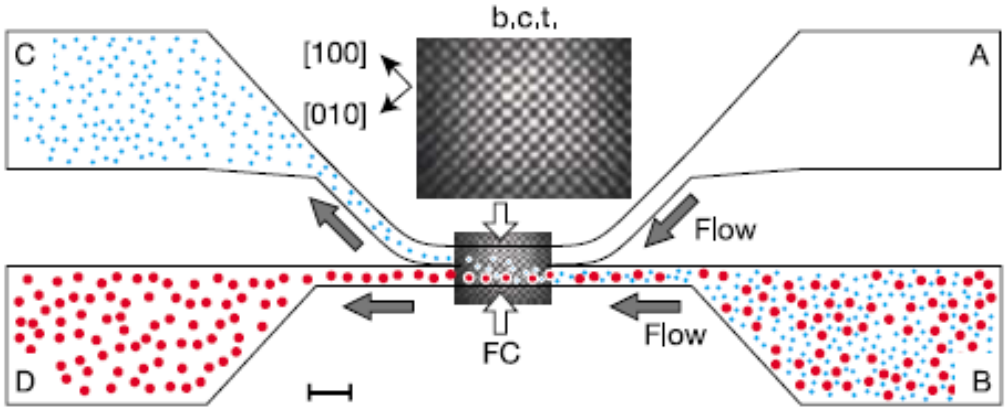

Figure 1.5 Separation of the particles with optical fractionation method [17].

In this method, a laser beam perpendicular to a PDMS microchannel is used. Scattering force of the laser causes vertical displacements of the particles while they are moving through the beam (Figure 1.6). The amount of displacement is proportional with laser beam parameters and size of the particles.

An optical tweezer is integrated with a microfluidic channel for single cell analysis in [19]. In this system, yeast cells are directed towards to the measurement region with optical manipulation and behaviors of the cells are analyzed under perturbations.

Optical manipulation is one of the promising techniques in cell biology by allowing contactless and contamination free manipulation. Nevertheless, the systems used in optical manipulation include not easy to use and expensive equipment that limits portability and LOC operation.

1.1.4 Acoustic Manipulation

Sound waves are widely used in particle manipulation due to the advantages of its contact and label free structure and acoustic manipulation methods do not alter cell characteristics. By using acoustic waves, various types of manipulations including enrichment, alignment or separation can be achieved [20], [21], [22]. Surface acoustic wave based method is presented to move cells and particles in [23]. In this study, 3D acoustic waves are generated to construct 3D traps for the particles. Positions of the traps can be determined by changing the phase or power of the acoustic wave. Moreover, acoustic tweezers can further be used to generate 3D cell structures by precisely transport cells in 3D domain. In a recent study, acoustic field is used to rotate cells and organisms in a microfluidic channel to detect mutations morphologically (Figure 1.7) [24].

In this method, microbubbles trapped into cavities underneath the microfluidic channel. Then, acoustic waves are utilized to manipulate trapped microbubbles

resulting in microvortices. Cells and organisms can be precisely rotated to detect anomalies by using microvortices.

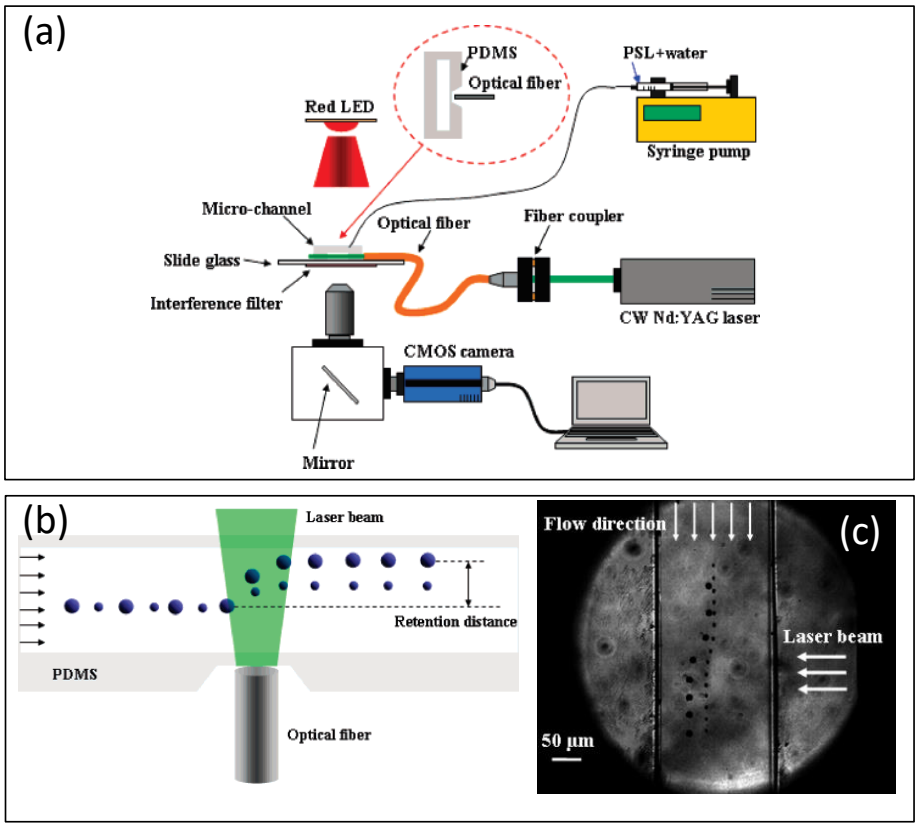

Figure 1.6 Manipulation of the particles with optical excitation (a) system setup (b) deflection of particles with laser excitation (c) microscopy image of manipulated particles [18].

Acoustic manipulation technique does not cause any damage to biological particles. Additionally, it is cost effective, allows manipulation of particles under continuous flow and has simple implementation so that, acoustic manipulation can be effectively used in high throughput LOC applications.

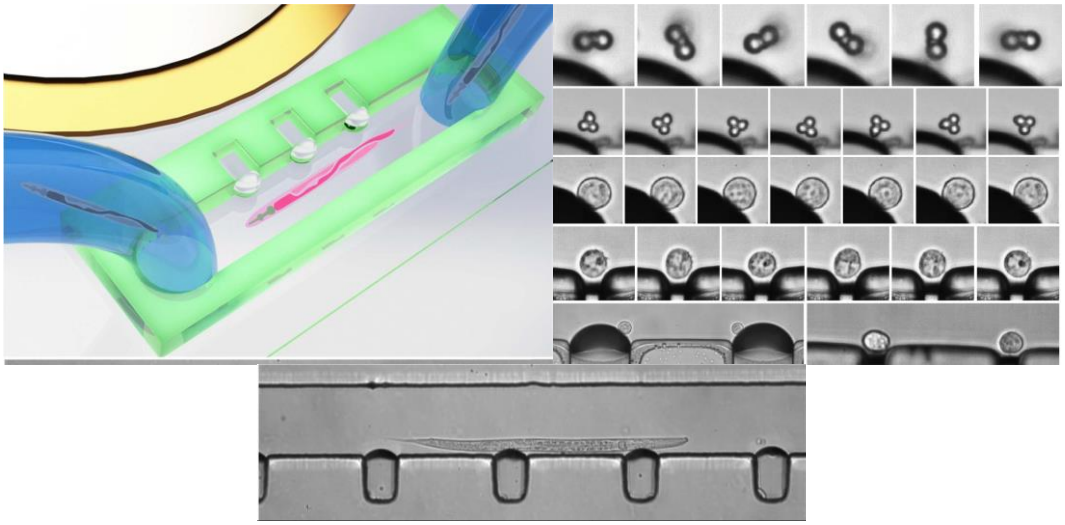

Figure 1.7 Illustration of microfluidic device rotates organisms with acoustic manipulation technique [24].

1.1.5 Electrical Manipulation

Electrical properties of the biological particles such as cytoplasmic conductivity are unique for different particles. By exploiting these properties, electrical manipulation techniques are being widely used in particle manipulation. The main advantages of electrical manipulation can be listed as (i) it allows label free implementation and (ii) electrical properties of the particles are more distinctive than optical or mechanical properties. Methods in electrical manipulation can be grouped as electrophoresis (EP) (based on applying DC electrical field) and dielectrophoresis (DEP) (utilized by applying AC electrical field) which are described in detail below.

1.1.5.1 Electrophoresis

EP method is based on manipulating charged particles under steady electrical field. In this method, biological particles such as DNA, hemoglobin can be migrated according to their charges. The charges of the particles directly affect electrophoretic force magnitude and direction. Additionally, migration velocity

directly related to size and mass of the particles. Therefore, by using EP particles with different sizes, masses or charges can be separated.

Traditionally, EP method is utilized in several clinical applications at macroscale such as sickle hemoglobin detection, differentiating bacterial cell types. Recently, EP systems are miniaturized with the integration with microfluidics. Therefore, samples can be analyzed in shorter times with multiple processing by consuming very small volumes of reagents (~10µL). In [25], a microfluidic EP device is introduced for manipulating yeast cells to gene analysis. In this system, microfluidic channel with analytical chambers used to measure gene activity with an electrochemical method (Figure 1.8). The cells flowing through the channel are trapped into dead end traps by using electrophoretic forces. After electrochemical measurements are made, controlled releasing of the cells is performed by applying opposite electrophoretic force with negative voltage. Another LOC EP system is presented in [26]. In this study, *casein* and *whey* proteins in milk are separated with a LOC system by integrating separation channels with molecular mass markers and standardizing migration times.

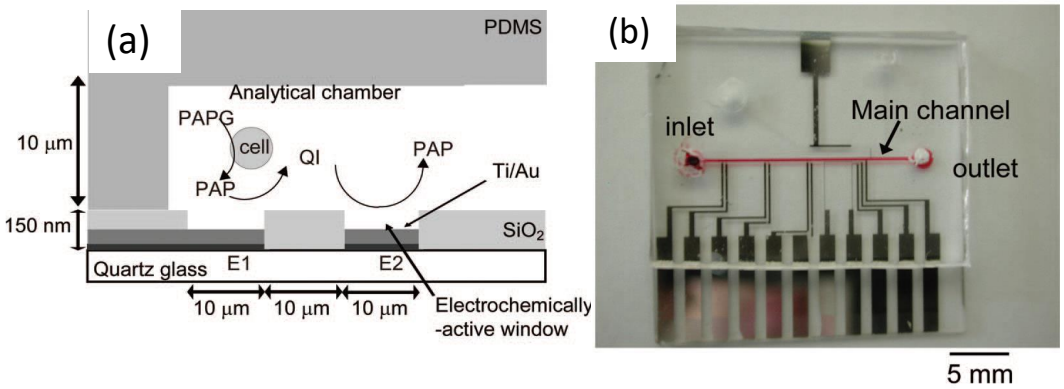

Figure 1.8 Electrophoresis based gene analysis device (a) design of the device (b) fabricated device [25].

1.1.5.2 Dielectrophoresis

DEP is a technique, based on manipulation of the dielectric particles under non-uniform electric field due to spatial gradient of the electric field [27]. In microfluidic based cell manipulation applications, DEP has been intensively employed by allowing separation and trapping of the cells [28]–[31].

DEP method is based on cells' distinguishing and unique electrical properties such as cytoplasmic conductivity or membrane capacitance. The advantages of DEP over other methods in cell manipulation can be specified as: (i) simplicity of the implementation, (ii) not requiring any labeling or surface modifications e.g. antibody immobilization, (iii) ability to obtain both positive and negative DEP forces by parameters of the instrumentation.

DEP methods can be mainly grouped as DC-DEP and AC-DEP which are operated with DC and AC currents respectively. In DC-DEP, external electrodes are used and non-uniform electric field is generated with special structures inside the channel such as electrically insulated obstacles (iDEP). In [32], mixture of particles are separated with iDEP method. In this device, non-uniformity in electric field is utilized by using cylindrical posts located inside the microfluidic channel as presented in Figure 1.9. Then, 1 and 4 μm polystyrene beads are separated by applying 1000 V voltage and directed towards different outlets (Figure 1.10). iDEP based devices have simple fabrication scheme however, high voltages should be used in DC-DEP results in Joule heating inside the channel. This phenomenon can lead bubble formation and also the temperature increase may be fatal for the cells under analysis.

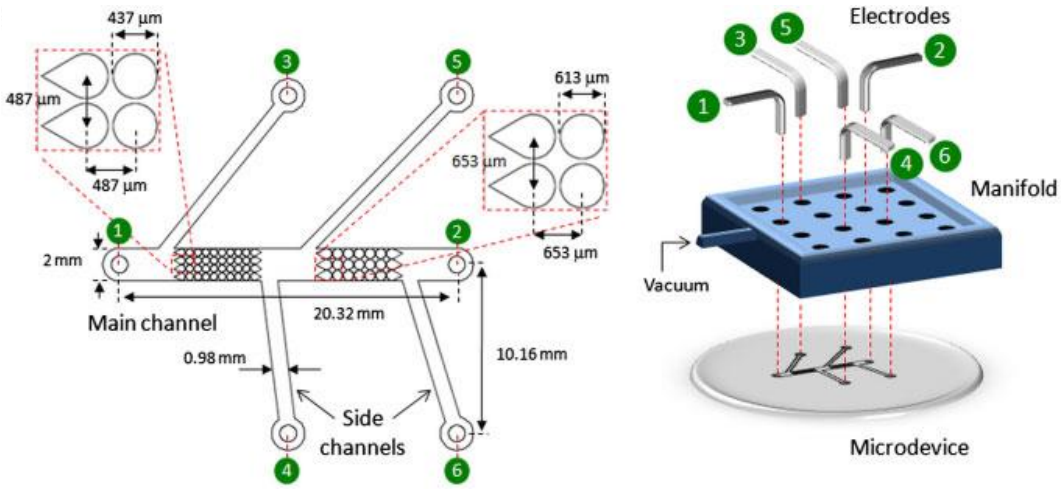

Figure 1.9 iDEP based particle separation device [32].

Although AC-DEP devices require complex fabrication steps, they are operated with lower voltages that overcome Joule heating. Additionally, using of low operating voltages makes AC-DEP compatible with portable systems. AC-DEP based cell manipulation has several applications such as separation by size or properties, concentration, focusing, sorting, trapping, filtering and patterning. In another study [33], 3D electrode based AC-DEP is employed for particle separation. In this system, one short and long electrode placed at the sidewalls of the microfluidic channel (Figure 1.11). Yeast and white blood cells are separated according to their sizes. However, this system is ineffective in separation of the particles have similar sizes.

DEP is a powerful tool for label free quantification of the cells by allowing different types of manipulation including separation, sorting or trapping. Furthermore, DEP based microfluidic devices are widely being used in LOC cancer quantification systems in a high throughput manner.

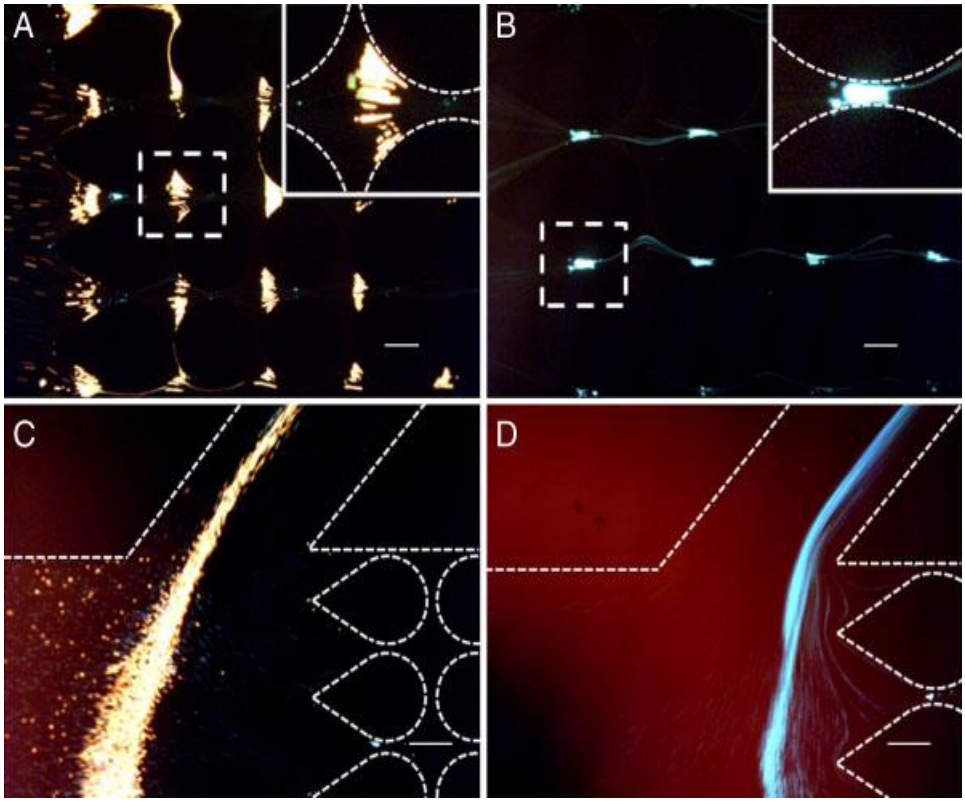

Figure 1.10 Experimental results of iDEP based particle separation device [32].

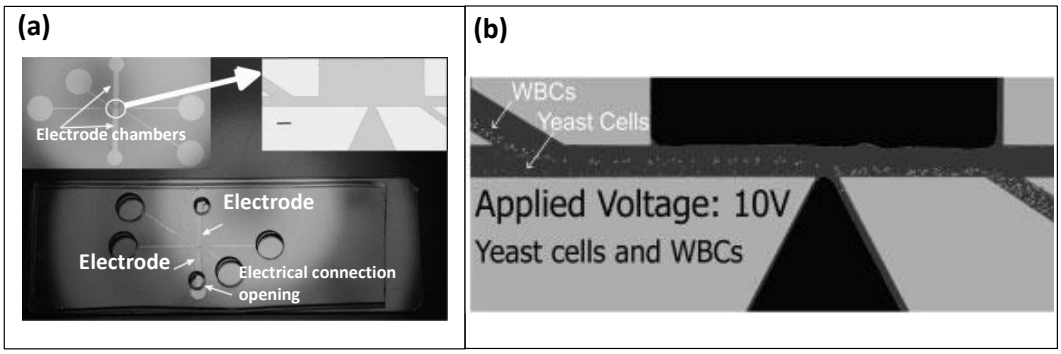

Figure 1.11 Cell separation device with 3D electrodes (a) device schematic (b) experimental result [33].

1.2 Lens-free Imaging Techniques

Developments in semiconductor technology allow microfabrication of lab-on-a-chip systems that have both sensing blocks and other circuitry including amplifiers, digital filters or read out circuits. Recently, lens-free imaging (using CMOS or CCD sensor) becomes significant technology in biological applications enabling cost effective, easy-to-use, and portable detection of the cells. Photonic cell detection is based on capturing photons fall on to surface of the image sensor. According to number of photons captured (i.e. how much light is absorbed), shadow images of the cells are generated. With this structure cells can be imaged without employing fluorescent tagging and microscope imaging achieved with bulky and expensive equipment. By exploiting this advantage, lens-free imaging can be easily used for point of care diagnosis at especially resource limited regions. Lens-free imaging techniques can be investigated into three parts based on properties of the illumination source (coherent, incoherent or partially coherent).

In coherent source based systems, a coherent illumination source (laser) and a small aperture (~1 μm) are used as shown in the Figure 1.12a. The distance between object and light source (z_1 ~4-7 mm) is generally smaller than the object to image sensor distance (z_2 ~40-70 mm). Therefore, fringe magnification ($(z_1+z_2)/z_1$) is nearly equal to 10 in these systems. Using this structure, it is possible to reconstruct lens-free images of biological particles with a resolution better than 1μm [34], [35].

Lens-free imaging systems can also be constructed by using incoherent illumination sources e.g. LEDs. These systems are simple to implement and the object is located just above the image sensor ($z_2 << z_1$) (Figure 1.13). Therefore, field of view (FOV) is relatively large i.e. 10-20 cm^2. In this method, the shadow of the object is recorded with the image sensor that yields low spatial resolution.

However, by utilizing specific shadows or patterns of the cells it is possible to detect different types of cells in a heterogeneous solution (Figure 1.13) [36]–[38].

Partially coherent imaging systems include an incoherent light source and a pinhole that has a radius of 50-500 μm (Figure 1.12b). Different from incoherent light based systems, using a pinhole gives the advantage of adjusting both temporal and spatial coherence properties. Then, lens-free holograms of the objects can be reconstructed with image processing. The object is located closer to the image sensor than pinhole ($z_2<z_1$). In this method, RBCs, bacteria or other biological specimen can be imaged with a resolution better than 1 μm.

Lens-free imaging techniques offer several advantages including simple implementation, cost effectiveness and portability. Moreover, due to wide FOV, high throughput systems can be designed with lens-free imaging whereas spatial resolution is significantly high (<1 μm) using image reconstruction techniques (Figure 1.13). Therefore, lens-free imaging becomes a powerful tool for cell quantification purposes especially in portable, LOC systems.

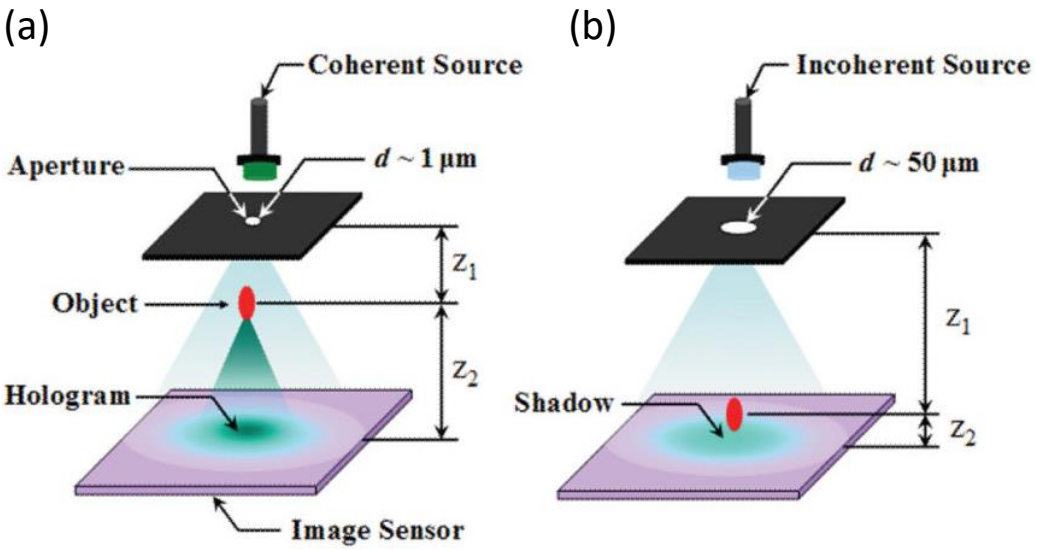

Figure 1.12 Illustration of the (a) coherent source and (b) partially coherent source based lens-free imaging [39].

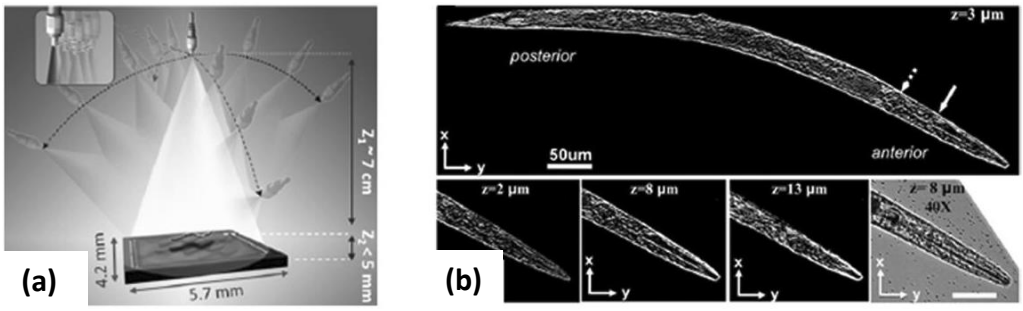

Figure 1.13 Lenfree optical tomography (a) illumination of the sample with various angles (b) lens-free imaging of C.elegans bacteria [39].

1.3 Research Objectives and Thesis Organization

The main objective of the thesis is to design, fabricate and implement a LOC device integrating a CMOS image sensor and a microfluidic DEP device for label and lens-free quantification of the cancer cells. To achieve this objective, following research studies are carried out:

- Dielectric modeling of the cancer and blood cells using MATLAB software and electrical properties of the cells.
- To design of the microfluidic DEP device for trapping of the cancer cells whereas trapping area should be properly imaged with a CMOS image sensor for quantification purposes.
- Electrical and hydrodynamic simulation of the designed DEP devices with COMSOL software tool utilizing finite element model.
- Fabrication of the DEP devices according to prepared fabrication process after verification of the simulation results.
- Development of a CMOS imaging system with sufficient resolution for cell imaging and mechanical integration of the sensor with microfluidic DEP device.
- To design and implement a portable signal generator used to operate DEP device.

- To develop an image processing application for automated quantification of the trapped cells.
- Testing of the designed system with cancer cells and obtaining both DEP trapping efficiency results and cell counting efficiency.

Thesis is organized as follows:

In Chapter 2, dielectric modeling of the cells is presented by investigating analogy between electrical circuit elements and cells. Then, DEP theory is explained in detail by giving frequency dependent formulation of the DEP force. Additionally, CMOS imaging technique is introduced with analysis parameters.

Chapter 3 presents the design of the two different LOC systems for automated count of cancer cells. Design steps of the both systems including COMSOL simulations of the DEP devices, designing parameters of the signal generator circuitry and functionality of the Android application are represented in this chapter.

Chapter 4 includes fabrication steps of the DEP device and 3D printed holder for mechanical integration of the whole system.

In Chapter 5, test setup and experimental procedure are explained. Additionally, performance of the LOC system is discussed in terms of cell trapping and counting efficiency. Furthermore, different application of the proposed system is also introduced.

Finally, in Chapter 6 concluding remarks are given by summarizing the accomplishments and future improvements are presented.

CHAPTER 2

THEORY & MODELING

2.1 Dielectrophoresis

Dielectrophoresis (DEP) (comes from the Greek word “phoresis” which means motion), is a technique based on applying inhomogeneous electric field to manipulate dielectric particles. DEP method is first introduced by Pohl et. al. in 1951 at macro scales by applying 10kV voltage to separate carbon black fillers from chloride [40]. With the development of microfabrication and microfluidics technology, DEP devices are being miniaturized so that they are used to manipulate biological agents inside microfluidic structures.

DEP force is generated from interaction of particle’s dipole and non-uniform electrical field. The particle’s dipole is resulted from either intrinsic properties of the particle (orientations of atomic structures) or reorientation of the surface charges of the particle due to presence of the electrical field. The DEP force can be calculated by using two different methods (i) point dipole method (ii) Maxwell-stress tension (MST) method.

2.1.1 Point Dipole Method

In this method, the particle is modeled as a point charge that generates the same electrical potential distribution. In an electric field, the force exerted on the dipole can be derived as below:

$$\boldsymbol{F_d} = (\boldsymbol{P}.\boldsymbol{\nabla})\boldsymbol{E} \tag{2.1}$$

where $\boldsymbol{E}$ is the electrical field and $\boldsymbol{P}$ is the dipole moment. The other higher order multipolar moments are ignored in this formula which is reasonable approximation for most of the cases in microfluidic DEP applications. However, at extreme cases i.e. at very strong electric field gradients or zero gradients these moments should be taken into account by modifying the formula accordingly.

2.1.2 Maxwell-Stress Tension Method

In another method, called as Maxwell-stress tension, firstly, the surface stress of the particle induced by the potential distribution is obtained. Then, the force is calculated by integrating the stress over the surface of the particle. Therefore, the DEP force can be written as:

$$\boldsymbol{F_{DEP}} = \oint_{\boldsymbol{S}} (\boldsymbol{T}.\boldsymbol{n})\boldsymbol{dS} \tag{2.2}$$

where $\boldsymbol{S}$ is the particle surface and **n** is the surface normal and the stress tensor $\boldsymbol{T}$ can be expressed as:

$$\boldsymbol{T} = \varepsilon\left(\boldsymbol{E}\otimes\boldsymbol{E} - \frac{\mathbf{1}}{\mathbf{2}}\boldsymbol{E^2U}\right) + \mu\left(\boldsymbol{H}\otimes\boldsymbol{H} - \frac{\mathbf{1}}{\mathbf{2}}\boldsymbol{H^2U}\right) \tag{2.3}$$

In this expression, $\otimes$ represents dyadic product, $\boldsymbol{U}$ is unit tensor, $\boldsymbol{E}$ is electrical field and $\boldsymbol{H}$ is magnetic field. As a further simplification, for the frequencies less than 100 MHz, magnetic field component of the above expression can be neglected. Therefore, in calculation of the DEP force, both methods give similar results.

DEP force mainly depends on magnitude and polarity of the charges induced on a particle under non uniform electric field. Assuming that cells have sphere shapes, the dipole moment $\boldsymbol{P}$ in equation Eqn. 2.1 can be written as:

$$\boldsymbol{P} = 4\pi r^3 \varepsilon_0 \varepsilon_m f_{CM} \boldsymbol{E} \tag{2.4}$$

where is r is the cell radius, f_{CM} is the complex Clausius-Mossotti factor, ε_0 and ε_m dielectric constants for the vacuum and surrounding medium respectively. By putting Eqn. 2.4 into Eqn. 2.1 we can obtain equation for the DEP force as presented below:

$$\boldsymbol{F_{DEP}} = 2\pi\varepsilon_m r^3 Re(f_{CM})(\boldsymbol{\nabla E_{rms}^2}) \tag{2.5}$$

where ε_m absolute permittivity the surrounding medium, Re(f_{CM}) is the real part of the Clausius-Mossotti factor and E_{rms} is the root mean square of the applied electric field. Furthermore, Clausius-Mossotti factor can be expressed as:

$$f_{CM} = \left(\frac{\varepsilon_p^* - \varepsilon_m^*}{\varepsilon_p^* + 2\varepsilon_m^*}\right) \tag{2.6}$$

where ε_p^* and ε_m^* are complex permittivity of the particle and medium respectively. Complex dielectric constant ε^* is also defined as:

$$\varepsilon^* = \varepsilon - \frac{j\sigma}{\omega} \tag{2.7}$$

where σ is the conductivity and ω is the angular frequency of the electric field. A dipole moment (that can move the particle) can be constructed by changing the frequency. Re(f_{CM}) varies between -0.5 and +1 depending on the electrical properties of the particle and medium. Particles that have higher permeability than the medium ($f_{CM} > 0$) move towards higher electric field (pDEP). Oppositely, particles lower permeability than the medium ($f_{CM} < 0$) repelled from weaker electric field regions (nDEP) as illustrated in Figure 2.1.

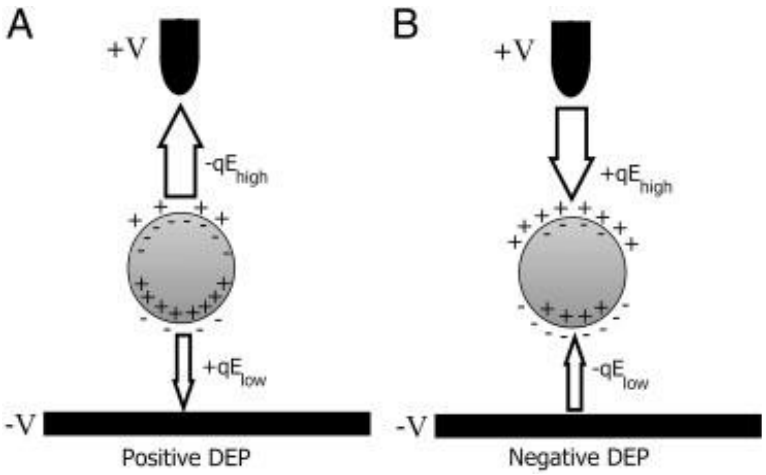

Figure 2.1 Positive and negative DEP effects on a polarizable particle [27] .

Hence, relative conductivity of the test medium to the particle under test, directly affects the sign of the DEP force. Re(f_{CM}) is also dependent on the applied frequency of the electrical field. Therefore, it is possible to exert both positive and negative DEP force on the particle by adjusting the operation frequency. General properties of the DEP force can be summarized as:

- DEP force is non-linear and will be zero under uniform electrical field.
- DEP force is dependent of particle radius i.e. particles that have larger volumes face with higher DEP forces (proportional with r^3) so that size based separation is possible with DEP method.
- DEP force is also dependent of both applied frequency and dielectric constants of the medium and particle under test. Therefore, particles can be also manipulated due to their unique electrical properties.
- Polarity of the electrical field does not affect the DEP force.
- The type of the DEP force (repulsive or attractive) is determined from the relationship between particle and medium permeability. Particles that have higher permeability than the medium ($f_{CM} > 0$) tend to be attracted by the

electrodes (pDEP) whereas particles lower permeability than the medium ($f_{CM} < 0$) is pushed away from weaker electric field regions (nDEP).

2.2 Electrode Configurations Used for DEP Devices

Dielectrophoresis is based on generating nonuniform electric field inside the microchannels to manipulate particles. DEP method has several applications in cell manipulation including trapping, separation or sorting. According to application type and desired electrical field, selection of electrode configuration is important in DEP systems. Common electrode configurations employed in DEP can be specified as: interdigitated, castellated, oblique, quadrupole, spiral, dot type and 3D electrodes. In interdigitated configuration, electrodes are micropatterned bottom of the microchannel. The electrodes are energized by applying two sinusoidal voltages that are out of phase. At the edges of the electrodes, the gradient of the electric field is maximum whereas other parts of the electrodes have weaker electric field. Therefore, particles are mostly attracted with the edges.

Castellated electrode configuration consists of castellated array of electrodes geometrically similar to interdigitated structure. Electrodes are activated by utilizing sinusoidal signals at opposite phases. Stronger electrical field gradients occur at the edges of the electrodes. This configuration is useful for high flow rate applications whereas with castellated structure single cell cannot be analyzed.

In oblique configuration, electrodes are placed at obliquely along the microchannel. In this configuration, generally, two oblique electrode arrays (symmetrical around the midline of the channel) are excited with signals have 180° phase difference. Electric field is strong at the tips of the electrodes located at the middle of the channel. This configuration is useful for manipulating particles under continuous flow however; it is not practical in single cell analysis.

Another configuration is called as quadrupole includes four electrodes placed at the four symmetrical sides with an offset of 90°. Sequential electrodes are excited with signals have 180° phase difference. Stronger electric field occurs at the sharp edges of the electrodes whereas at the center electric field is weak. This configuration is feasible for single cell analysis instead of flow analysis.

Spiral shaped electrodes are used to manipulate particles according to their movement inside of the spiral channels. The velocity of movement is both depend on size and type of the particle which determines the type of the DEP force.

In dot type configuration, dot shaped electrode arrays are microfabricated. The higher electric field is observed at the edges of the dots. This configuration is useful for trapping and isolation applications.

3D electrodes offer uniform DEP force along the height of the microchannel. 3D electrodes can be achieved with extruded electrodes from planar electrodes or side wall patterned electrodes. In extruded electrodes, any planar type electrode can be extruded along the direction normal to the substrate surface. Thereore, uniform DEP force is achieved. The electrodes can be excited by applying signals have 180° phase difference.

3D electrodes can be also patterned at the sidewalls of the microfluidic channel. With this configuration large population of the cells can be manipulated under uniform electric field. However, electric field is weak at the midline of the microfluidic channel so, to work at wider channels or at high flow rates extra mechanical structures such as hydrodynamic focusing is needed.

2.3 Cell Dielectric Modeling

DEP force mainly depends on real part of Claussius–Mossotti factor. This value is determined both electrical properties of the medium and cell. Electrical properties of the medium can be changed and adjusted accordingly. However, electrical

properties of the cells should be measured and electrical models for the cells should be developed to simulate device designs.

Cell membrane consists of both phospholipid layer that includes structural proteins inside of it. The membrane can be electrically modeled with a capacitor and a resistor since, lipid layers between phosphate groups are dielectric whereas phosphate layer is conductive. Moreover, cell membrane impedance can be determined by calculating both resistor and capacitor values as follows:

$$R = \frac{L}{\sigma . A} \tag{2.8}$$

$$C = \varepsilon \frac{A}{d} \tag{2.9}$$

where R is resistance, C is capacitance, σ and ε is conductivity and permittivity, respectively. L is the perimeter of the cell can be calculated as $2\pi r$ where r is the radius of the cell and A is the crossectional area equals to πr^2. Note that L/A is equals to $2/r$. Electrical model for the cell is illustrated in the Figure 2.2.

Cell cytoplasm mainly consists of cytosol and organelles. Cytosol includes water, some proteins and ions. Due to the ions, conductivity of the cytoplasm is higher than the membrane. Moreover, cytoplasm can be modeled as impedance.

In microfluidic applications, electrical properties of the cells should be represented as complex permittivity formula. Cells can be modeled as spheres or ellipsoidal. Most of the cells have nonhomogeneous structure, so that cells are modeled according to number of shells around cells. In single shell modeling Claussius–Mossotti factor can be expressed as:

$$f_{CM} = \frac{\varepsilon^*_{cell} - \varepsilon^*_{med}}{\varepsilon^*_{cell} + 2.\varepsilon^*_{med}} \tag{2.10}$$

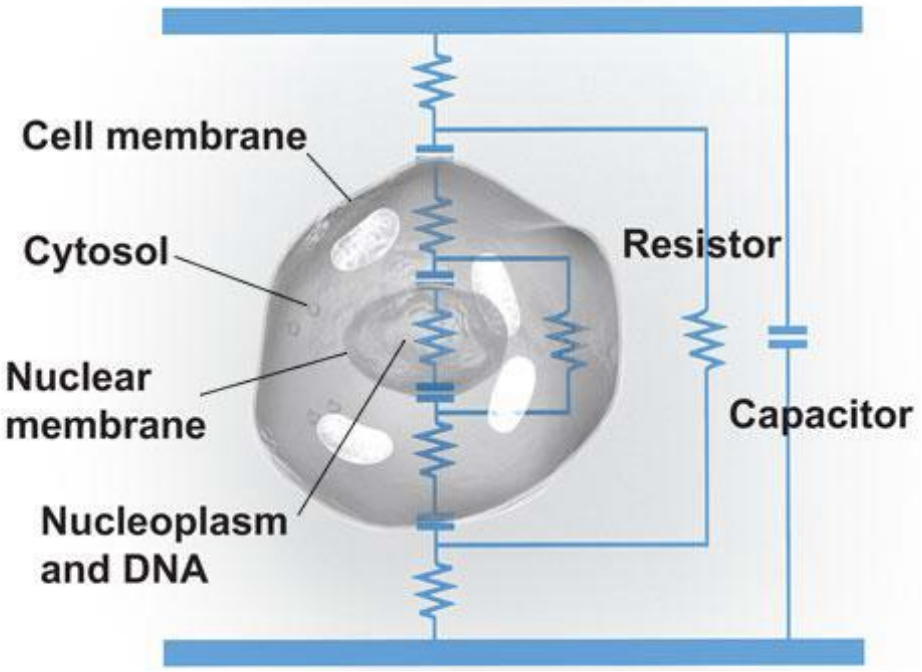

Figure 2.2 Electrical model for the cells [49].

In this expression, ε^*_{cell} and ε^*_{med} are the complex permittivity of the cell and the medium. The cell is assumed as smooth sphere in this expression. Real and imaginary parts of Clausis-Mossotti factor represents dielectrophoretic force and electrorotational torque, respectively. ε^*_{cell} can further be expressed as:

$$\varepsilon^*_{cell} = \varepsilon^*_{mem,eff} \cdot \frac{\left(\frac{r}{r-d}\right)^3 + 2.\frac{\varepsilon^*_{int} - \varepsilon^*_{mem,eff}}{\varepsilon^*_{int} + 2.\varepsilon^*_{mem,eff}}}{\left(\frac{r}{r-d}\right)^3 - \frac{\varepsilon^*_{int} - \varepsilon^*_{mem,eff}}{\varepsilon^*_{int} + 2.\varepsilon^*_{mem,eff}}} \tag{2.11}$$

In this formula, $\varepsilon^*_{mem,eff}$ and ε^*_{int} equal to complex permittivity of cell membrane and cell interior whereas [41] r and d is the cell radius and membrane thickness, respectively.

2.3.1 Dielectric Modeling of MCF7 (Human Breast Adenocarcinoma) Cell Lines

Breast cancer cells have heterogeneous and complex structure and to model the cancer cells, generally cell lines are used [42]. One of the common cell line used in breast cancer is MCF7 cell lines which are established at Michigan Cancer Foundation in 1973. The advantage of MCF7 cell lines their excellent hormone sensitivity due to estrogen receptor so, the MCF7 cell lines are commonly used in hormone response based researches.

In literature, there is limited information about electrical properties of the MCF7 cells. The important electrical parameters are given in the Table 2.1.

Table 2.1 The dielectric parameters of MCF7 cells

Reference	r_{cell} **(μm)**	C_{mem} **(mF/m^2)**	σ_{cyto}**(S/m)**	ε_{cyto}
[43]	12.7	N/A	N/A	N/A
[44]	9.1	22.20	N/A	N/A
[45]	N/A	12.4	0.23	N/A
Average	10.9	17.3	0.23	N/A

Cytoplasmic permittivity of the MCF7 cells is not defined in the literature. Therefore, the value is taken as 50 which is the permittivity value of MDA-MB231 cell line similar to MCF7.

ε_{mem} of $MCF7s_{average}$ value can be calculated as 16.69 by using the formula 2.11 and the parameters listed in the Table. Similar to K562 cells, thickness of the cell membrane is taken as 10 nm whereas membrane conductivity is assumed $1.8x10^{-6}$ S/m. Real part of Clausis-Mossotti factor is plotted versus changing frequency values and for two different medium conductivity values in MATLAB. Therefore, negative and positive DEP region can be examined as shown in the Figure 2.3.

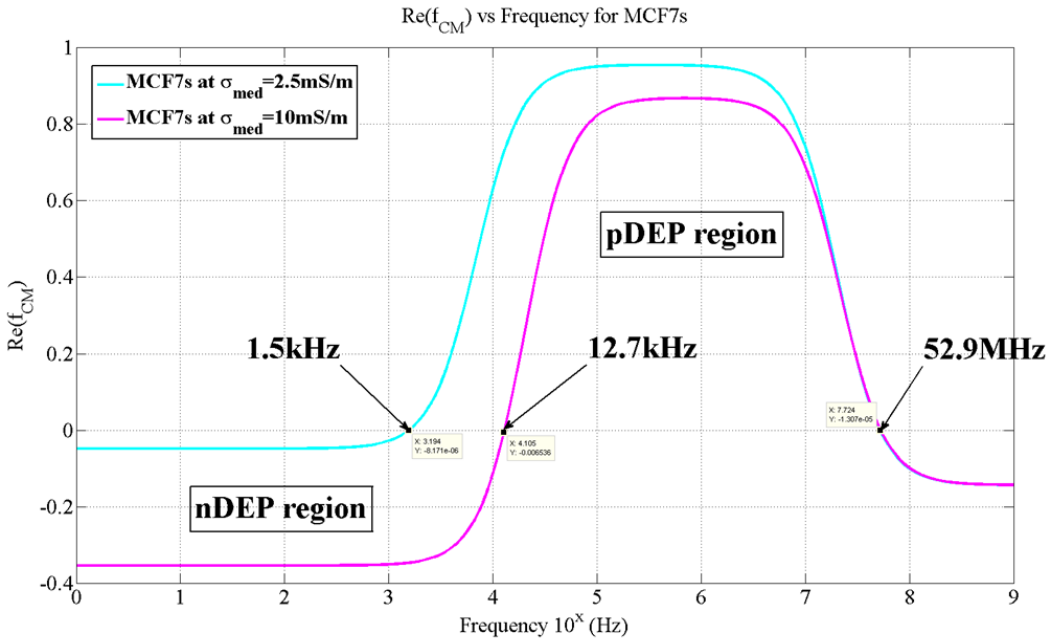

Figure 2.3 Re(f_{CM}) vs frequency graph for MCF7s [49].

As inferred from the Figure 2.3, there are two crossover frequencies for each medium where polarity of the DEP force is changed. For 2.5 mS/m, the crossover frequencies are noted as 1.5 kHz and 52.9 MHz whereas for 10 mS/m medium conductivity, 12.7 kHz and 52.9 MHz frequency values are the crossover frequencies. After the frequencies higher than 52.9 MHz, real part of Clausis-Mossotti factor is always negative which means negative DEP force is effective on the cell.

2.4 CMOS Imaging

CMOS technology allows microfabrication of lab-on-a-chip systems that have both sensing blocks and other circuitry including amplifiers, filters or read out circuits. Photonic cell detection is based on capturing photons fall on to surface of the CMOS image sensor. According to number of photons captured i.e. how much light is absorbed a shadow image of the cells is generated. CMOS imaging is a significant technology for cell imaging because of its lens-free structure. With this

structure cells can be imaged without employing fluorescent tagging and microscope imaging. By exploiting this advantage CMOS imaging can be easily used for point of care diagnosis at especially resource limited regions. Figure 2.4 presents basic structure of conventional and contact imaging techniques.

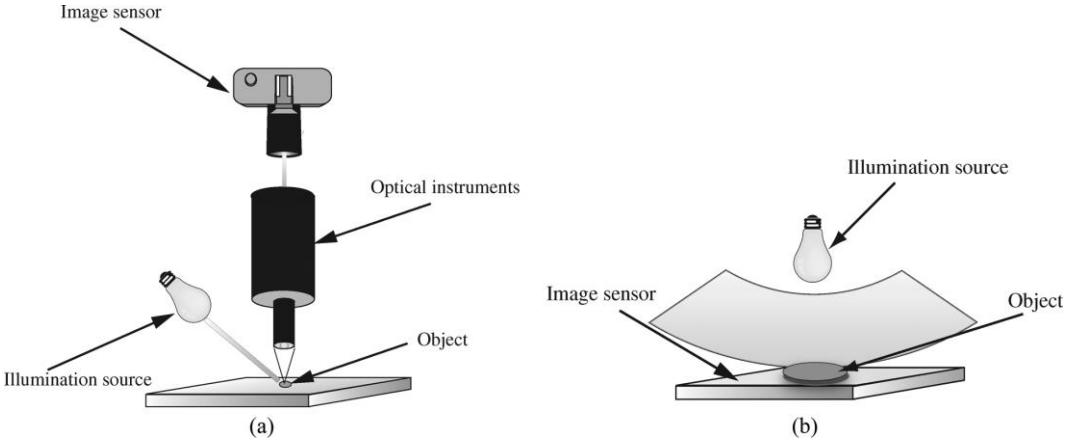

Figure 2.4 Illustration of conventional and contact imaging techniques [46].

The important issue for lens-free CMOS imaging is adjusting the sample to CMOS imager (D_{obj}) and sample to light source (D_{ls}) distances (Figure 2.5). The quality of an image can be quantified by contrast (C) that can be defined as:

$$C = \left(\frac{m_i - m_b}{a}\right)^2 \tag{2.12}$$

where m_i and m_b is the mean values of the object and background images respectively and a^2 is the background variance.

The contrast also depends on D_{obj} with the following function

$$C \subseteq f(D_{obj}{}^{-1}, m_i, m_b) = \frac{b}{1 + \left(\frac{D_{obj}}{d}\right)^n} \tag{2.12}$$

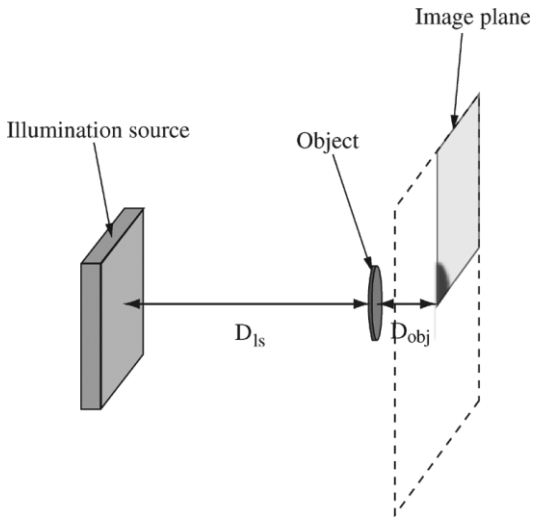

Figure 2.5 Simulation setup for the contact imaging system [46].

So, the contrast is inversely proportional to D_{obj} and also it is proportional to D_{la} (Figure 2.6). Therefore, D_{obj} should be minimized whereas D_{la} should be maximized in order to have the maximum contrast therefore quality. However, if D_{la} is too large then illuminance diminishes significantly and so the object may not be imaged properly. In our design D_{obj} parameter is fixed to 500 μm which the thickness of the glass substrate and D_{la} distance will be optimized experimentally.

In this chapter, dielectrophoresis theory is explained in detail by providing electrical model for the cells. Moreover, using single shell modeling, dependence of DEP force to the applied frequency is investigated. Additionally, CMOS imaging technique is presented by focusing on the effect of imager and sample to light source distances to the image quality.

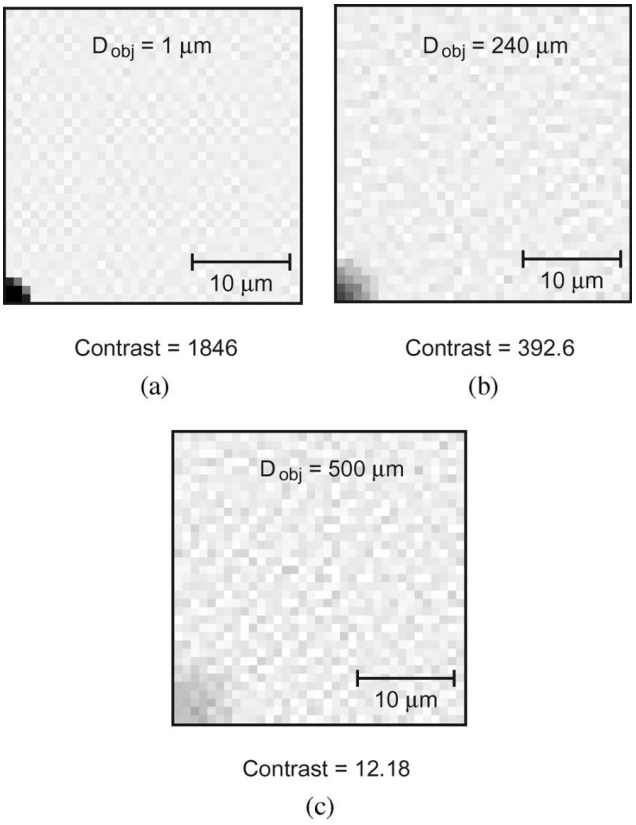

Figure 2.6 Simulation results at different distances [46].

CHAPTER 3

DESIGN AND SIMULATION

In this chapter, designs of the LOC systems for quantification of dielectrophoretically manipulated cancer cells are presented. The first generation system includes a CMOS image sensor, a DEP device and readout circuitry. Second generation system brings portability and easy-to-use operation. The system mainly consists of four parts: (i) DEP device design, (ii) CMOS image sensor circuitry design (iii) Sinusoidal waveform generator design and (iv) Android application design for automatic detection of the cells from raw CMOS images.

3.1 The Design of 1st Generation System

1st generation system includes a DEP device for the trapping of the cancer cells, a CMOS image sensor to image trapped cells and FPGA board with a computer software to acquire and process raw CMOS images.

The DEP device consists of 27 3D-electrodes having 40 μm width, the interelectrode gap between the electrodes 15 μm as it is presented in Figure 3.1. CMOS image sensor has 32 x 32 pixel array and pixel size is 15 μmx15 μm. Pixel structure of the CMOS image sensor is illustrated in Figure 3.2.

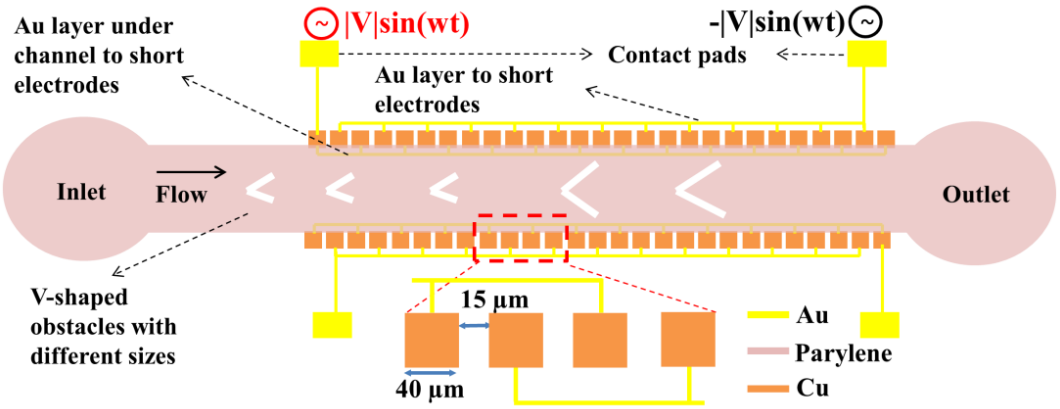

Figure 3.1 Structure of the DEP device with 3D electrodes [47].

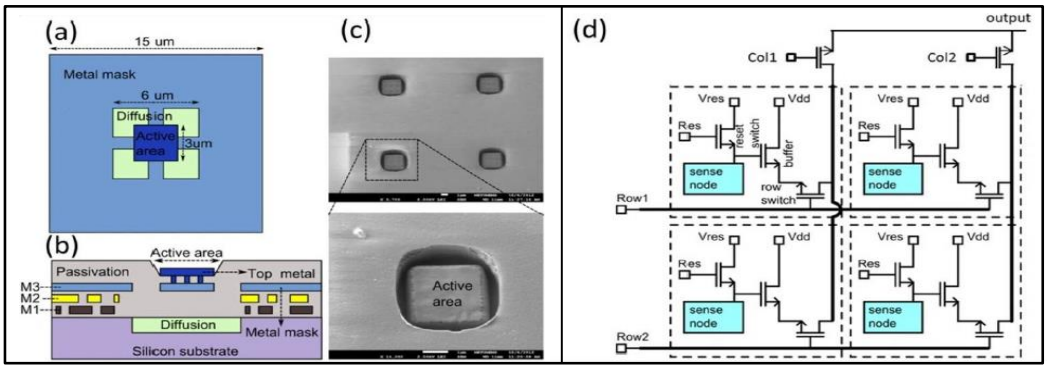

Figure 3.2 Pixel structure of the CMOS imager. (a) Pixel top view schematic with (b) cross section (c) SEM image and (d) pixel electronics [48].

In the proposed system, the DEP device is integrated with the CMOS image sensor with a PMMA frame. Raw CMOS images are captured with readout circuitry and FPGA board. Then, raw CMOS images are processed utilizing custom designed MATLAB program as shown in Figure 3.3. Image processing steps applied on to raw CMOS images are summarized below:

- *Noise Suppression:* Raw CMOS images are filtered with median filtering with a kernel size of 5 by 5 to eliminate the background noise.
- *Background Subtraction and Binarization:* Background image is subtracted from the current frame to detect the released cells. Then, the

differential image is binarized with a level of 0.02 determined by obtaining several cell images with the CMOS image sensor.

- *Morphological Operations:* After binarization, to eliminate background noise, the image is eroded with a disk element has 5 pixels size. Then, dilation operation with the same structural element is performed to fill the gaps inside the cell images.
- *Cell Counting:* Gaps inside the segmented regions are filled and the regions are counted for every differential image. Total cell count is obtained by summing the cell counts in the differential images. The video is down sampled consistent with the flow rate of the cells so that every cell is counted once in a video sequence.

The system includes a DEP device with 3D electrode structure. Therefore, cell experiments show that trapped cells cannot be distinguished properly and also image sensor has low spatial resolution (pixel size is 15 μm x15 μm that is close to cells' size). Moreover, the system has bulky equipment such as signal generator, computer or DC power supply limiting portability.

3.2 The Design of 2nd Generation System

To overcome with the limitations of the 1st generation system, an Android based portable imaging system is designed for automated quantification of the cancer cells.

3.3 DEP Device Design

The interdigitated electrode design is used for trapping the cancer cells. This structure eliminates unwanted shadows of the 3D electrodes falls onto trapped cells which limits detectability as shown in the Figure 3.4.

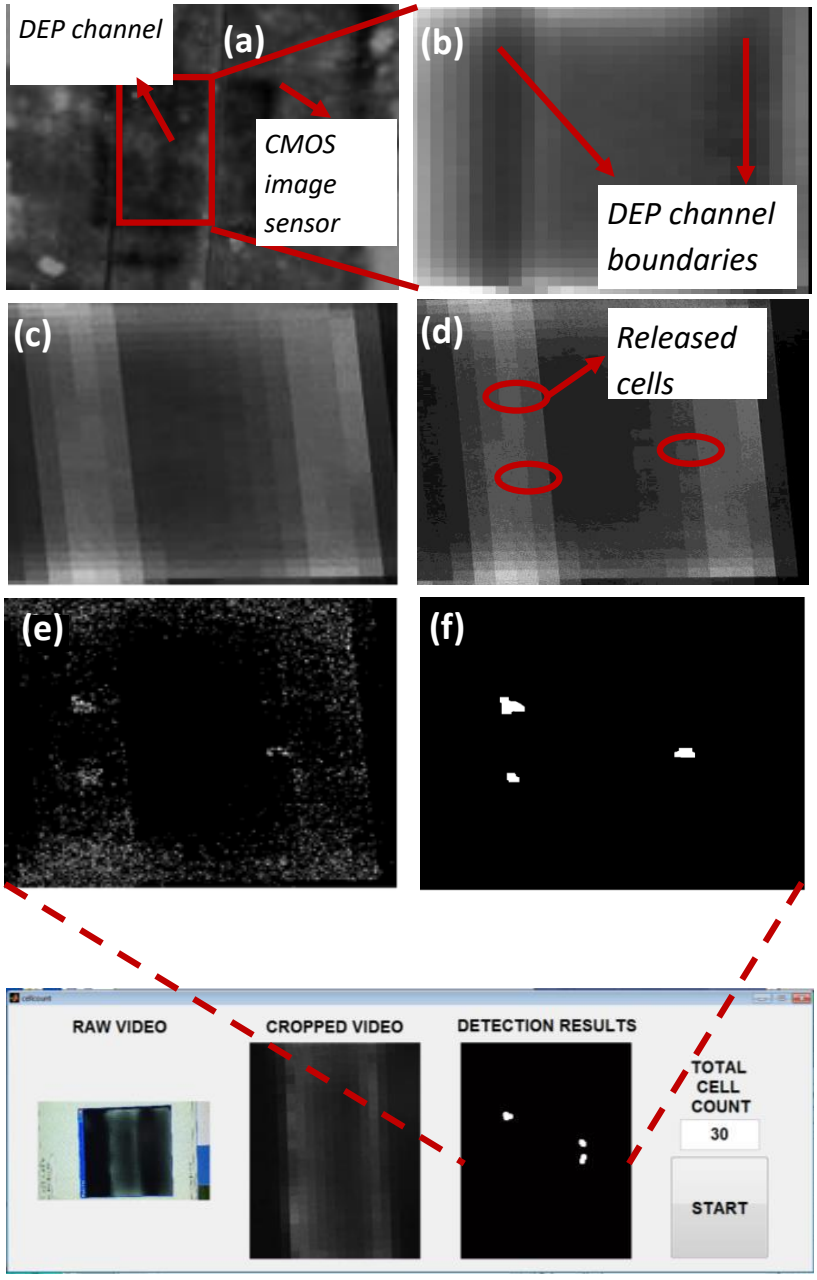

Figure 3.3 Microscope (a) and raw CMOS sensor images when DEP channel is empty (b), under medium flow with (c) no cells, (d) cells which are indistinguishable without using image processing , (e) binary differential image of (c) and (d), (f) final binary image after image processing.

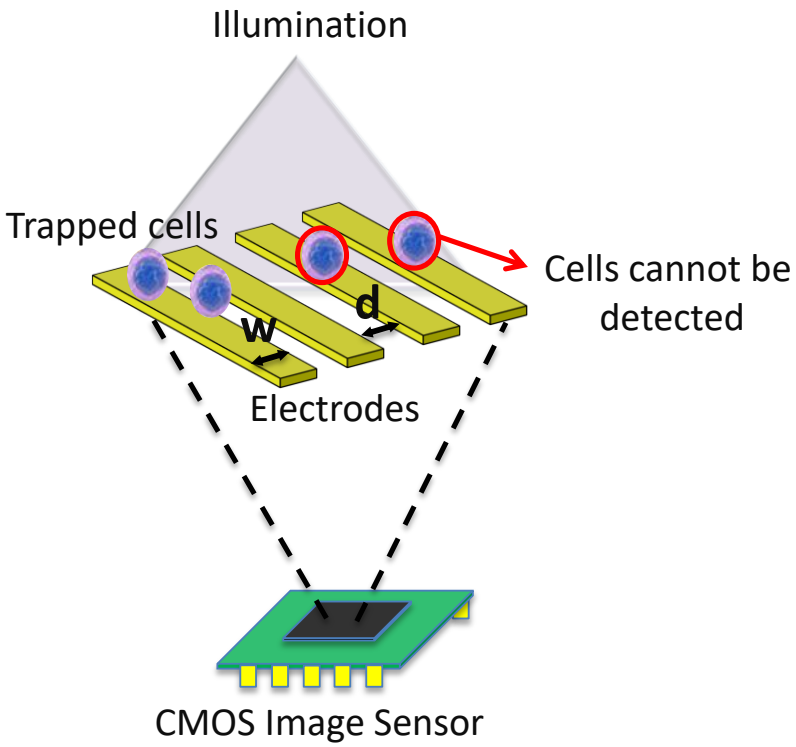

Figure 3.4 Illustration of the shadow problem in interdigitated electrodes.

However, the parameters electrode width *w* and distance between electrodes *d* still should be chosen carefully as illustrated in Figure 3.4 *w* should be as small as possible for proper cell imaging while allowing sufficiently large DEP trapping surface for the cells and *d* also should be as large as possible for clear distinction of the electrodes by maintaining sufficient electric field gradient between two electrodes. Therefore, four different designs summarized in Table 3.1 that have different *w* and *d* values are simulated in COMSOL for optimizing both *w* and *d*. The block diagram of the design is illustrated in the Figure 3.5.

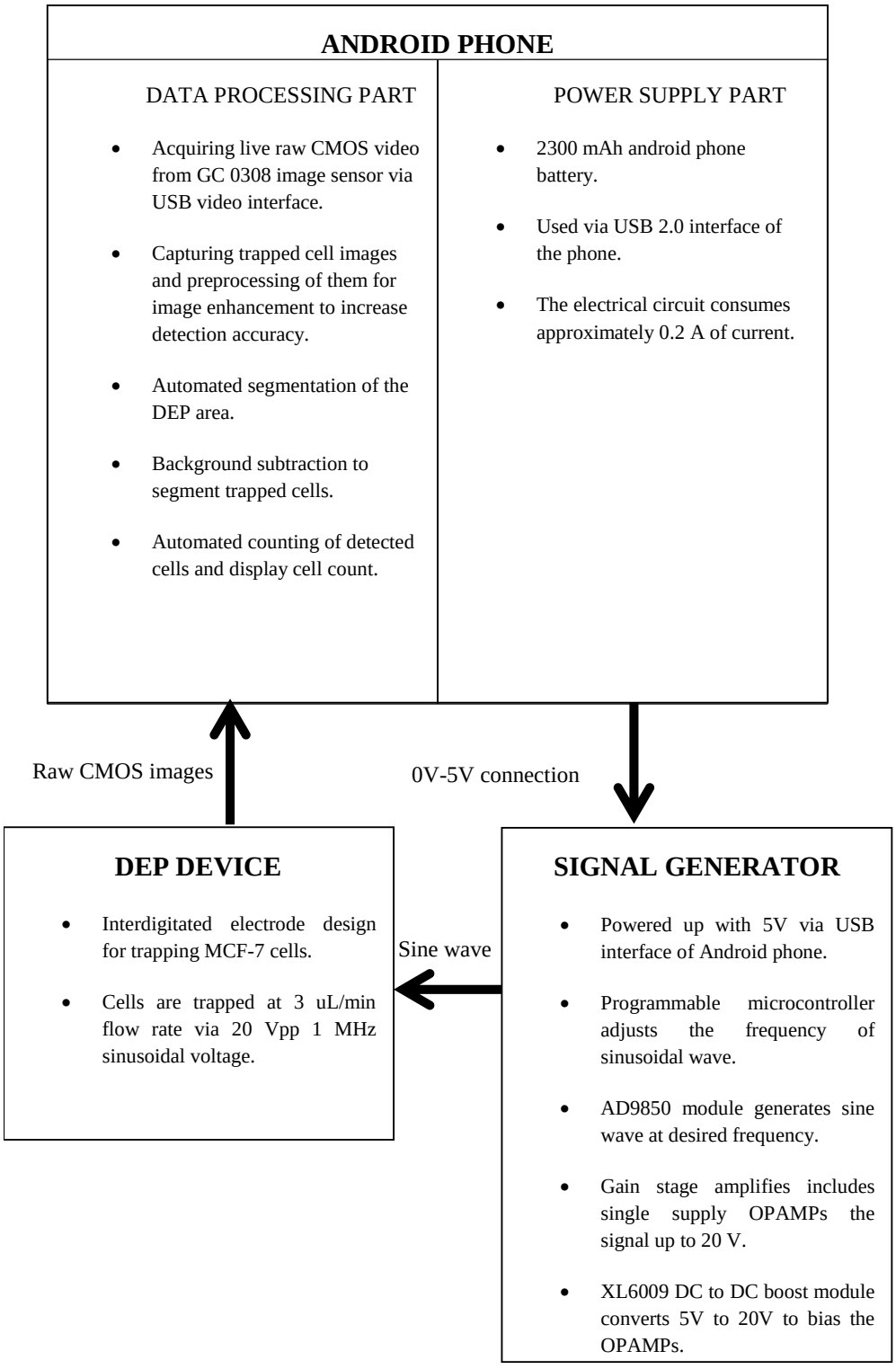

Figure 3.5 Block diagram of the system.

Table 3.1 Design parameters of the DEP devices

DESIGN NO	ELECTRODE WIDTH (w)	GAP WIDTH (d)
1	10 µm	10 µm
2	10 µm	20 µm
3	8 µm	20 µm
4	6 µm	20 µm
5	20 µm	10 µm

The total length of the channel will be 5000 µm since the active horizontal length of the CMOS sensor is approximately 5000 µm. There will be two 2000 µm long regions after and before the DEP area in order to have a steady state flow profile at the inlet and outlet of the DEP region. Therefore, DEP region will be 1000 µm long which will be sufficient for reasonable amount of cell trapping. Figure 3.6 illustrates the general design schematic of the DEP devices.

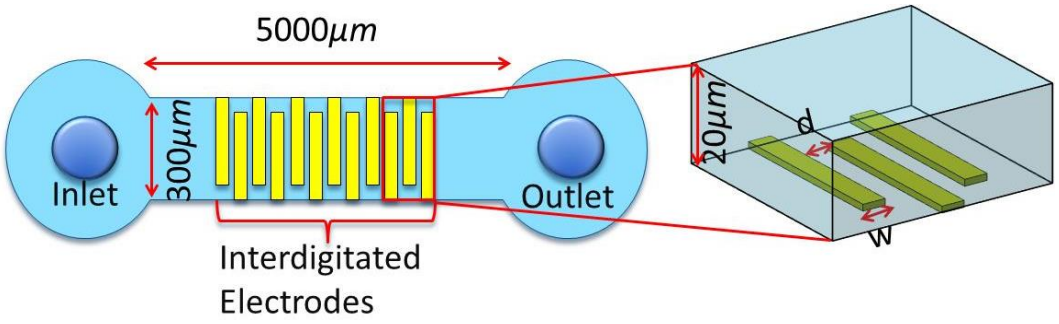

Figure 3.6 Illustration of the interdigitated electrode DEP device design.

3.3.1 Simulation Results of the DEP Devices

COMSOL Multiphysics 3.4 is used for simulation of the proposed design. Purpose of the simulation is testing the both DEP force and drag force exerted on

the cell before fabrication. All of the simulations are done in 2D to obtain faster results by decreasing the computational cost.

Two modules which are “Electrostatics” and “Incompressible Navier-Stokes” are employed in COMSOL. Electrostatics module is used for simulating DEP force inside the channel by solving Laplace with insulating boundary conditions since the microchannel walls are made of Parylene-C. Equation for the Electrostatics module is given as:

$$-\boldsymbol{\nabla}\cdot\left(\left(\sigma+\frac{\varepsilon_0\varepsilon_r}{T}\right)\boldsymbol{\nabla V}-\boldsymbol{J^e}\right)=\frac{\rho_0}{T} \tag{3.1}$$

Interdigitated electrode array is excited by applying sinusoidal signals have 180° phase difference. Hence, boundary condition for the electrodes is determined with ±|V| sin (ωt) formula. As it is mentioned before, in DEP equation, every term is constant except gradient of the electric field square. This term is position dependent and expressed as:

$$\boldsymbol{\nabla E^2}=\left|\begin{matrix}\left(\frac{\partial^3}{\partial x^3}+\frac{\partial^3}{\partial y^2\partial x}+\frac{\partial^3}{\partial z^2\partial x}\right)\hat{x}\\ \left(\frac{\partial^3}{\partial y^3}+\frac{\partial^3}{\partial x^2\partial y}+\frac{\partial^3}{\partial z^2\partial y}\right)\hat{y}\\ \left(\frac{\partial^3}{\partial z^3}+\frac{\partial^3}{\partial x^2\partial z}+\frac{\partial^3}{\partial y^2\partial z}\right)\hat{z}\end{matrix}\right|*\boldsymbol{V^2} \tag{3.2}$$

For 3D simulations, this expression can be converted to COMSOL language as follows:

“*sqrt(((2*(Vx*Vxx+Vy*Vyx+Vz*Vzx))^2)+((2*(Vx*Vxy+Vy*Vyy+Vz*Vzy))^2)+((2*(Vx*Vxz+Vy*Vyz+Vz*Vzz))^2))*”

Additionally, Navier-Stokes module is implemented in order to model microfluidic flow inside the channel by using Incompressible Navier-Stokes equation given by

$$\rho\left(\frac{\partial \boldsymbol{V}}{\partial t} + \mathbf{V}\cdot\boldsymbol{\nabla V}\right) = -\nabla \boldsymbol{P} + \mu\boldsymbol{\nabla^2 V} + f \tag{3.3}$$

To track the cell movements inside the microfluidic channel both effect of electrostatic force and drag force should be taken into account. For that purpose, cells can be modeled as particles and particle tracing simulations in 3D can be made by using the formulas below

$$\begin{aligned} &u+((constant)*(2*(Vx*Vxx+Vy*Vyx+Vz*Vzx))) \\ &v+((constant)*(2*(Vx*Vxy+Vy*Vyy+Vz*Vzy))) \\ &w+((constant)*(2*(Vx*Vxz+Vy*Vyz+Vz*Vzz))) \end{aligned} \tag{3.4}$$

for the positive DEP force applications and

$$\begin{aligned} &u-((constant)*(2*(Vx*Vxx+Vy*Vyx+Vz*Vzx))) \\ &v-((constant)*(2*(Vx*Vxy+Vy*Vyy+Vz*Vzy))) \\ &w-((constant)*(2*(Vx*Vxz+Vy*Vyz+Vz*Vzz))) \end{aligned} \tag{3.5}$$

for the negative DEP force applications.

Note that *u*, *v* and *w* are the medium velocities in *x*, *y* and *z* directions respectively, and the constant term can be expressed:

$$constant = \frac{\varepsilon_m}{\mu}\frac{r^2}{3}\,Re(F_{CM}) \tag{3.6}$$

Constants calculated at different frequency values for RBCs and MCF7s given in the Table 3.2.

Table 3.2 Cell parameters and constants with different frequencies utilized

	MCF7s	RBCs
Radius (μm)	10.9	3.2
Medium Permittivity	78	78
Medium Viscosity	$8.92\text{x}10^{-4}$	$8.92\text{x}10^{-4}$
Constant @ 5 kHz	$-8.653\text{x}10^{-18}$	$-1.188\text{x}10^{-18}$

Constant @ 12.7 kHz	5.61×10^{-21}	-1.135×10^{-18}

The designed DEP devices are simulated in COMSOL combining electrostatics module (for electric field simulation) with Navier-Stokes module (for fluid flow simulation).

In the electrostatics module, the electrodes are specified as gold and conductivity (σ) and relative permittivity of the medium) are set to 2.5×10^{-3} S/m and 78 respectively. 10 Vpp, 1 MHz sinusoidal voltage is applied to the electrodes. The constants used in Navier-Stokes module are, $\eta = 8.9 \times 10^{-4}$ Pa.s, $\sigma = 1000 kg.m^{-3}$ dynamic viscosity and density of the medium respectively.

After the constants are entered, firstly, time dependent simulation is made in Electrostatics module. Then, by using a stored solution (solution at a time when sinusoidal voltage peaks) stationary analysis is made in Navier-Stokes module. Figure 3.7-3.11 illustrates the simulation results (electric field gradient and particle tracing) for the different designs.

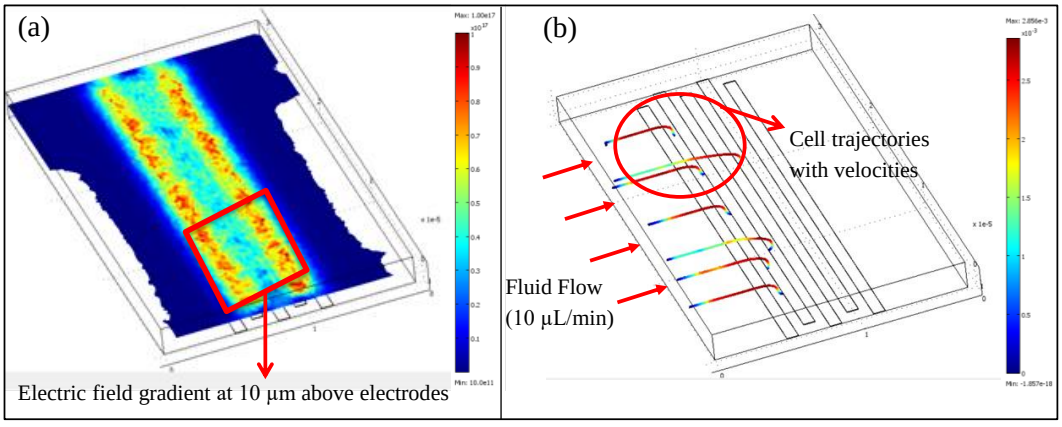

Figure 3.7 (a) Electric field gradient (b) particle tracing of the DEP device 1 (w=10 µm and d=10 µm).

In simulations, electric field gradient at 10 µm above the electrodes is investigated. Since, average diameter of the cancer cells is 20 µm (the height of

the microfluidic channel), so center of the cancer cells are located at the 10 μm (midpoint of the channel) while they are flowing through the microchannel. Also, Therefore, it is a reasonable approach to analyze the DEP force exerted at the center locations of the cells.

To trap cells on to electrodes, the minimum electric field gradient value should be 10^{12} kg^2m/s^6A^2. Hence, minimum limit in electric field simulations is set to 10^{12} kg^2m/s^6A^2. Additionally, to observe the cell movements under two dominant forces (electrical and drag) particle tracing is performed by applying fluid flow at 10 μL/min. Particle tracing simulation is made utilizing the Eqn. 3.4 and 3.5.

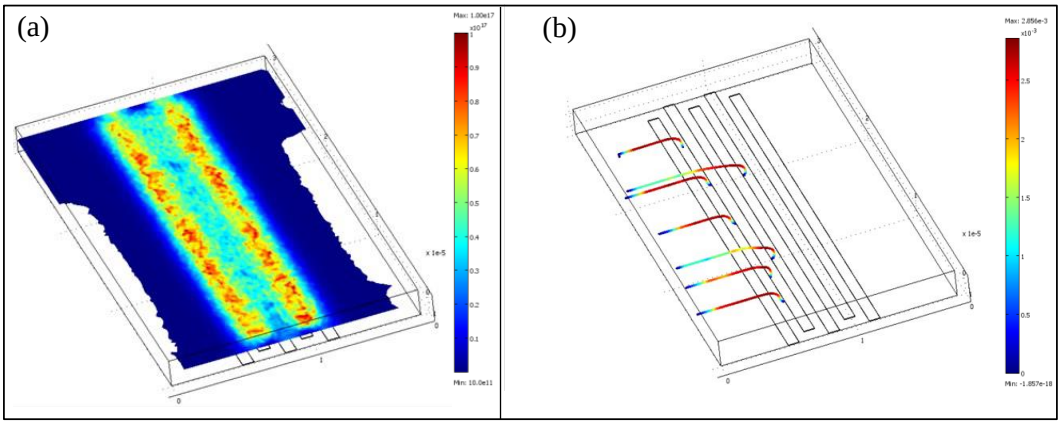

Figure 3.8 (a) Electric field gradient (b) particle tracing of the DEP device 2 (w=10 μm and d=20 μm).

Initial positions of the cells are randomly chosen at different locations of the microfluidic channel. Particle tracing is also correlated with the velocities of the cells at the flow direction to simultaneously observe effects of the drag force. When electrode width is decreased or interelectrode gap is increased, maximum value for electric field gradient diminishes.

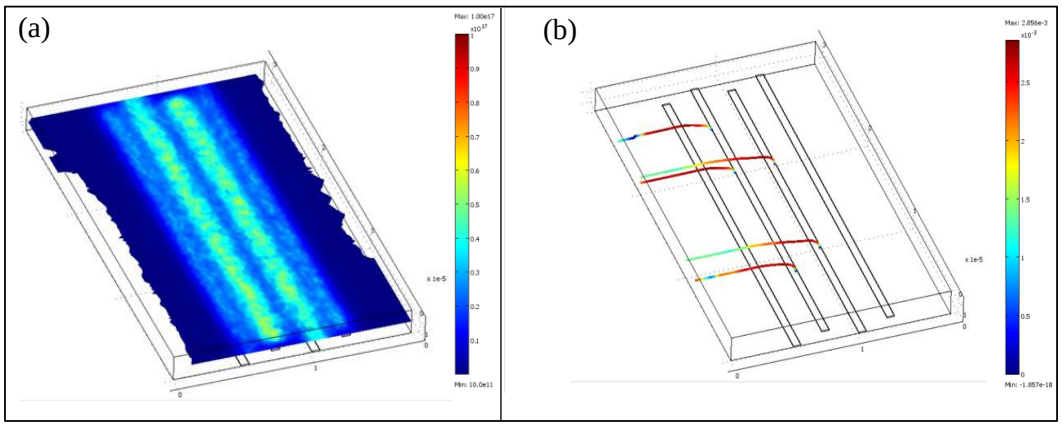

Figure 3.9 (a) Electric field gradient (b) particle tracing of the DEP device 3 (w=8 μm and d=20 μm).

As it is seen from the simulation results, the gradient of electric field square for this design is higher than 10^{12} kg^2m/s^6A^2 at 10 μm above the electrodes (the maximum height that cells can flow) which is the expected value for cell trapping for all of the designs. However, highest electric field gradient can be generated with 20 μm width electrodes. On the other hand, 6 μm and 8 μm electrodes will be better for cell imaging by minimizing shadow problems caused by electrodes.

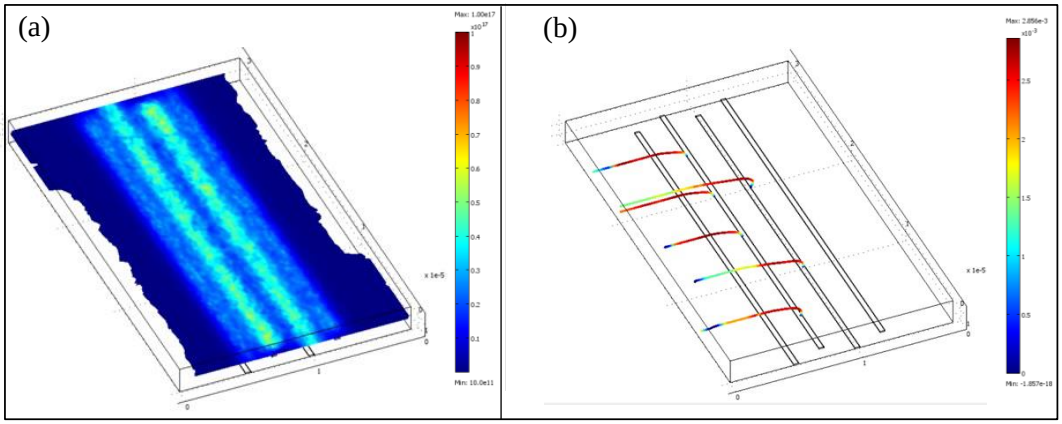

Figure 3.10 (a) Electric field gradient (b) particle tracing of the DEP device 4 (w=6 μm and d=20 μm).

Therefore, optimum w and d values can be found by making real experiments. To sum up, the device has 20 μm electrodes with 10 μm spacing provides highest trapping capability whereas the device has 6 μm electrodes with 20 μm spacing will be most suitable for imaging purposes.

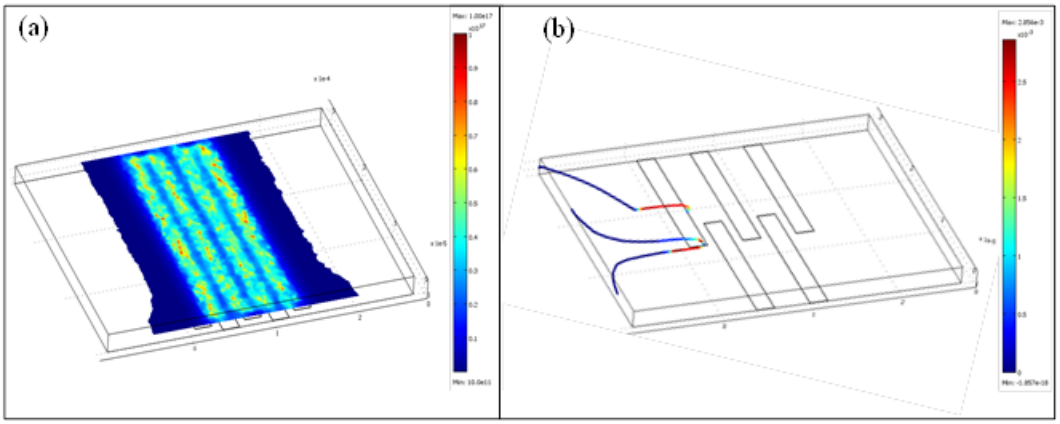

Figure 3.11 (a) Electric field gradient (b) particle tracing of the DEP device 4 (w=6 μm and d=20 μm).

3.4 CMOS Image Sensor

In order to image the trapped cells on the electrodes, 1/6.5'' VGA CMOS Image Sensor GC0308 is used. It is cost effective (~10$) and has 3.7 mm^2 field of view which is adequate to image whole microfluidic channel. Additionally, pixel dimension of the sensor is 3.4μmx3.4μm which is sufficient for imaging cancer cells (~10 μm-20 μm). It is also USB powered and have plug and play interface so it is suitable for portable applications.

Internal block diagram of the sensor is illustrated in the Figure 3.12. Additionally, important parameters of the CMOS sensor are given below in Table 3.3.

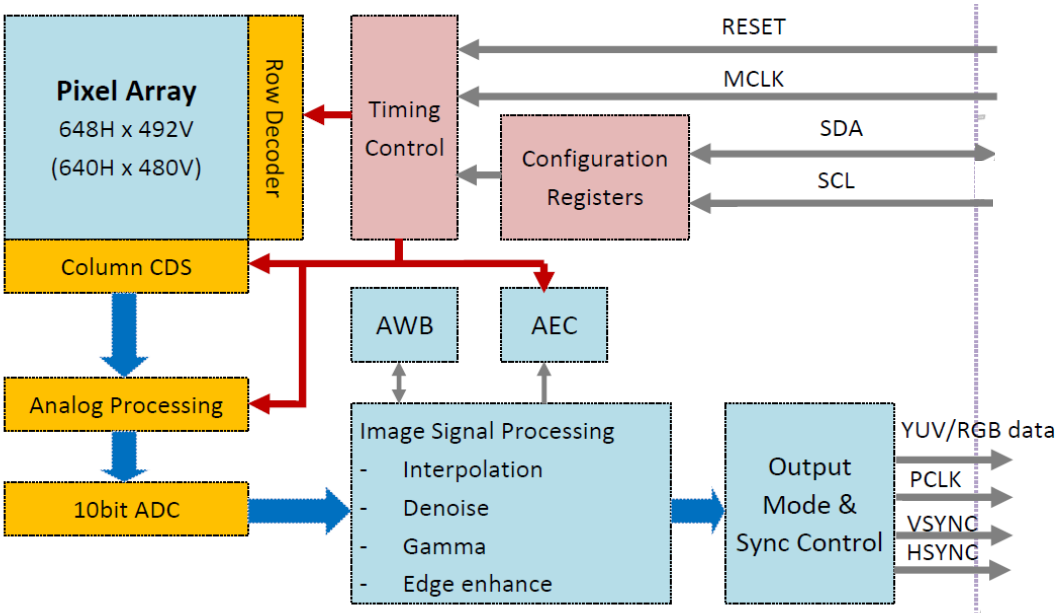

Figure 3.12 Internal block diagram of the GC0308 image sensor.

Table 3.3 Fundamental properties of the GC0308 CMOS image sensor.

Pixel Size	3.4 μm x 3.4 μm
Active Pixel Array	648 x 488
Max Frame Rate	30 fps @ 24 MHz, VGA

As a readout circuitry of the image sensor, a commercial USB 2.0 interface board is used due to its high data transfer rate which is 60 MByte per second. Figure 3.13 shows basic structure of the CMOS imaging with CMOS imager board.

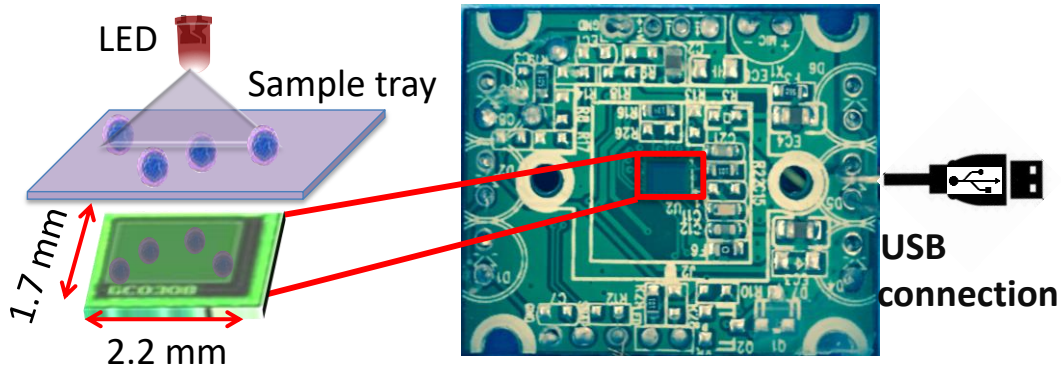

Figure 3.13 Illustration of the CMOS Imaging technique.

3.5 Signal Generator Circuitry

A portable USB powered signal generator circuitry is designed to energize interdigitated electrodes for cell trapping. The frequency that yields highest DEP force is 1 MHz for the MCF7 cancer cells. Moreover, magnitude of the applied sinusoidal voltage should be at least 10 Vpp to generate sufficient electrical field gradient inside the microfluidic channel to trap the cells.

By taking into account these constraints the signal generator circuitry having both adjustable frequency and amplitude is designed. Designed circuit includes ATmega microcontroller, XL 6009 DC to DC boost circuitry and AD9850 waveform generator IC. Additionally, the circuitry has a voltage amplifier stage.

The microcontroller coded with an Arduino board controls the AD9850 IC with control signals (clk, Freq. load, data and reset). The frequency of generated sinusoidal is adjustable with the microcontroller. AD 9850 IC is able to generate sinusoidal signals having 180 phase difference at the frequency values between 0 and 40 MHz. However, the generated signals have the magnitude of 1.2 Vpp that is insufficient to excite electrodes to obtain the intended DEP force. Therefore, a voltage amplifier circuit based on single supply OPAMP topology is designed. Since only available supply voltages are 0 and 5V (USB interface) the DC bias voltage is also boosted by using XL 6009 IC. Additionally, gain of the amplifier

can be adjusted with a potentiometer. Therefore, the signal generator circuit can generate sinusoidal voltages (have 180 phase difference) between 0-40 MHz and from 0 to 20 Vpp. Figure 3.14 shows the block diagram of the signal generator circuitry and PCB of the circuitry is illustrated in Figure 3.15.

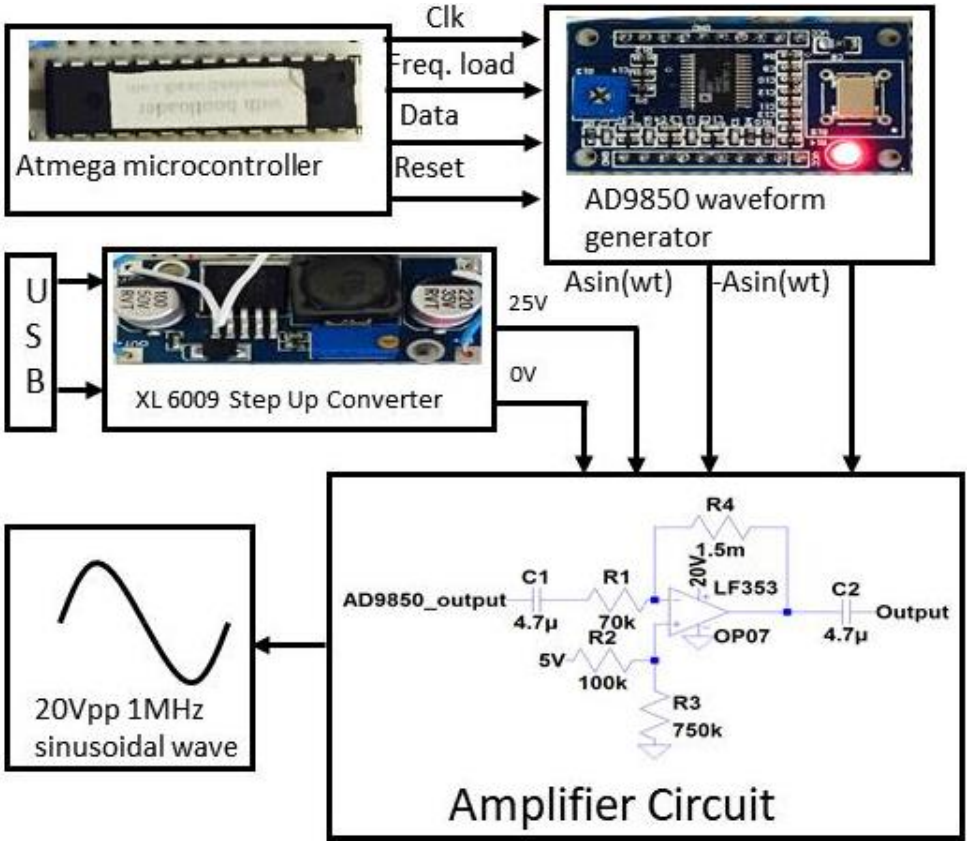

Figure 3.14 Block diagram of the signal generator circuit.

3.6 Android Application

An android application performing image processing operations for automatic quantification of the trapped cells is developed. Moreover, the smartphone is used for supplying power to the whole circuitry via USB interface. The application uses UVC (USB Video Class) interface to acquire raw CMOS image data from CMOS imager interface board and by using OpenCV (Open Source Computer

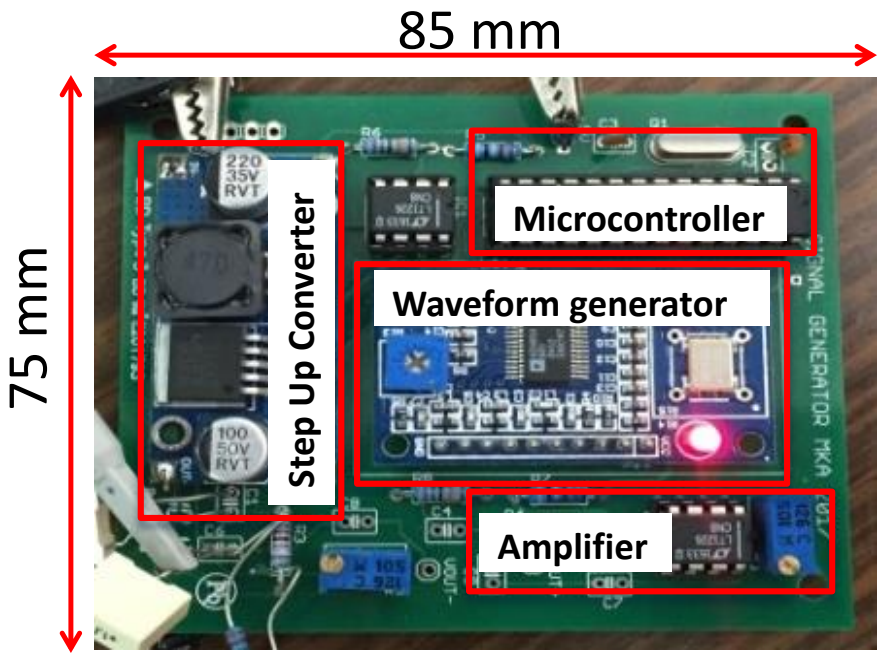

Figure 3.15 PCB layout of the signal generator circuit.

Vision) library functions captured images are processed and cell counts are automatically obtained.

Cancer cells are trapped with the microfluidic DEP device and then imaged via CMOS image sensor underneath the trapping area of the microfluidic channel. Image sensor is connected to the smartphone via USB interface utilizing an Android application.

The application automatically counts the trapped cells from raw CMOS images based on background subtraction technique. In the application, the live CMOS images are transferred via USB and displayed on the screen. Firstly, background image is set with "*Set BG*" button. The cells are trapped only onto DEP region so that DEP region with interdigitated electrodes should be segmented. For that purpose, raw CMOS image is enhanced with median filtering operation and bounding electrodes are detected with edge detection technique. Then, using spatial information, DEP region is automatically detected and segmented. Finally,

background image of the DEP region is captured and coordinates of the DEP area are recorded. After cells are trapped with dielectrophoretic force, trapped cell images inside the DEP region (according to the automatically recorded coordinates) are captured pressing *"Capture"* button. Trapped cells are detected with background subtraction algorithm based on differential analysis between trapped cell image and background image captured before. Cells are segmented by utilizing further image processing operations such as binarization, dilation and erosion. Cell count is automatically obtained with *"Analyze"* button which counts segmented regions as candidates for cells and displays on the screen. The GUI of the Android application and block diagram of the proposed image processing operations is given in the Figure 3.16 and 3.17.

Chapter 3 presents the design of the two different generations of imaging systems combine DEP device with CMOS image sensor. 1st generation system has limitations such as low spatial resolution, low field of view and bulky structure. In the 2st generation system, these limitations are overcome by designing an Android based imaging system. Additionally, different designs for the DEP device are proposed and verified with COMSOL.

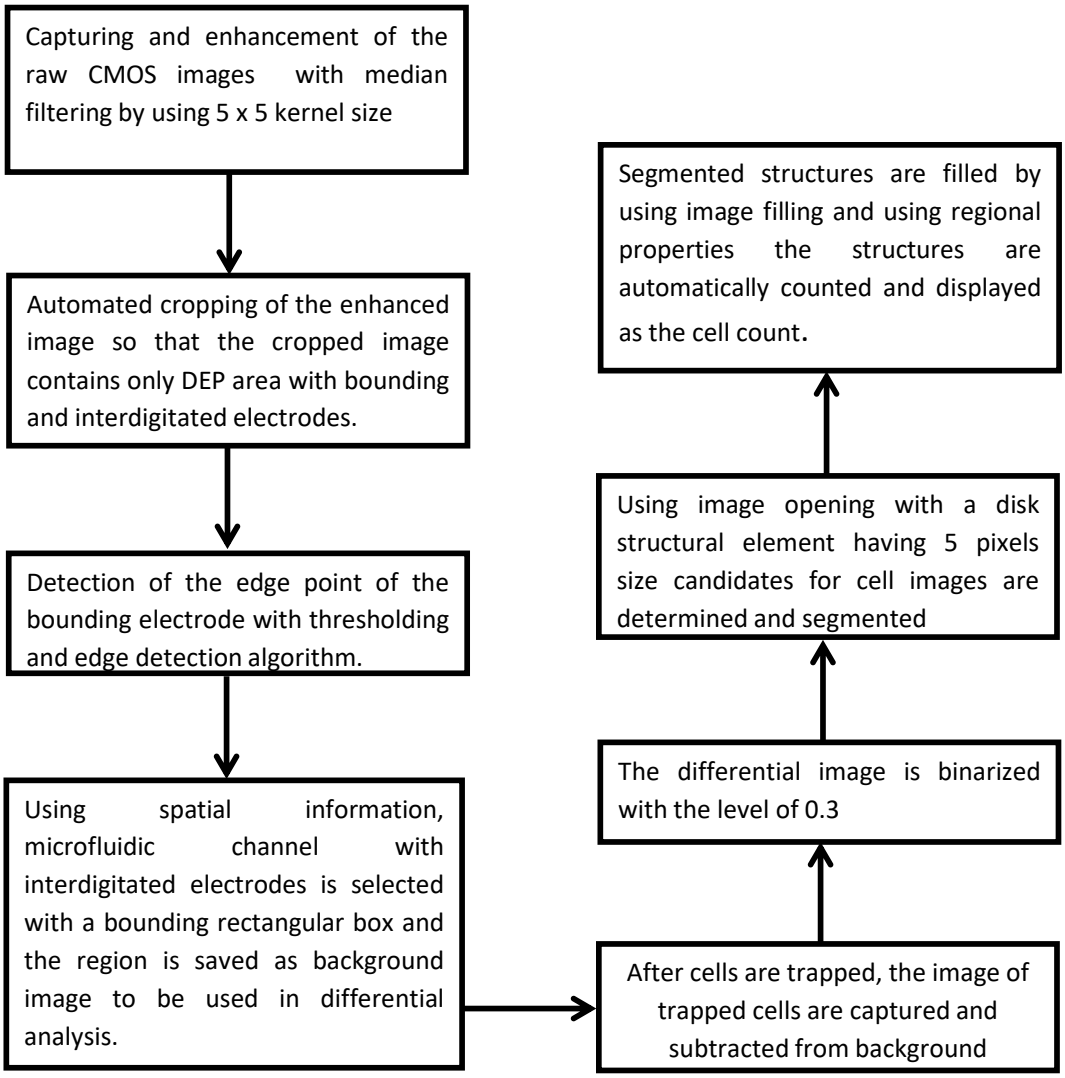

Figure 3.16 Block diagram of the image processing operations.

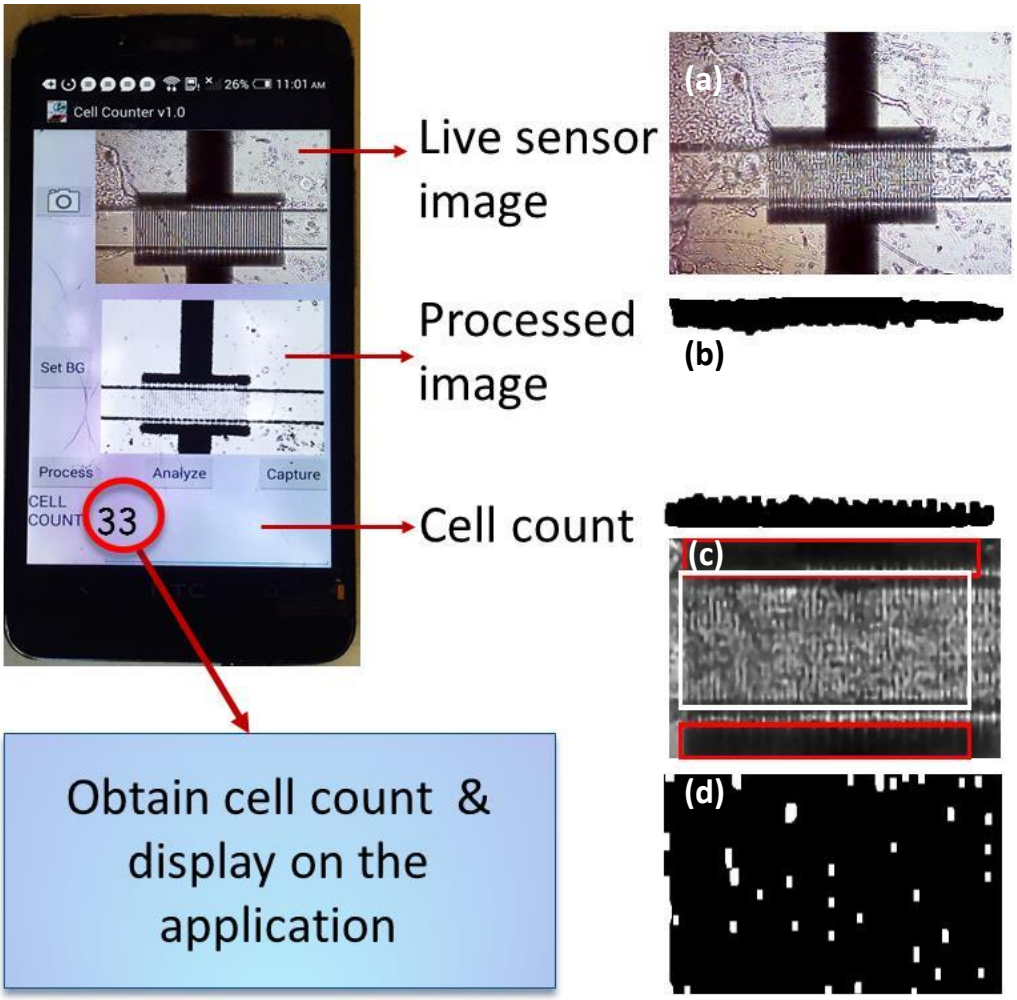

Figure 3.17 Android application and image processing operations (a) raw CMOS image (b) segmentation of electrodes (c) segmentation of the DEP region (d) detected cells.

CHAPTER 4

FABRICATION

In this chapter, fabrication process of the DEP devices is explained by giving mask drawings, fabrication steps and fabricated devices. Additionally, fabrication of the holder with 3D printer is presented.

4.1 Fabrication of the DEP Devices

Fabrication of the DEP devices is made by using surface micromachining techniques such as etching, sputtering and photolithography. Fabrication process of the DEP devices includes three masks that are electrode formation, parylene microfluidic channel mask and mask for the both electrode and channel openings.

The masks for the five designs verified in COMSOL are drawn in CADENCE as shown in the Figures 4.1-4.3. All of the designs are drawn in the mask since although all of them operate properly in COMSOL, in order to optimize the values for d and w real life experiments with DEP devices have different d and w values are needed. The masks for all four devices are given below. Note that because of some process variations in wet etching step of the microfabrication (undercut) electrode widths are drawn 2 μm bigger and so spacing are left 2 μm smaller.

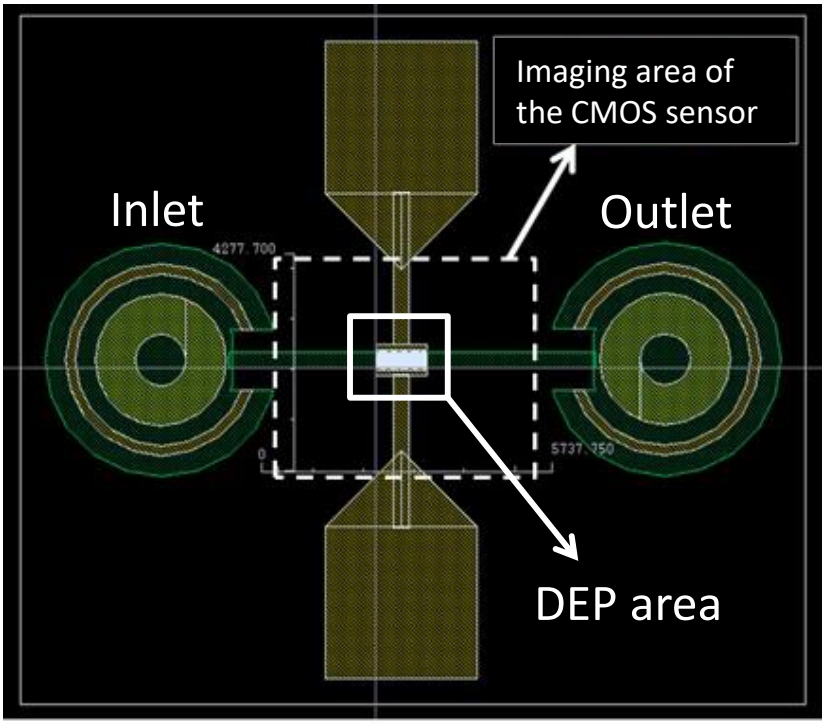

Figure 4.1 General mask of the DEP device and sensor alignment.

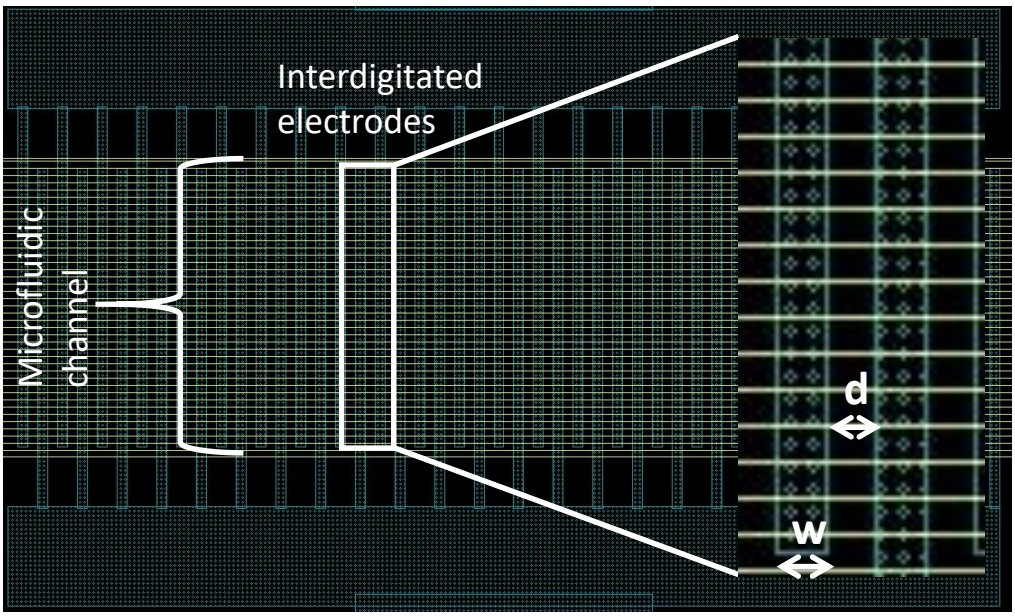

Figure 4.2 Mask layout of the DEP region.

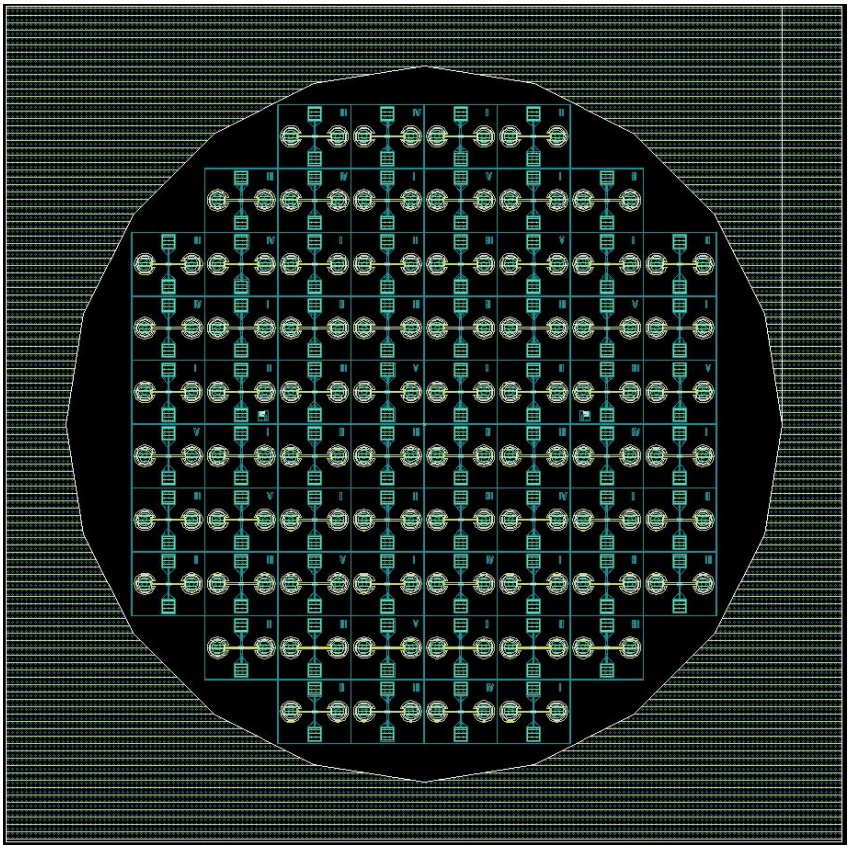

Figure 4.3 Mask layout of the die.

In the fabrication process, glass wafer is used for the substrate because of its transparency. In our case, verification step includes microscope investigation so that all of the structural material should be optically transparent. Parylene is coated as channel forming material due to its advantages such as biocompatibility and bio-stability, allowing conformal coating, optical transparency, pinhole and stress free application, and cost effectiveness. The electrodes are also covered with thin film of parylene (~0.5 μm) in order to prevent Joule heating. Fabrication steps are illustrated in Figure 4.4.

Fabrication starts with 6" glass substrate cleaning with piranha and etched with BHF. Then, 30 nm Ti and 400 nm Au layer is sputtered onto glass. Then, AZ9260

positive photoresist coated on the surface of the substrate and soft baked. Wet etching is applied to the regions specified after lithography steps. For the channel formation, another mask is used and channels are defined with photoresist. Parylene is coated onto photoresist and then channel openings are made with DRIE. Finally, photoresist inside the channel is released with acetone. Figure 4.5 illustrates the fabricated DEP device.

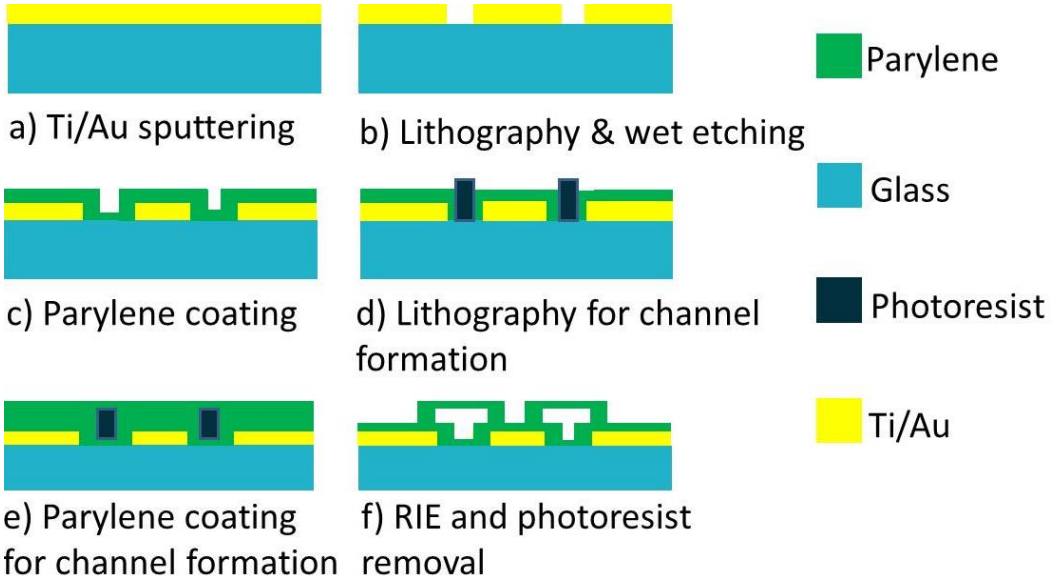

Figure 4.4 The fabrication flow of the DEP device.

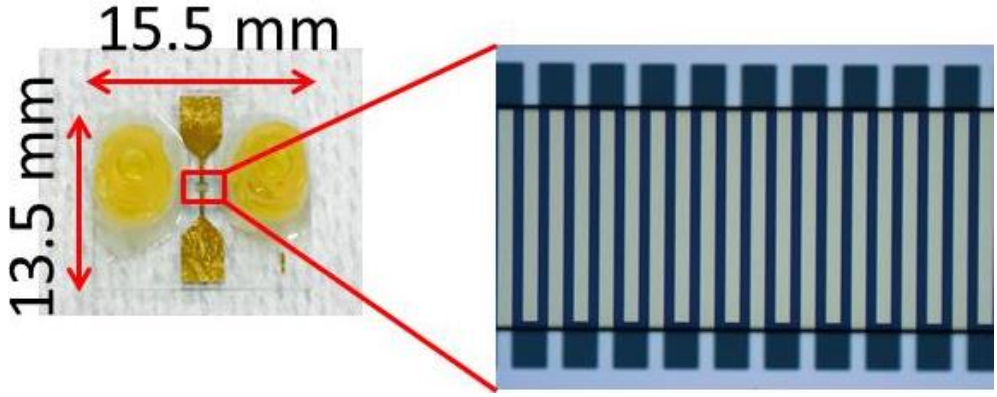

Figure 4.5 Picture of the fabricated DEP device.

4.2 Holder Fabrication

For mechanical integration of the DEP device onto CMOS imager, Polylactic Acid (PLA) based holder is designed. The holder consists of three subparts: (i) DEP device frame (ii) CMOS imager holder and (iii) Main holder. In order to have accurate positioning of the DEP device on CMOS image sensor, holder for the DEP device is designed as shown in the Figure 4.6.

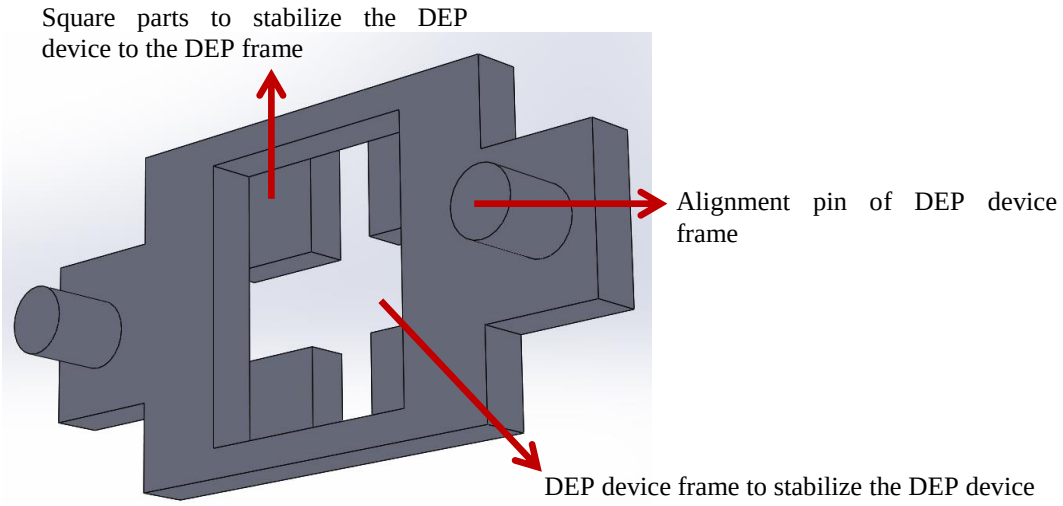

Figure 4.6 Illustration of the DEP device frame

To stabilize both CMOS image sensor board and DEP device frame the CMOS imager holder is designed. Figure 4.7 shows the designed CMOS imager holder.

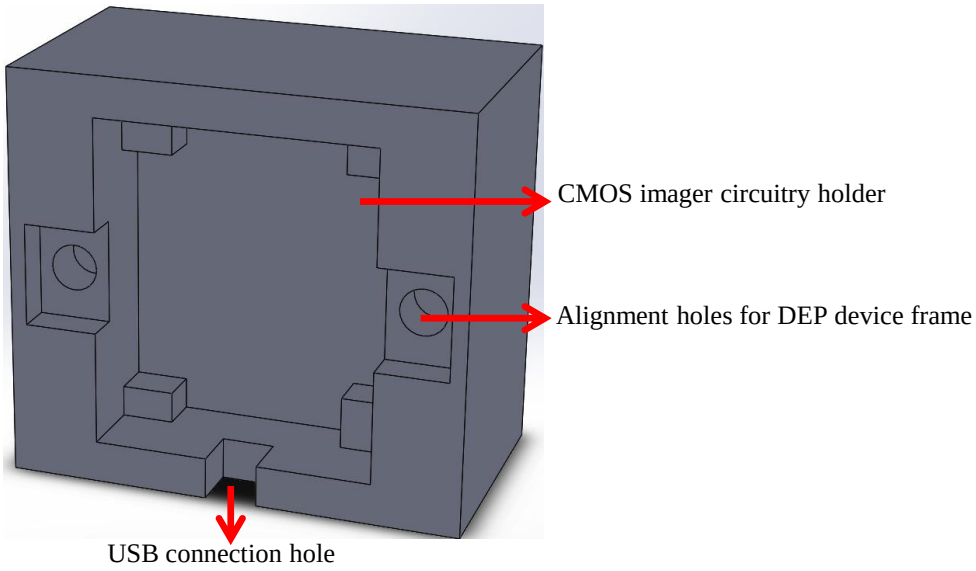

Figure 4.7 Illustration of the CMOS imager holder

Finally, the main holder illustrated in the Figure 4.8 designed to integrate both parts with the signal generator circuitry.

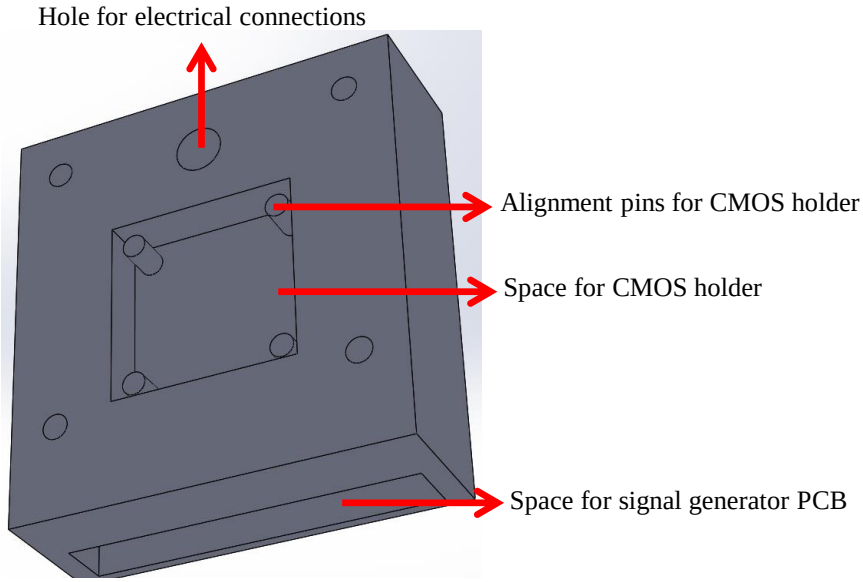

Figure 4.8 Illustration of the main holder

The parts are fabricated with 3D printer and 3D printed holders are presented in the Figure 4.9.

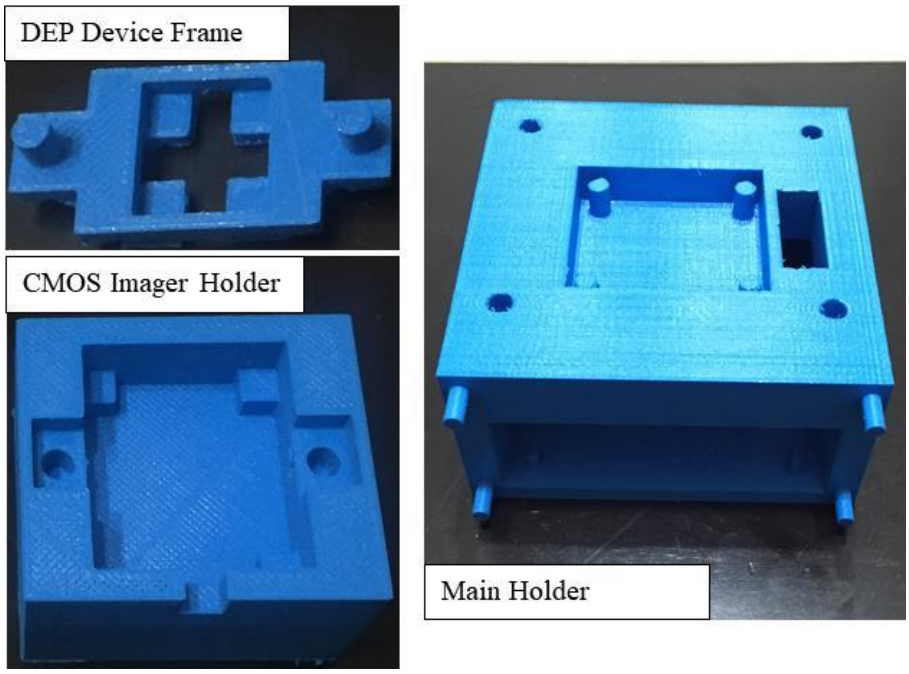

Figure 4.9 3D printed holders.

In this chapter, microfabrication of the DEP devices are explained in detail by summarizing fabrication processes and illustrating fabrication masks. Additionally, to complete mechanical integration of the whole system, 3D holders are designed and fabricated.

CHAPTER 5

RESULTS AND DISCUSSION

In this chapter, both experimental results of the DEP device and CMOS image sensor are presented. Firstly, cell preparation procedure is explained and then both trapping efficiency of the different DEP devices and counting efficiency of the CMOS imager system are given. Furthermore, a different application of the proposed LOC system is introduced.

5.1 Preparation of the Cells

In trapping experiments with the DEP devices, MCF7 cell are prepared. Cell culture of the MCF7 (RPMI 1640 medium) includes 0.2% (w/v) gentamicin, and 10% (w/v) fetal bovine serum. The incubator for the cells is at 37 °C with 5% CO_2. In order to obtain an electric field gradient inside the microfluidic channel, cells should be suspended in a conductive medium. Therefore, a DEP medium is prepared which has a conductivity of 25 mS/m and the medium also contains 0.3% (w/v) dextrose and 8.5% (w/v) sucrose as nutrients for the cells.

MCF7 cells are fluorescently labeled fluorescein diacetate (FDA), for observing inside the DEP channel. Fluorescent dye is prepared by dissolving FDA in DMSO (10 μg/ml). To label 10^6 cells in 1 ml 2.5 μl of dye solution is used. Stained cells are monitored under the fluorescence microscope.

5.2 Experimental Setup

To proof of concept, DEP devices are tested with MCF7 cells in in Class 10.000 Clean Room. The experimental setup illustrated in Figure 5.1 includes:

- Florescence Microscope: Olympus SZX12 microscope integrated with Photometrix Evolve 128 camera is employed to monitor trapping of the fluorescently labeled cancer cells in the DEP region. Microscope images are processed and recorded with WinFluor software.
- Syringe Pump: Lab Smith programmable syringe pump with automated µProcess Scanner software is utilized to precisely control the flow rate of the cells.

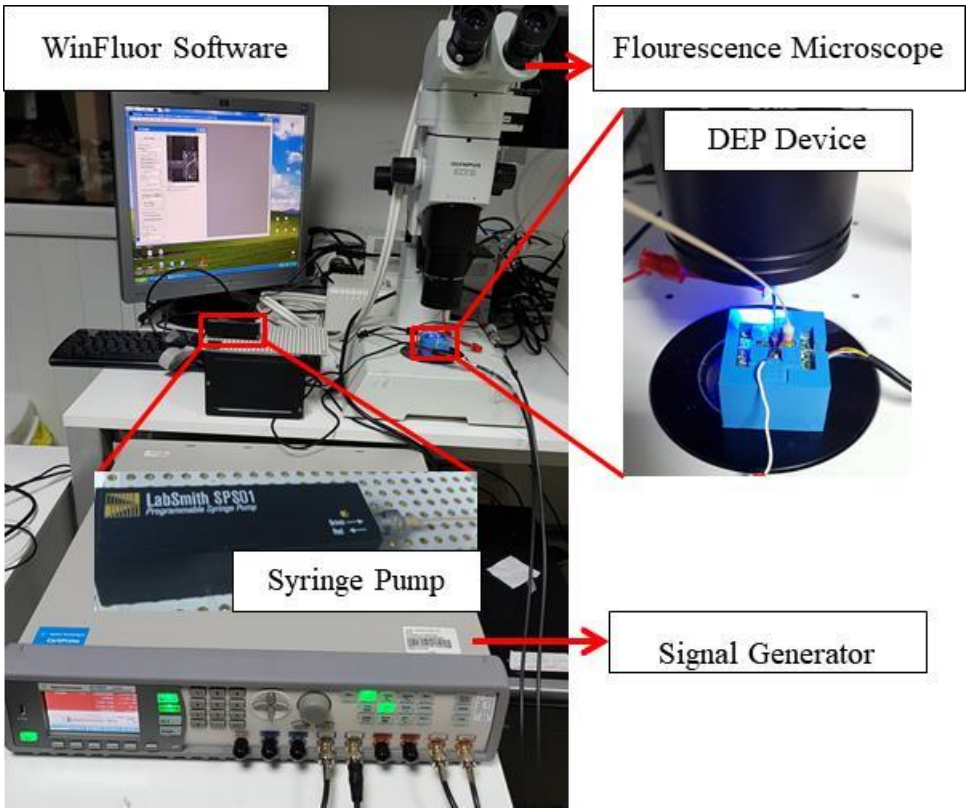

Figure 5.1 Picture of the experimental setup.

- Signal Generator: To excite the interdigitated electrodes via 20Vpp sinusoidal signals having 180° phase difference at 1 MHz, Agilent, 81150A signal generator is used.
- DEP Device: Microfluidic DEP device includes interdigitated electrode structure is used to trap the cancer cells inside the DEP region under continuous flow.

5.3 Experimental Results for the 1st Generation System

1st generation system consists of a DEP device, CMOS image sensor and FPGA board as shown in Figure 5.2. Additionally, raw CMOS images are acquired and imaged with computer software.

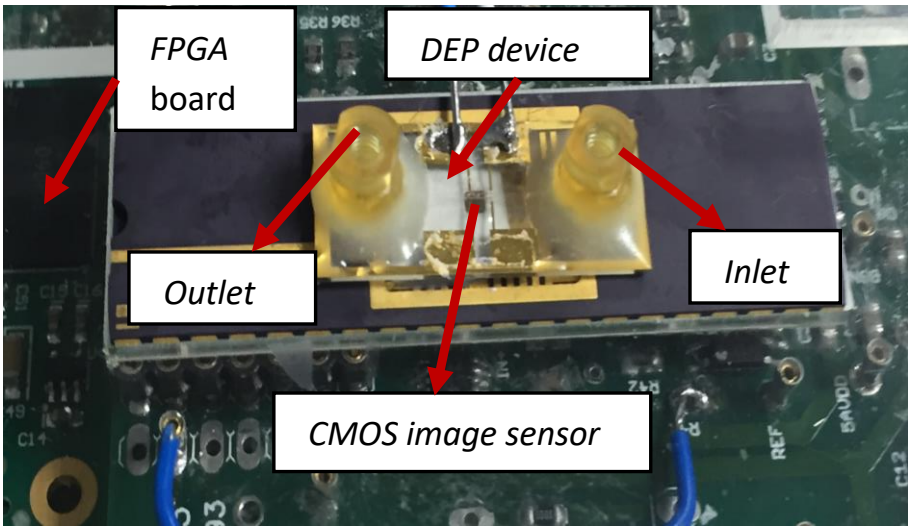

Figure 5.2 Illustration of the 1st generation system.

Figure 5.3 illustrates the image of the DEP device and corresponding CMOS sensor image. As it is observed from the Figure 5.3, trapping area cannot be distinguished due to both shadow problem of the 3D electrode structure and low spatial resolution of the image sensor. Therefore, in this system, trapped cells cannot be segmented from the CMOS sensor images. Moreover, field of view of the sensor is small so that microfluidic channel cannot be imaged completely.

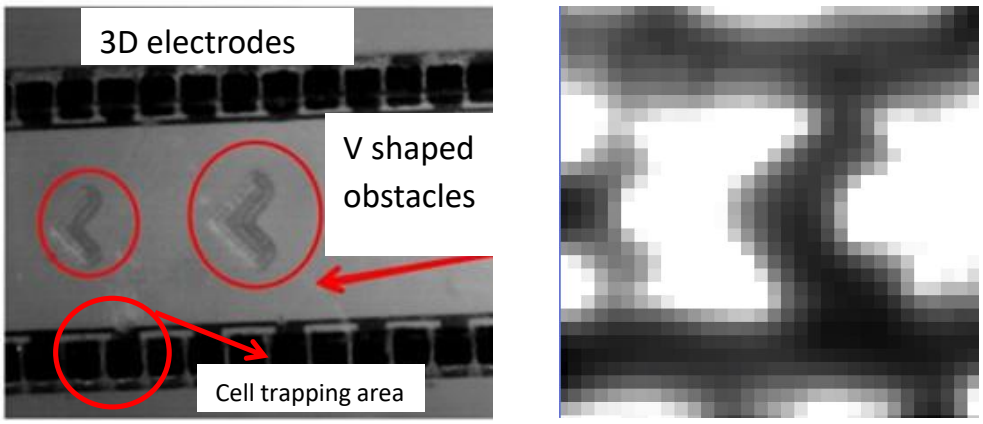

Figure 5.3 Microscope and corresponding sensor image of the DEP device.

Since trapped cells cannot be detected with this system, an alternative technique is used for detection. In this approach, cells are firstly trapped with the DEP device under 10 µl/min flow rate at 9 V_{pp}, 47.97 MHz. Then, trapped cells are released by washing the channel with the medium at 20 µl/min flow rate and cutting the applied voltage off. The CMOS image sensor is located at the output of the DEP region so released cells are imaged.

Custom designed MATLAB program automatically processes raw images and counts the flowing cells based on differential analysis (Figure 5.4). Figure 5.5 shows the CMOS sensor count and fluorescence microscope count respectively.

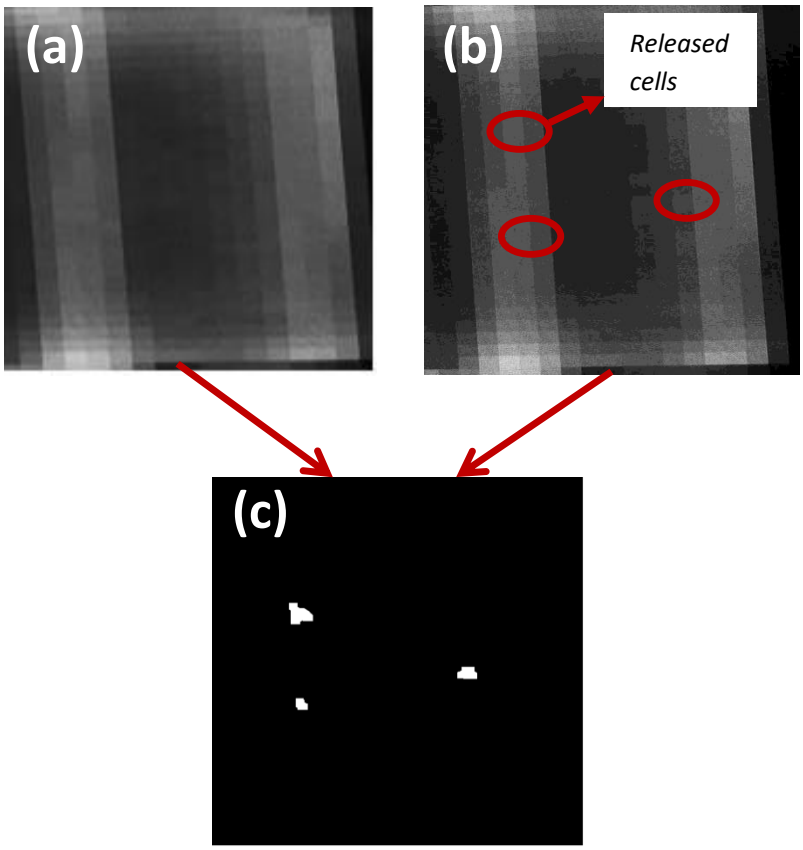

Figure 5.4 Differential image analysis (a) empty channel (b) released cells (c) detection results

The counting accuracy of the system is achieved up to 95%. However, the proposed system has still disadvantages such as: (i) low spatial resolution (15 μm), (ii) small field of view (~0.23 mm^2) and (iii) includes bulky equipment limiting portability.

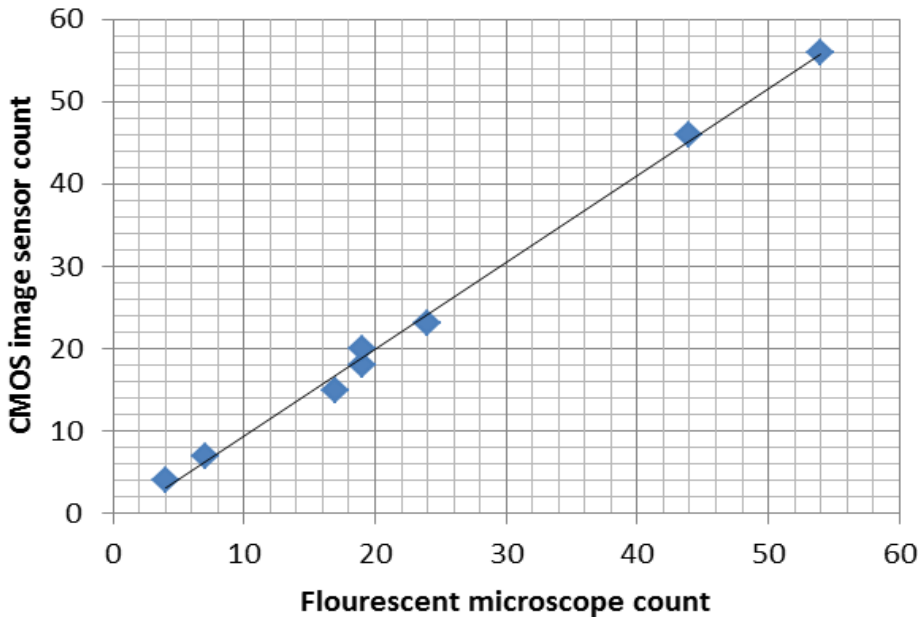

Figure 5.5 CMOS sensor count versus fluorescence microscope count.

5.4 2nd Generation LOC System

To eliminate the disadvantages of the 1st generation system, a smartphone based, portable imaging system is utilized. The proposed system consists of (i) CMOS imager: For imaging of the trapped cells for quantification (ii) Signal generator circuit: To energize the electrodes of the DEP device to manipulate cancer cells and (iii) Smartphone: Both acquires raw CMOS images from the sensor and supplies power to the whole system. Also, custom Android application utilizes image processing operations to obtain automated cell count. Figure 5.6 presents the LOC system.

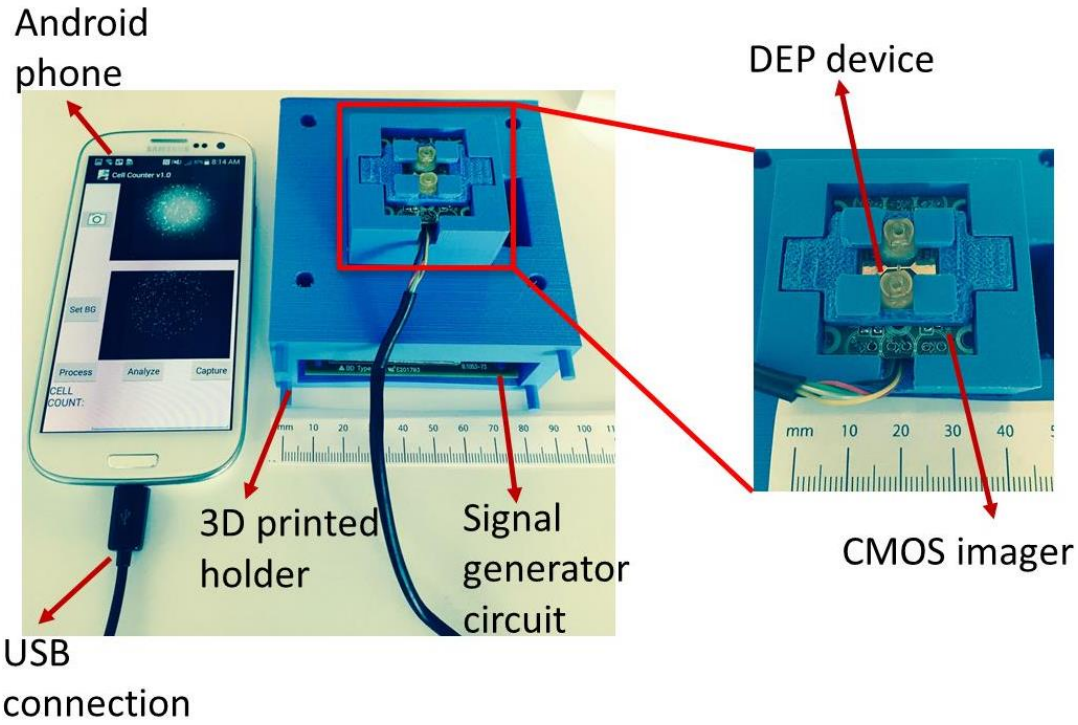

Figure 5.6 Smartphone based LOC system.

5.5 Test Results

5.5.1 DEP Device Characterization

Five different DEP devices (having various electrode width and interelectrode gap) with interdigitated electrodes are tested in terms of trapping efficiency. For that purpose, each design is tested under various flow rates by applying 20Vpp sinusoidal signal at 1MHz frequency. The detailed test procedure is given in the Table 5.1 and test results is illustrated the Figure 5.7-5.16.

Table 5.1 Test parameters for the DEP device characterization.

DEP Device	Flow Rate	Voltage	Frequency
Design 1: 10 μm electrode with 10 μm spacing	0.5, 0.75, 1, 1.25, 1.5, 2, 2.25, 2.5, 2.75 and 3 μL/min	20 Vpp	1 MHz
Design 2: 10 μm electrode with 20 μm spacing	0.5, 0.75, 1, 1.25, 1.5, 2, 2.25, 2.5, 2.75 and 3 μL/min	20 Vpp	1 MHz
Design 3: 8 μm electrode with 20 μm spacing	0.5, 0.75, 1, 1.25, 1.5, 2, 2.25, 2.5, 2.75 and 3 μL/min	20 Vpp	1 MHz
Design 4: 6 μm electrode with 20 μm spacing	0.5, 0.75, 1, 1.25, 1.5, 2, 2.25, 2.5, 2.75 and 3 μL/min	20 Vpp	1 MHz
Design 5: 20 μm electrode with 10 μm spacing	0.5, 0.75, 1, 1.25, 1.5, 2, 2.25, 2.5, 2.75 and 3 μL/min	20 Vpp	1 MHz

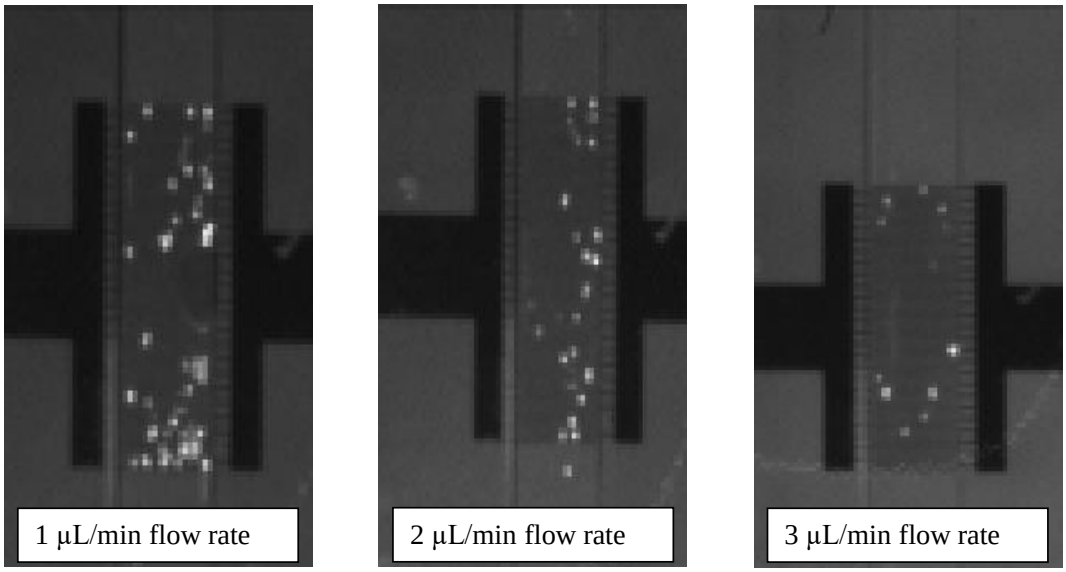

Figure 5.7 Fluorescence microscope images of trapped cells under 1,2 and 3 µL/min flow rate for the design 1.

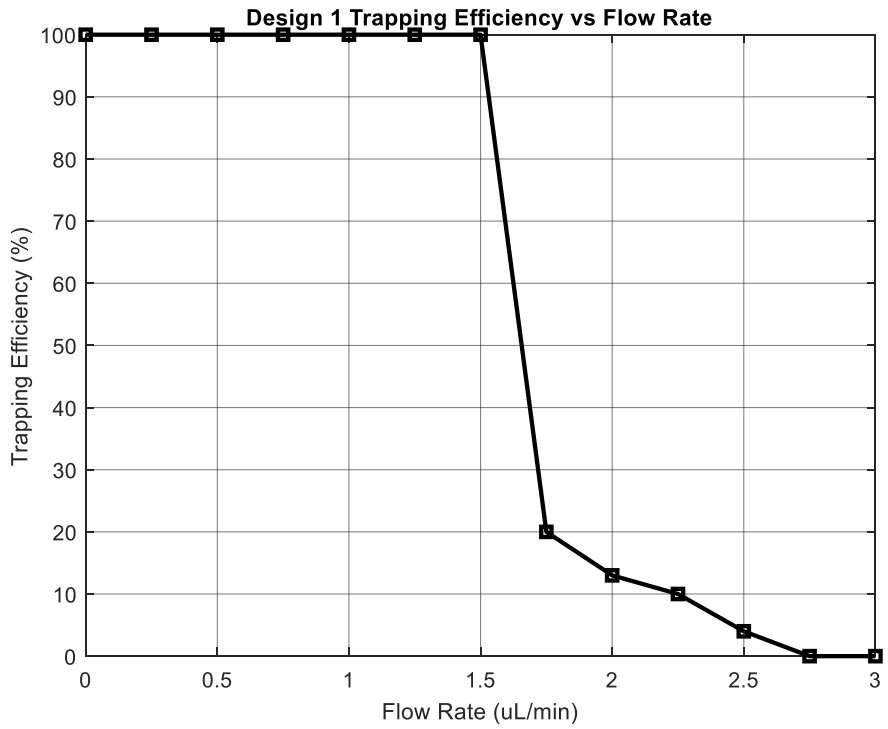

Figure 5.8 Trapping efficiency results for the device 1 under different flow rates.

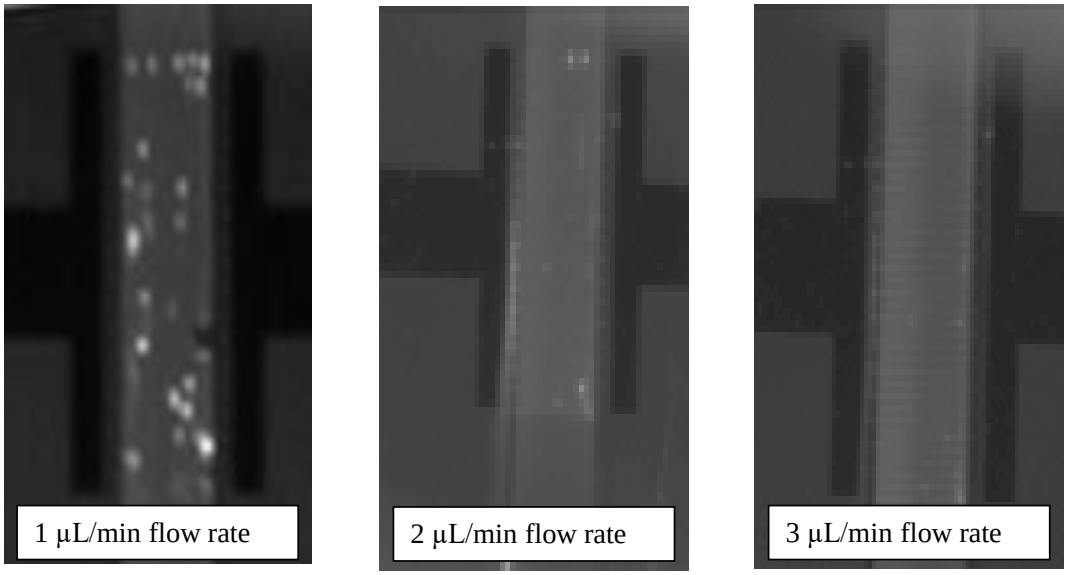

Figure 5.9 Fluorescence microscope images of trapped cells under 1,2 and 3 µL/min flow rate for the design 2.

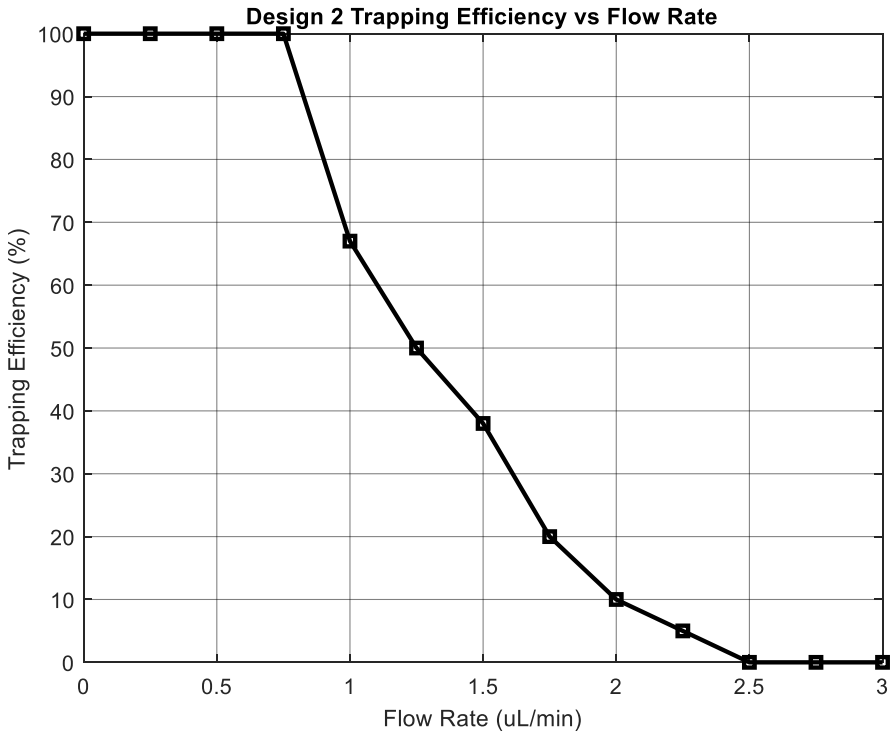

Figure 5.10 Trapping efficiency results for the device 2 under different flow rates.

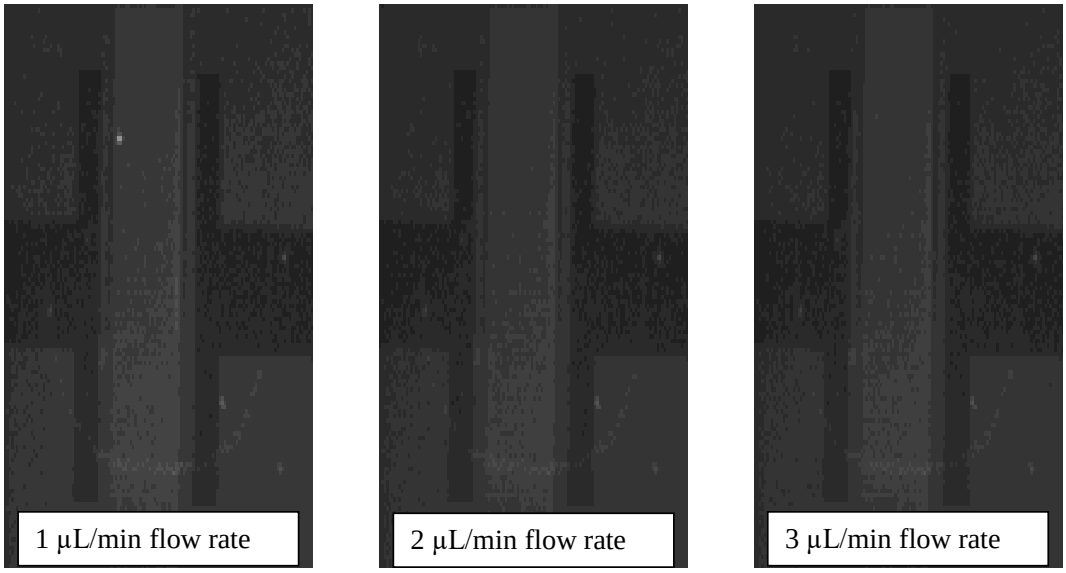

Figure 5.11 Fluorescence microscope images of trapped cells under 1,2 and 3 µL/min flow rate for the design 3

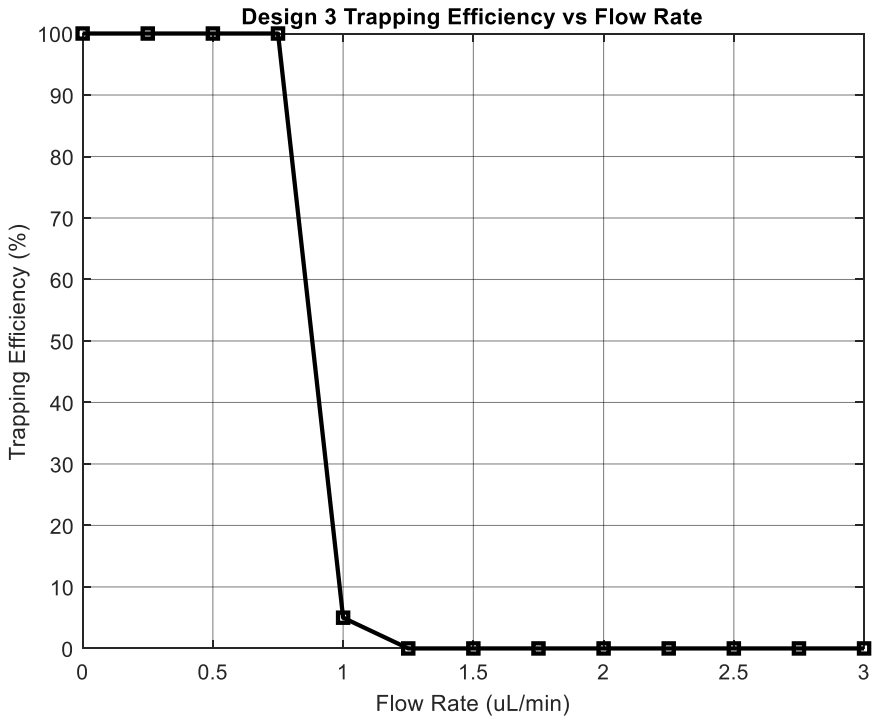

Figure 5.12 Trapping efficiency results for the device 3 under different flow rates

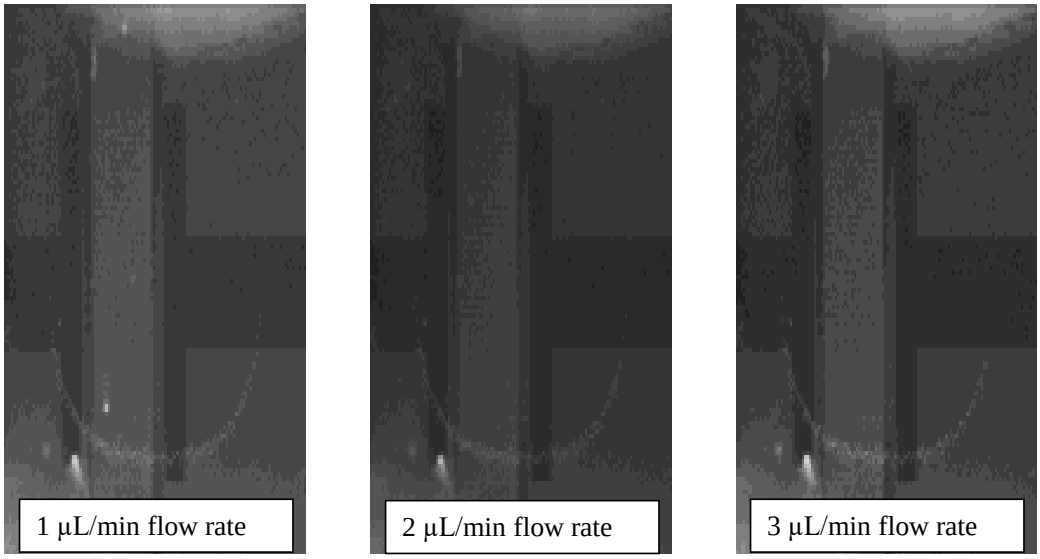

Figure 5.13 Fluorescence microscope images of trapped cells under 1,2 and 3 µL/min flow rate for the design 4.

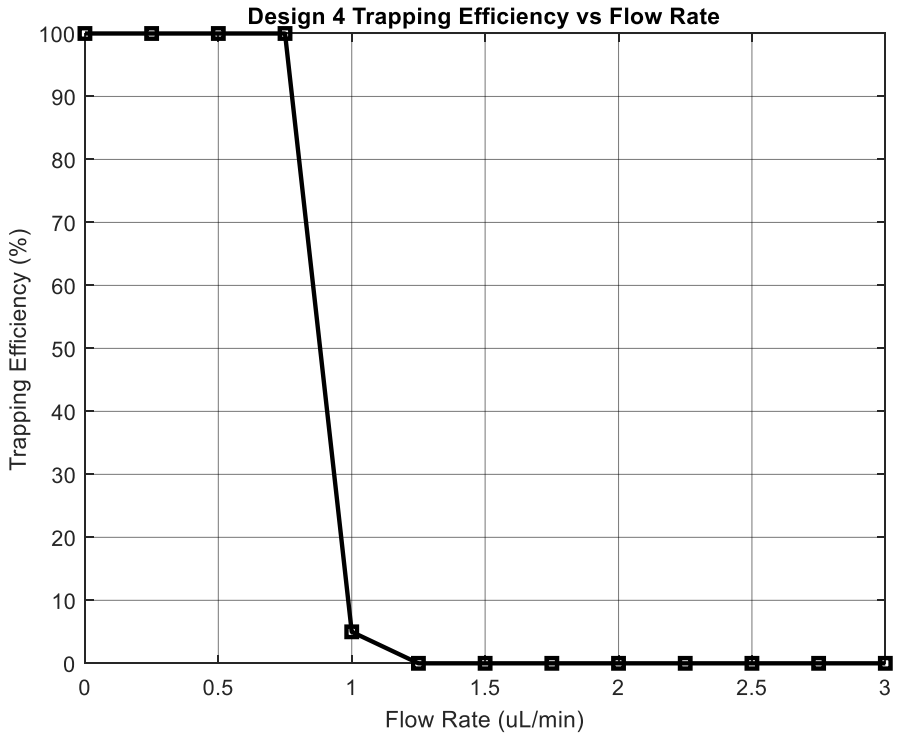

Figure 5.14 Trapping efficiency results for the device 4 under different flow rates.

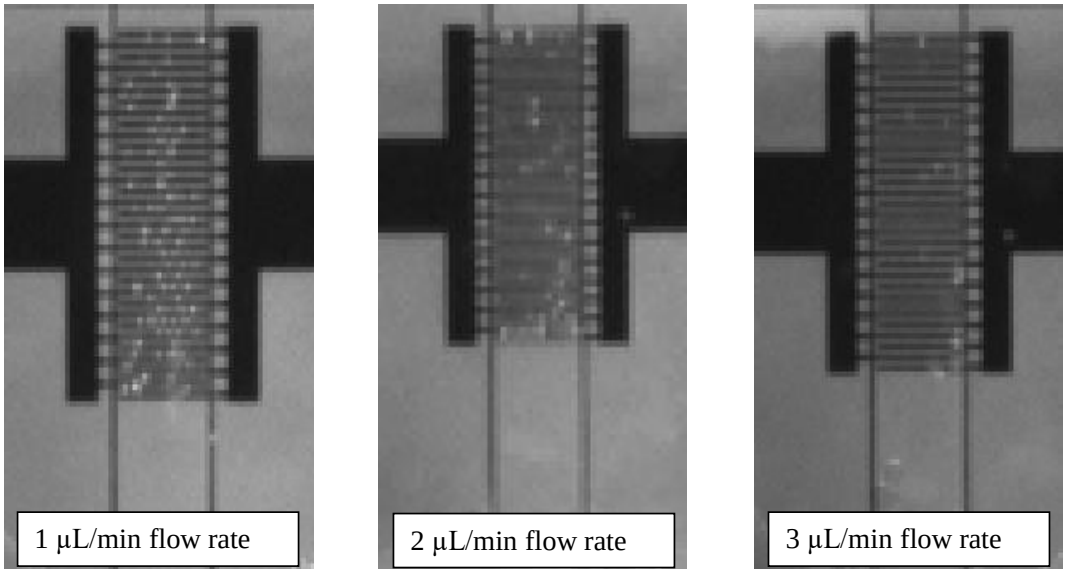

Figure 5.15 Fluorescence microscope images of trapped cells under 1,2 and 3 µL/min flow rate for the design 5.

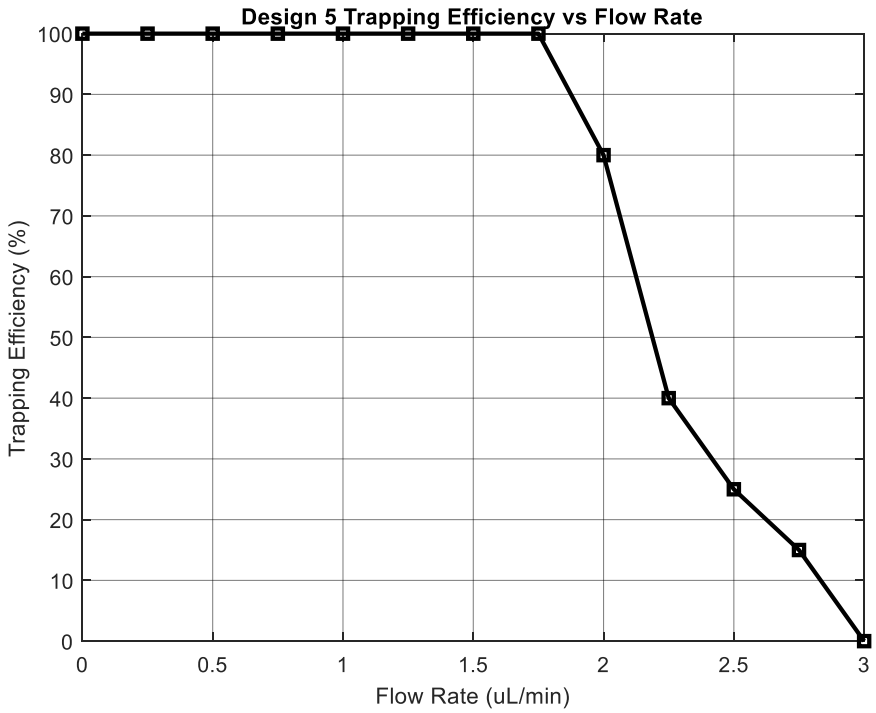

Figure 5.16 Trapping efficiency results for the device 5 under different flow rates.

In trapping efficiency experiments, the flow rate is changed from 0 to 3 μL/min with 0.25 μL/min intervals. Expectedly, design 5 which has largest electrode width, has highest trapping efficiency especially at high flow rates (>1.5 μL/min). Since, wider electrodes provide larger physical trapping area for the flowing cells. Additionally, if the interelectrode gap decreases, higher electrical field gradient is observed in a smaller region so that trapping efficiency increases.

All of the devices have 100% trapping efficiency up to 0.75 μL/min flow rate. After 1 μL/min flow rate, drag force becomes more dominant and trapping efficiencies of the design 2, 3 and 4 are dramatically decreased. Design 5 achieves 100% trapping efficiency at flow rates up to 1.75 μL/min and has an acceptable trapping efficiency (80%) at 2 μL/min. Therefore, design 5 has the best performance DEP characterization tests in terms of trapping efficiency as expected.

5.5.2 CMOS Imager Performance Tests

To obtain counting efficiency of the devices, five different devices are tested under optimum flow rates obtained in DEP characterization experiments. MCF7 cells are trapped and then imaged with CMOS image sensor for all of the designs. Additionally, fluorescence microscope is utilized for verification purposes. Table 5.2 summarizes the test procedure for counting efficiency experiments.

Table 5.2 Test parameters for the DEP device characterization.

DEP Device	Flow Rate	Voltage	Frequency
Design 1: 10 μm electrode with 10 μm spacing	1.5 μL/min	20 Vpp	1 MHz
Design 2: 10 μm electrode with 20 μm spacing	0.75 μL/min	20 Vpp	1 MHz

Table 5.2 (continued).

Design 3: 8 μm electrode with 20 μm spacing	0.75 μL/min	20 Vpp	1 MHz
Design 4: 6 μm electrode with 20 μm spacing	0.75 μL/min	20 Vpp	1 MHz
Design 5: 20 μm electrode with 10 μm spacing	1.75 μL/min	20 Vpp	1 MHz

Figure 5.17 illustrates the CMOS images of the empty DEP regions of the different designs. Expectedly, as electrode width increases, shadow images of the electrodes become darker i.e. having high contrast values it is more difficult to segment the trapped cells onto electrodes. Moreover, when interelectrode gap increases electrodes can be distinguished better.

Nonuniform noise patterns occur in the CMOS images due to surface contaminations both on to glass substrate and image sensor. However, with filtering operations and differential analysis method (background subtraction) most of the noise patterns are eliminated.

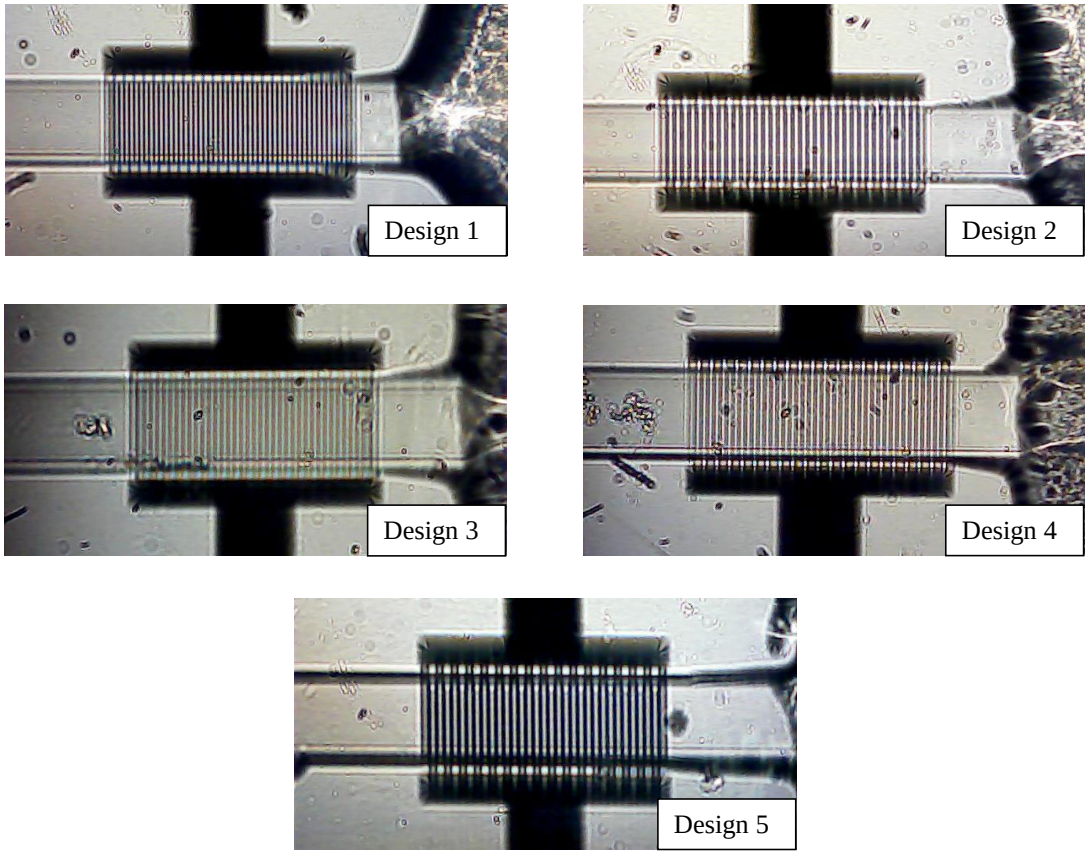

Figure 5.17 Raw CMOS sensor images of the empty DEP devices.

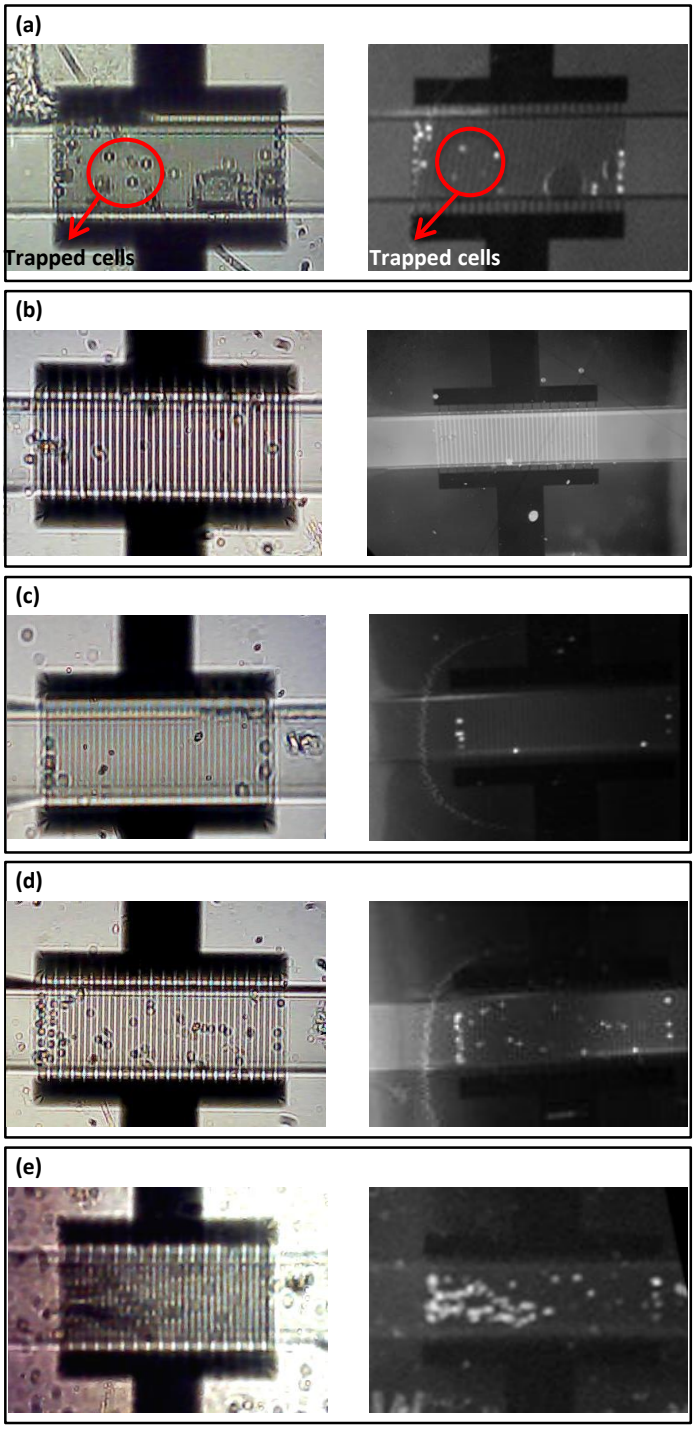

Figure 5.18 Raw CMOS and corresponding fluorescence microscope images for (a) design 1 (b) design 2 (c) design 3 (d) design 4 (e) design 5

Both CMOS and corresponding fluorescence microscope images of the trapped cells on to different designs are presented in the Figure 5.18. As shown in raw CMOS images, cells are clearly distinguishable from the electrodes and background in all of the designs. Nevertheless, cells trapped very close microfluidic channel boundaries may become undetectable as illustrated in the Figure 5.19.

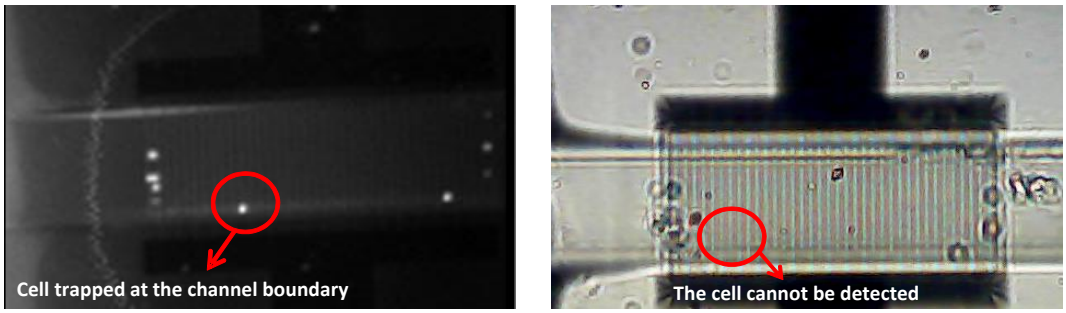

Figure 5.19 Illustration of the undetectable cell trapped at the channel boundary.

To overcome this problem, position of the illumination source (so the shadow images) is shifted and undetectable cells can be imaged in this new shadow image shown in Figure 5.20.

Another problem occurs when the number of trapped cells becomes high (~100). Due to lens-free structure, spatial resolution is limited in CMOS images and individual cells may not be detectable presented in the Figure 5.21.

Yet, thanks to differential analysis and image processing operations, the performance of the system is still acceptable. Figure 5.21 shows detection results of the differential analysis with counting accuracy of 83%.

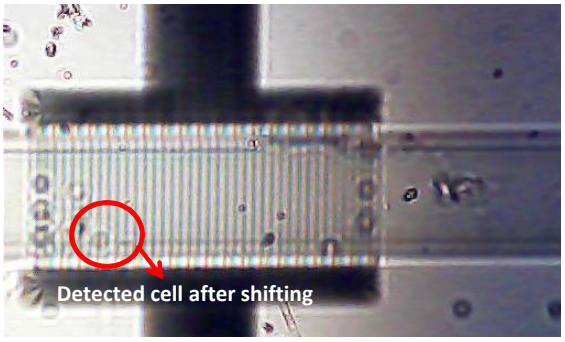

Figure 5.20 Detected trapped cell after shifting of the light source.

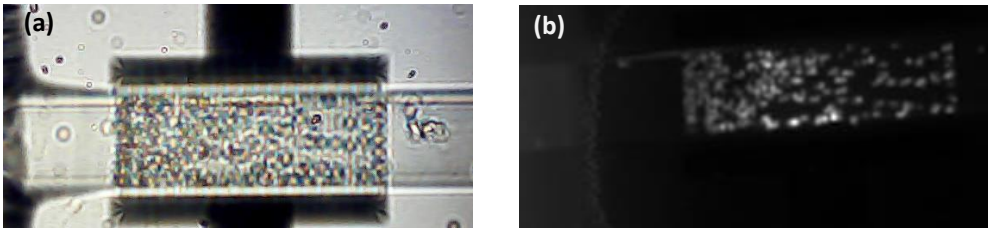

Figure 5.21 (a) Raw CMOS and (b) fluorescence microscope images of the DEP area when number of trapped cells is high.

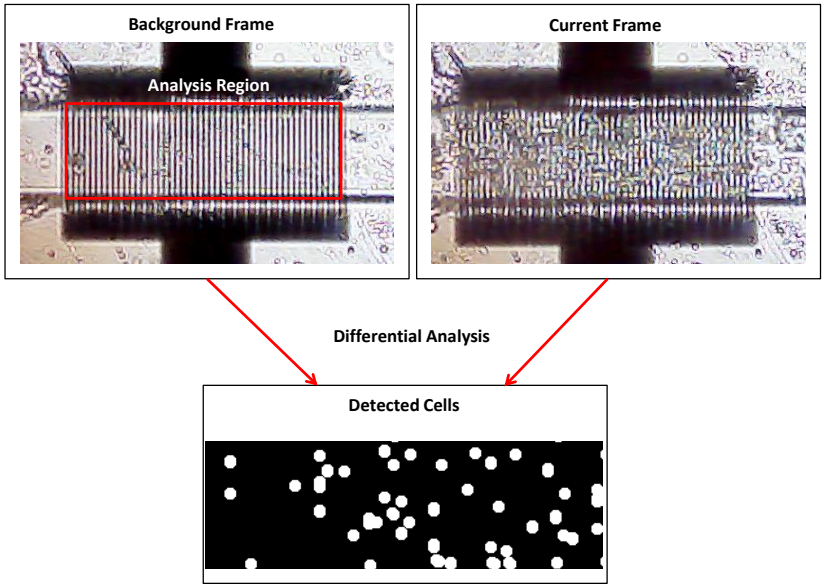

Figure 5.22 Detection of the cells from raw CMOS images based on background subtraction technique.

Average counting efficiencies of the CMOS imager with different designs are summarized in the Table 5.3.

Table 5.3 Average counting efficiencies of the different designs.

DEP Device	**Average Counting Efficiency**
Design 1: 10 μm electrode with 10 μm spacing	>90%
Design 2: 10 μm electrode with 20 μm spacing	>90%
Design 3: 8 μm electrode with 20 μm spacing	>90%
Design 4: 6 μm electrode with 20 μm spacing	>95%
Design 5: 20 μm electrode with 10 μm spacing	>85%

Counting efficiency values of the device 2, 3 and 4 are nearly same and better than the design 1 and 5 as expected. Since, interelectrode gaps in these devices (20 μm) are larger than the other designs (10 μm) that decreases the shadow effects of the electrodes cause misdetection of the cells. In addition, in some cases, (mostly occur when low number of cells (<30) are trapped in to DEP area) counting efficiency of the system reached to 100%. As it is compared with the previous system, 2nd generation system offers portability, easy-to-use operation, higher spatial resolution (3.4 μm), larger field of view (3.7 mm^2) and maximum counting accuracy (>95%).

Counting efficiency may be further improved with increasing spatial resolution by utilizing partially coherent or coherent illumination source with reconstruction techniques.

5.6 Droplet Based Cell Screening Application

As an alternative application, designed system is employed to real time monitoring of droplet encapsulated cancer cells. The system combines 2nd generation imaging system with microfluidic droplet formation device.

Microfluidic droplet device is microfabricated with soft lithography based techniques. The fabrication process and are illustrated the Figure 5.23 and 5.24 respectively.

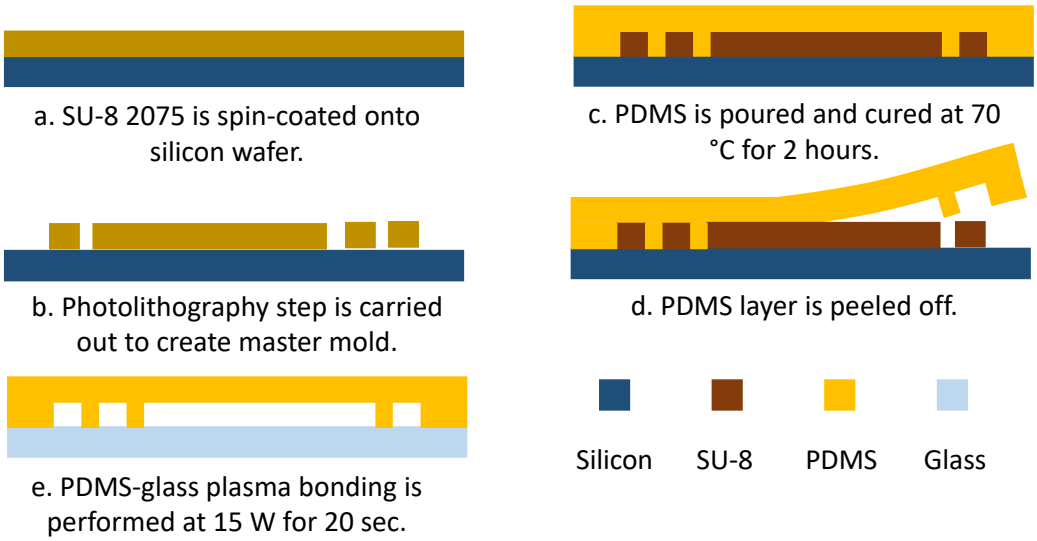

Figure 5.23 Fabrication process of the droplet formation device.

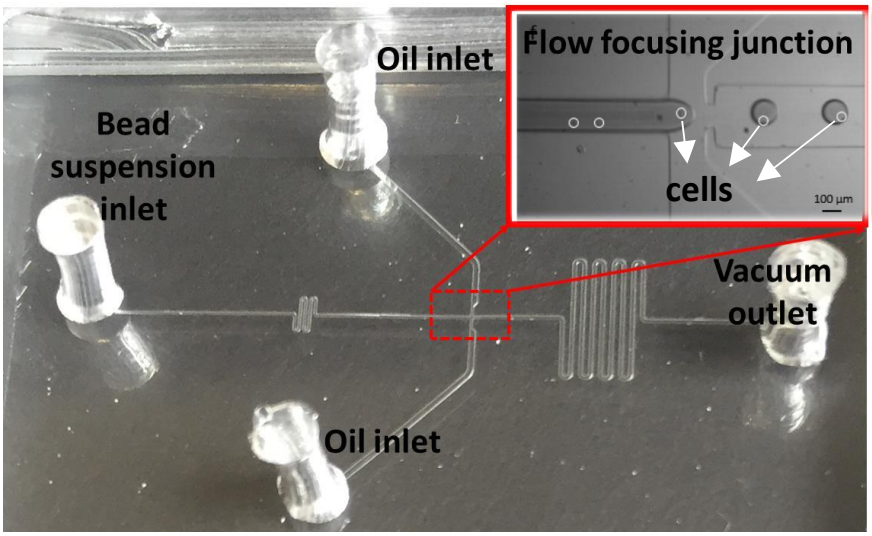

Figure 5.24 Fabricated droplet formation device.

The microfluidic droplet formation device and CMOS image sensor are integrated with a PMMA holder. In experiments, Myeloid leukemia (K-562) cells having $2x10^6$ cells/ml concentration and suspended in RPMI medium are used. Flow of the medium through the microfluidic channel is dispersed by the continuous flow of Novec-7500 fluorinated oil (2% Pico Surf-1). Therefore, cancer cells are were encapsulated in the droplets. Developed an LOC system monitors K562 cancer cells inside droplets by using a CMOS image sensor and Android application (Figure 5.25).

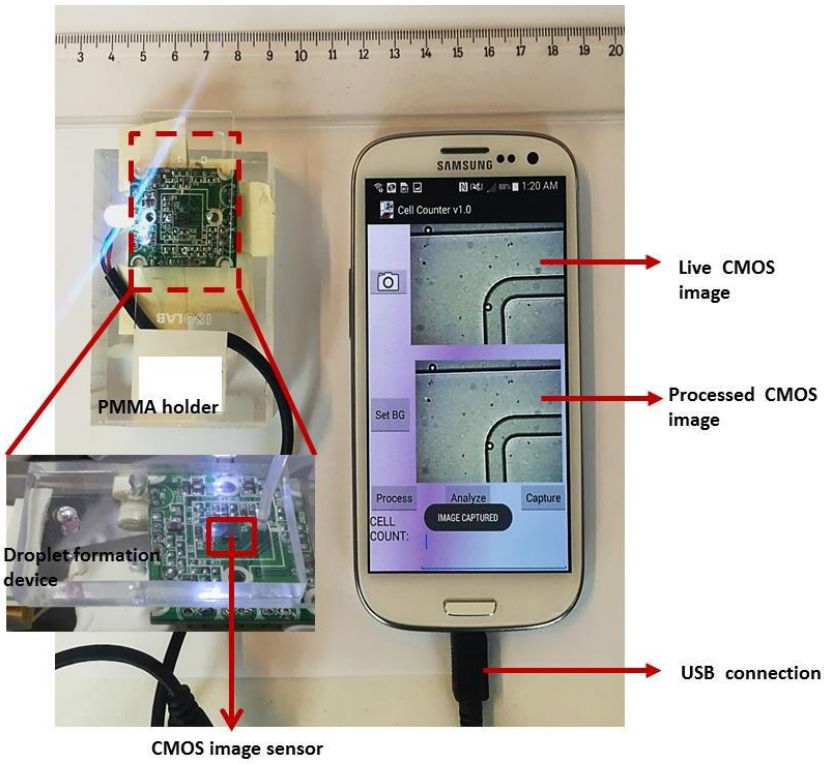

Figure 5.25 Smartphone based cell screening system combining CMOS imaging system with a microfluidic droplet formation device.

For proof-of-principle, images of an empty droplet, droplets including single cell and double cells are captured with both bright field microscope and CMOS imaging system (Figure 5.26). Raw CMOS images firstly enhanced with median filtering. Then, droplets are automatically detected utilizing Hough Transform.

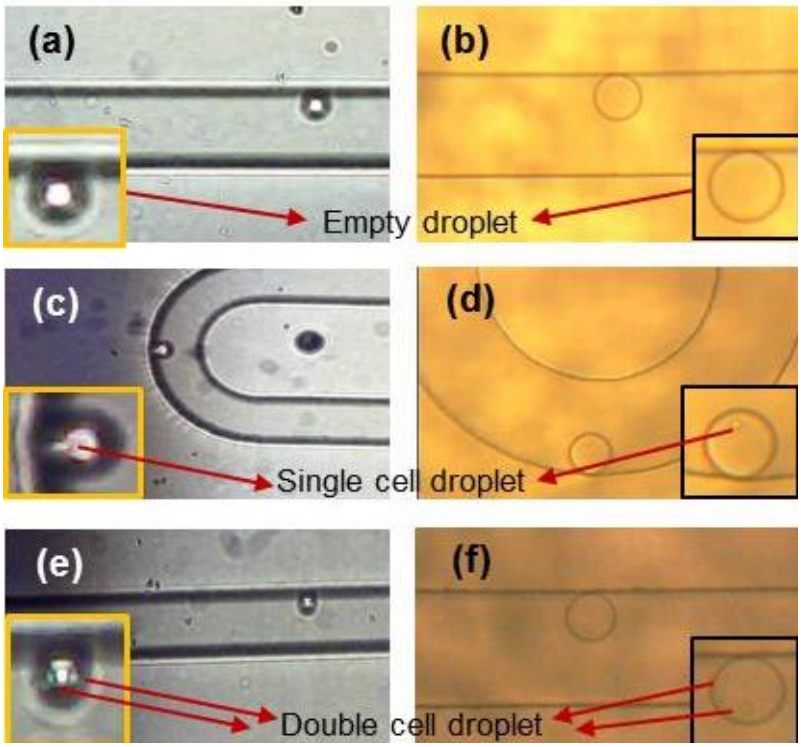

Figure 5.26 CMOS and microscope images of the (a), (b) empty droplets, (c), (d) single cell and (e), (f) double cell droplets.

The application segments and counts cells encapsulated with droplets by implementing edge detection and thresholding operations as shown in Figure 5.27.

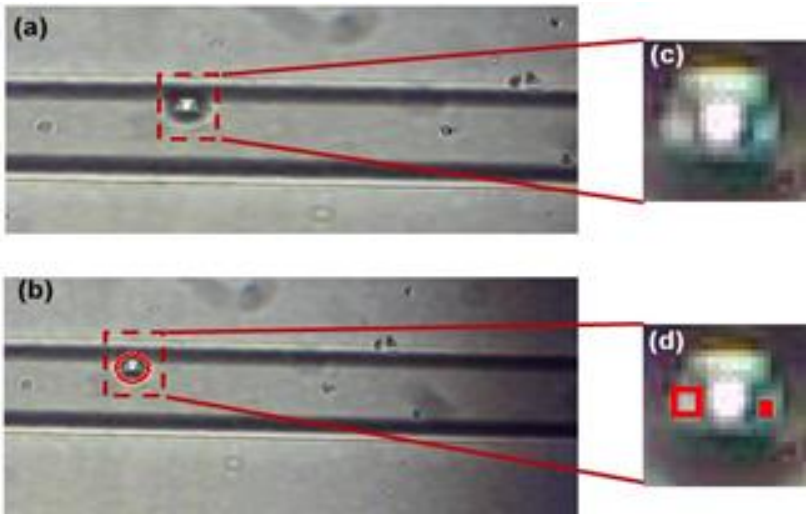

Figure 5.27 Detection of the droplet encapsulated cells (a), (b) raw CMOS image (b),(d) Hough transform based detection results

The results indicate that different number of the cancer cells encapsulated with droplets can be segmented, that can be employed for further analysis. As a future perspective, the proposed droplet screening system can be implemented in detection of apoptosis of cells in label-free manner. Moreover, the system can be used in chemosensitivity assays to monitor survival rate of the cancer cells under different drug dosages so that personalized cancer treatments may be effectively planned.

In this chapter, both experimental results of 1st and 2nd generation imaging systems are presented. 2nd generation system eliminates the drawbacks of the 1nd generation system including low spatial resolution, small field of view and having bulky components. Furthermore, counting accuracy of the 2nd generation system achieves up to 100% whereas trapping efficiency is reported as 100% up to 1.75 μL/min flow rate.

CHAPTER 7

CONCLUSION AND FUTURE WORK

Aim of this thesis is to develop an LOC system combining a microfluidic DEP device with a CMOS imager for label and lens-free quantification of the cancer cells. For that purpose, two different systems are designed, simulated and tested with cell experiments.

First generation system includes a DEP device with 3D electrode structure, a CMOS image sensor and FPGA board. Since, spatial resolution of the image sensor is limited and 3D electrode structure causes unwanted shadow patterns on to image sensor, trapped cells cannot be detected with this system. As an alternative approach, trapped and then released cells are detected with this system under continuous flow with the accuracy of 95%. However, the system still has disadvantages such as low resolution, small field of view and including bulky equipment limits portability.

To overcome these drawbacks, second generation imaging system is developed. Designed DEP device has interdigitated planar electrode configuration eliminates shadow problems observed in the previous design. Portable USB powered signal generator circuitry to operate DEP devices and Android application is utilized for obtain and process CMOS sensor images brings portability to the system. Furthermore, using cost effective GC0308 image sensor dramatically increased

the spatial resolution (~with a factor of 20). Experimental results using MCF7 cancer cells indicate that both counting and trapping accuracy of the second generation system can reach up to 100%. Some of the trapped cells cannot be detected due to low spatial resolution and this problem can be overcome with using different illumination and image reconstruction techniques as a future aspect. Additionally, as an alternative application, the system is integrated with a microfluidic droplet formation device to detect and monitor the cancer cells encapsulated inside the droplets. Preliminary results show that the system is able to segment single or double cells inside the droplet. As a future improvement, the system can be utilized for chemosensitivity assays to monitor survival rate of cancer cells by giving specific amounts of drug into the droplets and observing morphological changes of the cells.

In this thesis, design and experimental results of LOC imaging system is presented. As a future work, following developments can be made:

- To increase spatial resolution, the distance between CMOS image sensor and microfluidic channel can be decreased with microfabrication. Moreover, partially coherent imaging technique can be used in conjunction with image reconstruction techniques to obtain better resolution.

- A machine learning based method can be implemented by obtaining several cell image data with CMOS sensor under different illumination conditions to train the system.

- Using specific and distinct shadows of the cells, different types of the cells can be separated in a heterogeneous solution by utilizing image processing techniques.

- Design of the DEP device can be improved with mechanical separation structures to distinguish rare cells inside a heterogeneous cell solution or whole blood.

REFERENCES

[1] World Health Organization, *World Health Statistics 2015*. 2015.

[2] B. W. Stewart and C. P. Wild, “World cancer report 2014,” *World Heal. Organ.*, pp. 1–2, 2014.

[3] “The American Cancer Society.” .

[4] W. E. Svendsen, *Lab-on-a-Chip Devices and Micro-Total Analysis Systems*. 2015.

[5] G. M. Whitesides, “The origins and the future of microfluidics,” *Nature*, vol. 442, no. 7101, pp. 368–373, Jul. 2006.

[6] H. Yun, K. Kim, and W. G. Lee, “Cell manipulation in microfluidics,” *Biofabrication*, vol. 5, no. 2, p. 22001, 2013.

[7] J. D. Adams, U. Kim, and H. T. Soh, “Multitarget magnetic activated cell sorter,” *Proc. Natl. Acad. Sci.*, vol. 105, no. 47, pp. 18165–18170, 2008.

[8] J. H. Kang, S. Krause, H. Tobin, A. Mammoto, M. Kanapathipillai, and D. E. Ingber, “A combined micromagnetic-microfluidic device for rapid capture and culture of rare circulating tumor cells,” *Lab Chip*, vol. 12, no. 12, p. 2175, 2012.

[9] D. Melville, F. Paul, and S. Roath, “Direct magnetic separation of red cells from whole blood,” *Nature*, vol. 255, no. 5511, p. 706, Jun. 1975.

[10] M. Zborowski, G. R. Ostera, L. R. Moore, S. Milliron, J. J. Chalmers, and A. N. Schechter, “Red blood cell magnetophoresis,” *Biophys. J.*, vol. 84, no. 4, pp. 2638–2645, 2003.

[11] L. Zhu, Q. Zhang, H. Feng, S. Ang, F. S. Chau, and W.-T. Liu, “Filter-based microfluidic device as a platform for immunofluorescent assay of microbial cells.,” *Lab Chip*, vol. 4, pp. 337–341, 2004.

[12] H. Mohamed, L. D. McCurdy, D. H. Szarowski, S. Duva, J. N. Turner, and M. Caggana, “Development of a rare cell fractionation device: Application for cancer detection,” *IEEE Trans. Nanobioscience*, vol. 3, no. 4, pp. 251–256, 2004.

[13] A. Khademhosseini, J.Yeh, S. Jon, G. Eng, K. Y. Sun, J.A. Burdick and R. Langer “Molded polyethylene glycol microstructures for capturing cells within microfluidic channels.,” *Lab Chip*, vol. 4, no. 5, pp. 425–430, 2004.

[14] H. Tani, K. Maehana, and T. Kamidate, “On-Chip Bioassay Using Immobilized Sensing Bacteria in Three-Dimensional Microfluidic Network,” in *Microchip-based Assay Systems, Methods and Applications*, vol. 385, 2007, p. in press.

[15] N. Chronis and L. Lee, “Polymer MEMS-based microgripper for single cell manipulation,” *... Syst.*, pp. 17–20, 2004.

[16] D. Di Carlo, D. Irimia, R. G. Tompkins, and M. Toner, “Continuous inertial focusing, ordering, and separation of particles in microchannels.,” *Proc. Natl. Acad. Sci. U. S. A.*, vol. 104, no. 48, pp. 18892–18897, 2007.

[17] A. J. Mach, J. H. Kim, A. Arshi, S. C. Hur, and D. Di Carlo, “Automated cellular sample preparation using a Centrifuge-on-a-Chip,” *Lab Chip*, vol. 11, no. 17, pp. 2827–2834, 2011.

[18] M. P. MacDonald, G. C. Spalding, and K. Dholakia, “Microfluidic sorting in an optical lattice,” *Nature*, vol. 426, no. November, pp. 421–424, 2003.

[19] S. Kim, S. Yoon, H. Sung, and S. Kim, “Cross-Type Optical Particle Separation in a Microchannel,” *Anal. Chem.*, vol. 80, no. 7, pp. 2628–2630, 2008.

[20] E. Eriksson, K. Sott, F. Lundqvist, M. Sveningsson, J. Scrimgeour, D. Hanstorp, M. Goksör and A. Graneli “A microfluidic device for reversible environmental changes around single cells using optical tweezers for cell selection and positioning.,” *Lab Chip*, vol. 10, no. 5, pp. 617–625, 2010.

[21] F. Petersson, L. Åberg, A. M. Swärd-Nilsson, and T. Laurell, “Free flow acoustophoresis: Microfluidic-based mode of particle and cell separation,” *Anal. Chem.*, vol. 79, no. 14, pp. 5117–5123, 2007.

[22] J. Shi, D. Ahmed, X. Mao, S.-C. S. Lin, A. Lawit, and T. J. Huang, “Acoustic tweezers: patterning cells and microparticles using standing surface acoustic waves (SSAW).,” *Lab Chip*, vol. 9, no. 20, pp. 2890–5, 2009.

[23] Z. Ma, Q. Liu, H. Liu, H. Yang, J. X. Yun, M. Xu, C. A. Eisenberg, T. K. Borg, R. Markwald and B. Z. Gao “Cardiogenic regulation of stem-cell electrical properties in a laser-patterned biochip,” *Cellular and Molecular Bioengineering*, vol. 5, no. 3. pp. 327–336, 2012.

[24] F. Guo, Z. Mao, Y. Chen, Z. Xie, J. P. Lata, P. Li, L. Ren, J. Liu, J. Yang, M. Dao, S. Suresh and T. J. Huang “Three-dimensional manipulation of single cells using surface acoustic waves,” *Proc. Natl. Acad. Sci.*, vol. 113, no. 6, pp. 1522–1527, 2016.

[25] D. Ahmed, A. Ozcelik, N. Bojanala, N. Nama, A. Upadhyay, Y. Chen, W. Hanna-Rose and T. J. Huang “Rotational manipulation of single cells and organisms using acoustic waves,” *Nat Commun*, vol. 7, pp. 1–11, 2016.

[26] T. Yasukawa, K. Nagamine, Y. Horiguchi, H. Shiku, M. Koide, T. Itayama, F. Shiraishi and T. Matsue “Electrophoretic cell manipulation and electrochemical gene-function analysis based on a yeast two-hybrid system

in a microfluidic device," *Anal. Chem.*, vol. 80, no. 10, pp. 3722–3727, 2008.

[27] S. G. Anema, "The use of 'lab-on-a-chip' microfluidic SDS electrophoresis technology for the separation and quantification of milk proteins," *Int. Dairy J.*, vol. 19, no. 4, pp. 198–204, 2009.

[28] B. Cetin and D. Li, "Dielectrophoresis in microfluidics technology," *Electrophoresis*, vol. 32, no. 18. pp. 2410–2427, 2011.

[29] H. Shafiee, M. B. Sano, E. a Henslee, J. L. Caldwell, and R. V Davalos, "Selective isolation of live/dead cells using contactless dielectrophoresis (cDEP).," *Lab Chip*, vol. 10, no. 4, pp. 438–45, Feb. 2010.

[30] P. R. C. Gascoyne, X. Wang, Y. Huang, and F. F. Becker, "Dielectrophoretic Separation of Cancer Cells from Blood," *IEEE Trans. Ind. Appl.*, vol. 33, no. 3, pp. 670–678, 1997.

[31] F. Yang, X. Yang, H. Jiang, W. M. Butler, and G. Wang, "Dielectrophoretic separation of prostate cancer cells.," *Technol. Cancer Res. Treat.*, vol. 12, no. 1, pp. 61–70, Feb. 2013.

[32] H. Li and R. Bashir, "Dielectrophoretic separation and manipulation of live and heat-treated cells of Listeria on microfabricated devices with interdigitated electrodes," *Sensors Actuators, B Chem.*, vol. 86, no. 2–3, pp. 215–221, 2002.

[33] R. C. Gallo-Villanueva, V. H. Pérez-González, R. V. Davalos, and B. H. Lapizco-Encinas, "Separation of mixtures of particles in a multipart microdevice employing insulator-based dielectrophoresis," *Electrophoresis*, vol. 32, no. 18, pp. 2456–2465, 2011.

[34] B. Çetin, Y. Kang, Z. Wu, and D. Li, "Continuous particle separation by size via AC-dielectrophoresis using a lab-on-a-chip device with 3-D electrodes," *Electrophoresis*, vol. 30, no. 5, pp. 766–772, 2009.

[35] V. Micó and Z. Zalevsky, "Superresolved digital in-line holographic microscopy for high-resolution lensless biological imaging.," *J. Biomed. Opt.*, vol. 15, no. 4, p. 46027, 2015.

[36] W. Xu, M. H. Jericho, I. a. Meinertzhagen, and H. J. Kreuzer, "Digital in-line holography for biological applications.," *Proc. Natl. Acad. Sci. U. S. A.*, vol. 98, no. 20, pp. 11301–5, 2001.

[37] A. Ozcan and U. Demirci, "Ultra wide-field lens-free monitoring of cells on-chip.," *Lab Chip*, vol. 8, no. 1, pp. 98–106, 2008.

[38] S. J. Moon, H. O. Keles, Y. G. Kim, D. Kuritzkes, and U. Demirci, "Lensless imaging for point-of-care testing," in *Proceedings of the 31st Annual International Conference of the IEEE Engineering in Medicine and*

Biology Society: Engineering the Future of Biomedicine, EMBC 2009, 2009, pp. 6376–6379.

[39] S. B. Kim, H. Bae, J. M. Cha, S. J. Moon, M. R. Dokmeci, D. M. Cropek and A. Khademhosseini "A cell-based biosensor for real-time detection of cardiotoxicity using lensfree imaging.," *Lab Chip*, vol. 11, no. 10, pp. 1801–7, 2011.

[40] S. B. Kim, H. Bae, K.-I. Koo, M. R. Dokmeci, A. Ozcan, and A. Khademhosseini, "Lens-free imaging for biological applications.," *J. Lab. Autom.*, vol. 17, no. 1, pp. 43–9, 2012.

[41] X. Wang, F. F. Becker, and P. R. C. Gascoyne, "The fractal dimension of cell membrane correlates with its capacitance: a new fractal single-shell model.," *Chaos*, vol. 20, no. 4, p. 43133, Dec. 2010.

[42] D. L. Holliday and V. Speirs, "Choosing the right cell line for breast cancer research.," *Breast Cancer Res.*, vol. 13, no. 4, p. 215, 2011.

[43] J. An, J. Lee, Y. Kim, B. Kim, and S. Lee, "Analysis of Cell Separation Efficiency in Sorter, Dielectrophoresis-activated Cell," in *Proceedings of the 3rd IEEE Int. Conf. on Nano/Micro Engineered and Molecular Systems*, 2008, pp. 965–969.

[44] P. R. C. Gascoyne, S. Shim, J. Noshari, F. F. Becker, and K. Stemke-Hale, "Correlations between the dielectric properties and exterior morphology of cells revealed by dielectrophoretic field-flow fractionation," *Electrophoresis*, vol. 34, no. 7, pp. 1042–1050, 2013.

[45] H. M. Coley, F. H. Labeed, H. Thomas, and M. P. Hughes, "Biophysical characterization of MDR breast cancer cell lines reveals the cytoplasm is critical in determining drug sensitivity.," *Biochim. Biophys. Acta*, vol. 1770, no. 4, pp. 601–8, Apr. 2007.

[46] H. Ji, D. Sander, A. Haas, and P. A. Abshire, "Contact imaging: Simulation and experiment," *IEEE Trans. Circuits Syst. I Regul. Pap.*, vol. 54, no. 8, pp. 1698–1710, 2007.

[47] Y. Demircan, A. Koyuncuoğlu, M. Erdem, E. Özgür, U. Gündüz, and H. Külah, "Label-free detection of multidrug resistance in K562 cells through isolated 3D-electrode dielectrophoresis.," *Electrophoresis*, vol. 36, no. 9–10, pp. 1149–57, May 2015.

[48] J. Musayev, C. Altiner, Y. Adiguzel, H. Kulah, S. Eminoglu, and T. Akin, "Capturing and detection of MCF-7 breast cancer cells with a CMOS image sensor," *Sensors Actuators, A Phys.*, vol. 215, pp. 105–114, 2014.

[49] G. Ozkayar, "Rare cell enrichment from blood by using dielectrophoresis," M.S. Thesis, Middle East Technical University, 2014.